

UNIVERSITY OF CALIFORNIA, SAN DIEGO

Ocean fronts in the Southern California Current System and their role in
structuring zooplankton distributions, diel vertical migration, and size
composition

A dissertation submitted in partial satisfaction of the requirements for the
degree Doctor of Philosophy

in

Oceanography

by

Jesse Russell Powell

Committee in charge:

Professor Mark D. Ohman, Chair
Professor Russ E. Davis
Professor Peter J. S. Franks
Professor Michael R. Landry
Professor Jonathan B. Shurin

2013

Copyright

Jesse Russell Powell, 2013

All rights reserved.

The Dissertation of Jesse Russell Powell is approved, and it is acceptable in quality and form for publication on microfilm and electronically:

Chair

University of California, San Diego

2013

DEDICATION

To my parents, who taught me to wonder and explore,
and displayed great patience when I did so.

TABLE OF CONTENTS

| | |
|---|----------|
| SIGNATURE PAGE..... | iii |
| DEDICATION..... | iv |
| TABLE OF CONTENTS..... | v |
| LIST OF TABLES..... | xi |
| LIST OF FIGURES..... | xiii |
| ACKNOWLEDGEMENTS..... | xix |
| VITA..... | xxv |
| ABSTRACT OF THE DISSERTATION..... | xxvi |
| | |
| CHAPTER 1: Introduction..... | 1 |
| Physical oceanography of the California Current System..... | 3 |
| Major features..... | 3 |
| Water masses..... | 4 |
| Recurrent structures in the SCCS..... | 5 |
| Interannual and interdecadal variability..... | 5 |
| Winds..... | 7 |
| Mesoscale structure..... | 8 |
| Biological oceanography of the CCS..... | 9 |
| Eastern boundary upwelling ecosystems..... | 9 |
| Floristic and faunal provinces..... | 10 |
| Sources and sinks – the generation of pattern | 11 |
| Spring transition..... | 12 |

| | |
|--|----|
| Patterns in the zooplankton..... | 12 |
| Long-term trends..... | 13 |
| <i>Fronts in the CCS region.....</i> | 14 |
| Geostrophy and mesoscale features..... | 15 |
| Submesoscale frontogenesis..... | 15 |
| Stirring and filament formation | 16 |
| <i>Barrier or blender? Cross-front exchange</i> | 17 |
| <i>Modeling</i> | 17 |
| Fronts and zooplankton ecology | 18 |
| <i>Distributions and assemblages across fronts</i> | 19 |
| <i>Fronts and Diel Vertical Migration</i> | 20 |
| <i>Predator-prey interactions.....</i> | 21 |
| Example fronts in the CCS..... | 22 |
| <i>Coastal Transition Zone (CTZ) Program.....</i> | 22 |
| <i>The Ensenada Front.....</i> | 23 |
| <i>The A-Front.....</i> | 24 |
| Research questions..... | 25 |
| Research approach..... | 26 |
| Description of chapters..... | 28 |
| References..... | 30 |
| Tables..... | 43 |

| | |
|--|-----------|
| CHAPTER 2: Use of glider-class acoustic doppler profilers for estimating zooplankton biomass..... | 44 |
| Acknowledgements..... | 49 |
| Supplement to chapter 2..... | 178 |

**CHAPTER 3: Co-variability of zooplankton gradients with
glider-detected density fronts in the Southern California**

| | |
|--|-----------|
| Current System..... | 50 |
| Abstract..... | 50 |
| Introduction..... | 51 |
| Methods..... | 58 |
| Study area and duration..... | 58 |
| <i>Spray</i> glider and instrument payload..... | 59 |
| Glider data processing..... | 62 |
| Gradients, enhancement index and front detection..... | 63 |
| Results..... | 64 |
| Coincident biological and physical structures | 64 |
| Oceanic density fronts along lines 80 and 90..... | 65 |
| Covariability of density and MVBS, Chl-a gradients | 66 |
| Enhanced MVBS at ocean density fronts..... | 68 |
| Covariability of MVBS with other hydrographic variables... | 69 |
| Discussion..... | 70 |
| Acknowledgements..... | 76 |

| | |
|-----------------|----|
| References..... | 76 |
| Tables..... | 81 |
| Figures..... | 84 |

CHAPTER 4: Changes in zooplankton behavior and size distributions across glider-detected fronts in the Southern

| | |
|--|-----------|
| California Current System..... | 96 |
| Abstract..... | 96 |
| Introduction..... | 97 |
| Methods..... | 103 |
| Study area and duration..... | 103 |
| <i>Spray</i> glider and instrument payload | 103 |
| Glider Data Processing | 106 |
| Front Definition and Canonical Front Construction..... | 107 |
| Interbeam differencing and smoothing algorithms..... | 108 |
| Mocness sample processing and ZooScan analysis | 109 |
| Estimating depth of Chl- <i>a</i> max and the euphotic zone..... | 111 |
| DVM calculations..... | 112 |
| Acoustic modeling and Monte Carlo simulations | 112 |
| Inverse modeling of zooplankton size spectra..... | 114 |
| Results..... | 114 |
| Zooplankton habitat changes across fronts | 114 |
| Chl- <i>a</i> fluorescence maximum and euphotic zone depth..... | 115 |

| | |
|--|------------|
| DVM amplitude changes across fronts | 116 |
| Horizontal gradients of maxDSV..... | 116 |
| Cross-frontal water column scattering characteristics..... | 117 |
| Modeled changes in zooplankton size structure | 118 |
| Net samples: zooplankton assemblages and DVM..... | 120 |
| Discussion..... | 121 |
| Acknowledgements | 128 |
| References..... | 129 |
| Tables..... | 135 |
| Figures..... | 136 |
| CHAPTER 5: Summary and conclusions..... | 161 |
| Life in a turbulent ocean... as observed by <i>Spray</i> gliders..... | 161 |
| Estimating zooplankton biomass with the <i>Spray</i> ADP..... | 162 |
| Front distribution and seasonality in the SCCS, and their role in structuring plankton distributions..... | 163 |
| Fronts as boundaries between planktonic ecosystems..... | 167 |
| A new model for discovery in biological oceanography..... | 168 |
| A call to arms: what are the big questions? | 173 |
| References..... | 175 |
| Tables..... | 177 |
| APPENDIX I: Supplement to chapter 2..... | 178 |

APPENDIX II: ADP calibration procedures.....183

LIST OF TABLES

| | |
|---|-----|
| Table 1.1: Water masses of the California Current System (L= Low; H = High). After Simpson, 1984..... | 43 |
| Table 3.1: Spearman's rank correlation (r_s) of hydrographic and biotic variables and their respective gradients with MVBS and MVBS gradients. Asterisks indicate correlations that are not significant ($p > 0.05$)..... | 81 |
| Table 3.2: Comparison of median MVBS gradients at hydrographic or biotic fronts versus non-fronts..... | 82 |
| Table 3.3: Comparison of median hydrographic or biotic gradients at MVBS fronts versus non-fronts | 83 |
| Table 4.1: Comparison of inshore and offshore (relative to frontal location) scattering characteristics of daytime and nighttime layers of maximum backscatter | 135 |
| Table 5.1: Sensors that might be integrated into single multi- instrument package on future gliders | 177 |
| Table A1.1: Station locations for Moccness tows | 179 |
| Table A1.2: Taxon Categories Identified by Zooscan in this study..... | 179 |
| Table A2.1: ADP calibration results. All data reported in decibels. | 188 |

Table A2.2: Pairwise differences between each ADP instrument's mean calibration test result. The mean and standard deviation of these differences is shown at the bottom of the table. All data reported in decibels..... 190

LIST OF FIGURES

| | |
|--|----|
| <p>Figure 2.1: RMVBS measured by the ADP versus \log_{10} SAC ($\text{mm}^2 \text{m}^{-3}$). The line depicts a Model II regression ($y = 11.87x + 22.93$, $r^2 = 0.55$) fitted using a reduced major axis algorithm.</p> | 46 |
| <p>Figure 2.2: (Left) Coefficient of determination, r^2, for correlation of RMVBS with \log_{10} SAC of zooplankton of different size classes. (Right) Boxplots show the \log_{10} SAC of zooplankton in the size bins</p> | 46 |
| <p>Figure 2.3: (A–E) Partial response functions for \log_{10} SAC for each of the five explanatory variables used by the GAM. In each panel, the relative weighting of the smoothing function (ordinate) is plotted against \log_{10} SAC</p> | 47 |
| <p>Figure 3.1: CCE-LTER <i>Spray</i> glider transect lines 80 and 90.....</p> | 84 |
| <p>Figure 3.2: Schematic diagrams depicting the definition of gradients, fronts and enhancement indices</p> | 85 |
| <p>Figure 3.3: Glider sections along line 80 showing (A) density, (B) temperature, (C) salinity, D) spiciness, E) Chl-a (SFU), F) acoustic backscatter (MVBS), G) cross-track current velocity, and H) along-track current velocity.....</p> | 86 |
| <p>Figure 3.4: Seasonal and cross-shore distribution of density fronts along (A) line 80, and (B) line 90 Grey dots show the</p> | |

| | |
|---|----|
| distribution of all dives from October 2006 through November 2011..... | 87 |
| Figure 3.5: Incidence and gradient strength of density fronts along line 80 and line 90 by season and distance offshore..... | 88 |
| Figure 3.6: Figure 3.6. Median distance offshore of density fronts along (A) Line 80 and (B) Line 90 during bi-monthly periods throughout the year | 89 |
| Figure 3.7: Covariability of horizontal gradients in Acoustic Back- scatter (MVBS) and seawater density for (A and B) line 80 and (C and D) line 90 at fronts and non-frontal regions..... | 90 |
| Figure 3.8: Covariability of horizontal gradients in Standard Fluor- escence Units (SFU) and seawater density for (A and B) line 80 and (C and D) line 90 at fronts and non-frontal regions..... | 91 |
| Figure 3.9: (A and C) Line 80 and (B and D) Line 90 MVBS Enhance- ment Index values in relation to fronts..... | 92 |
| Figure 3.10: (A and C) Line 80 and (B and D) Line 90 Chl-a Fluor- escence enhancement index in relation to fronts..... | 93 |
| Figure 3.11: MVBS Enhancement Index at density fronts for (A) line 80, and (B) line 90. Red, blue and black dots indicate positive, negative and zero enhancement, respectively..... | 94 |
| Figure 3.12: Percent chance for a mobile predator of locating waters with higher mean acoustic backscatter (MVBS) by migrating up a local density gradient..... | 95 |

| | |
|---|-----|
| Figure 4.1: CCE-LTER <i>Spray</i> glider transect lines 80 and 90, off the Southern California coast superimposed on bathymetry. Inset shows location off North America..... | 136 |
| Figure 4.2: (A,B) Mean surface layer (0-50 m) temperatures and (C,D) Salinities across fronts along (A,C) Line 80 and (B,D) Line 90. | 137 |
| Figure 4.3: (A,B) Mean density, σ_θ , and (C,D) salinity structure inshore and offshore of canonical fronts for (A,C) Line 80 and (B,D) Line 90. | 138 |
| Figure 4.4: (A,B) Mean surface layer (0-50 m) mean volume backscatter and (C,D) Chl-a fluorescence across fronts along (A,C) Line 80 and (B,D) Line 90..... | 139 |
| Figure 4.5: (A,B) Mean volume backscatter (MVBS) and (C,D) Chl-a fluorescence structure inshore and offshore of canonical fronts for (A,C) Line 80 and (B,D) Line 90..... | 140 |
| Figure 4.6: Changes in the depth of Chl-a fluorescence maximum across ocean fronts in the Southern California Current System | 141 |
| Figure 4.7: Average inshore to offshore change in the depth of the (A,B) Chl-a fluorescence maximum and (C,D) euphotic zone across fronts compared to non-frontal regions for (A,C) line 80 and (B,D) line 90..... | 142 |
| Figure 4.8: Depth of the Chl-a maximum versus the modeled depth | |

| | |
|--|-----|
| of the euphotic zone. The black line shows a 1:1 relationship..... | 143 |
| Figure 4.9: Changes in DVM amplitude across ocean fronts. (A) | |
| Vertical section of MVBS along line 80..... | 144 |
| Figure 4.10: Average inshore to offshore change in DVM amplitude | |
| across fronts compared to non-frontal regions for (A) line 80 | |
| and (B) line 90..... | 145 |
| Figure 4.11: Relationship between median DVM amplitude and the | |
| median depth of the euphotic zone..... | 146 |
| Figure 4.12: Vertical sections of (A) MVBS and (B) maxDSV values | |
| along a line 80 transect. The position of an ocean front is indi- | |
| cated by the dotted white line..... | 147 |
| Figure 4.13: Horizontal gradients in maxDSV across frontal regions | |
| (white boxes) versus non-frontal regions (shaded boxes) for | |
| (A-C) line 80 and (D-F) line 90, for three depth strata (indi- | |
| cated above the panels)..... | 148 |
| Figure 4.14: Acoustic backscattering characteristics of different depth | |
| strata (A,C) offshore, and (B,D) inshore of (A,B) line 80 fronts | |
| (n=81), and (C,D) line 90 fronts (n=73)..... | 149 |
| Figure 4.15: Acoustic modeling of zooplankton assemblages. | |
| Acoustic model output from a Monte Carlo simulation of | |
| (A) expected MVBS, and (B) expected maxDSV..... | 150 |
| Figure 4.16: Expected size spectra of daytime and nighttime scat- | |
| tering layers. Size spectra of ensonified zooplankton assem- | |

| | |
|---|-----|
| blages were estimated with an inverse model..... | 151 |
| Figure 4.17: Inverse model output showing variation in expected slopes of size spectra of assemblages ensonified by the glider ADP along a line 80 transect..... | 152 |
| Figure 4.18: Expected size spectra of vertically stratified scattering layers. The blue and green lines show the size spectra of ensonified zooplankton assemblages of the 400-500 m and 100-200 m scattering layers..... | 153 |
| Figure 4.19: Day (D) and Night (N) weighted mean depths (WMD) of zooplankton in the offshore and inshore regions. Box plots show WMD of zooplankton collected by Mocness..... | 154 |
| Figure 4.20: Vertical distributions of carbon biomass of major zoo- plankton taxa in the inshore and offshore regions on three cruises: P0605, P0704, P0810..... | 155 |
| Figure 4.21: Comparison of inshore and offshore carbon biomass contributions of different taxonomic groups for the three cruises combined (P0605, P0704, P0810)..... | 157 |
| Figure 4.22: Vertical distributions of carbon biomass different zoo- plankton size categories in the inshore and offshore regions on three cruises: P0605, P0704, P0810..... | 158 |
| Figure 4.23: Comparison of inshore and offshore carbon biomass contributions of different size classes for three cruises com- bined (P0605, P0704, P0810)..... | 160 |

| | |
|---|-----|
| Figure A1.1: Sampling geometry of Mocness-mounted ADP. The ADP was mounted to the frame so that two of the three acoustic beams were roughly level with the mouth of the net. The third beam points up to the surface..... | 178 |
| Figure A1.2: Relationship between sample taxonomic composition and RMVBS. Each net sample’s taxonomic composition is displayed in terms of percentage biomass within the sample..... | 180 |
| Figure A1.3: Relationship between carbon biomass estimates and Summed Area Concentration, SAC..... | 181 |
| Figure A1.4: Relationship between log10 carbon biomass and Relative Mean Volume Backscatter (RMVBS, dB)..... | 182 |
| Figure A2.1: A) ADP testing set-up in the SIO OAR pool. The ADP is shown 2 m underwater in the photo at a distance of 5 m from the stepper motor system..... | 186 |
| Figure A2.2: Example beam map generated during the calibration of ADP M685 on March 23, 2011. The color scale depicts recorded acoustic backscatter in decibels | 197 |

ACKNOWLEDGEMENTS

I owe a tremendous debt to my advisor, Mark Ohman, without whom this dissertation would not have been possible. More than anyone I've ever met, Mark is a man entirely in his element, both as a scientist and an advisor. His enthusiasm for research and teaching is clear, as his belief that being a scientist is a privilege and an honor. As Mark tells his students, scientists are given the chance to advance the frontiers of knowledge, and contribute to the good of society. It is for these reasons, I believe, that Mark works so hard to give the next generation of scientists the tools they need to carry the torch high. Whether it is the finer points of scientific writing, or formulating hypotheses, or designing experiments, he urges us all to go further. These lessons were not lost. I, for one, will always value his notes and emails ending with the exhortation "Onward ever onward!" Additionally, Mark is an extraordinarily decent human being. A long line of students, including myself especially, have benefited from his support and advice.

I would also like to thank my committee for their excellent advice and constructive criticism. Peter Franks is the model of a good-natured professor whose positive outlook inspires students to see the best in themselves and their work. While Mark inspired me to do more, Peter inspired me to do less, in a good way. At my qualification exams, Peter impressed upon me the need to trim back my overly-ambitious (I would now say naïve) plans, and instead focus on the essence of my question. He urged me to cut away all the

extraneous diversions and try to demonstrate one true thing. Another lesson learned. I was also extremely fortunate to have Russ Davis on my committee. Besides his unparalleled knowledge of all things glider-related, I would have stumbled down many wrong paths and dead-ends if not for his advice at committee meetings. I appreciated his willingness, eagerness even, to call BS on something if it so merited it. As Feynman said, “The first principle is that you must not fool yourself, and you are the easiest person to fool.” In all of my committee meetings, Jonathan Shurin, continually tried to turn my focus back to the underlying ecological questions. It is true that I can get wrapped up in the technical details of a project. Jonathan urged me to broaden my thinking. Michael Landry joined my committee late in the process, stepping in for Jay Barlow when scheduling difficulties arose. Michael provided invaluable insight and help in wrangling some sloppy writing, especially in Chapter 4. Finally, I would like to thank Jay Barlow who was there at the start to help launch my dissertation, as well as provide guidance at several committee meetings.

The Biological Oceanography program at Scripps is exceptional in that it gives students the time and the tools they need to generate questions that are both important and original. I took many courses here that made me think in new and unexpected ways. Chief among these were Peter Frank’s Physical-Biological Interactions course, Mark Ohman’s course in Marine Zooplankton, and Farooq Azam’s Microbial Oceanography. I hope that Scripps will always be a place that encourages future marine scientists to find their own questions and explore their scientific curiosity.

Of course, I must thank my exceptional cohort: Alison Cawood, Miriam Goldstein, Meg Rippy, and Darcy Taniguchi. They are my friends, my colleagues, and my fellow girly-drink aficionados. Each one of us brought different strengths to the group, and together we were unbeatable. We studied together, practiced talks together, watched bad TV together, and went to sea together. Graduate school is a long, hard journey. Cohort, without you I wouldn't have made it. Thank you!

Yet more thanks go out to officemates Pete Davison (till he up and graduated) and, now, Natasha Gallo. A good officemate is a boon, and I was very fortunate to have Pete and Natasha with whom I could exchange ideas and theories, and enjoy a welcoming space. Pete and Natasha are excellent scientists and I have learned from them both.

We graduate students all owe a great many thanks to the amazing staff here at SIO. Shonna Dovel should be awarded a medal. She has come to the rescue of more graduate students in a pre-cruise panic than anyone. I can't count the times that I have run to her for flow meters, or filters, or plankton preservation supplies. She is a tremendous person. Double her salary already! And double Linsey Sala's salary also! I cannot fathom her patience with flaky grad students who never log samples correctly, or forget to add formaldehyde, or burst in with last-minute requests. She is a true professional, who keeps our collections, and our lab, running smoothly. Linsey learned the job from Annie Townsend, now retired, who is yet another person who helped me tremendously. There are many other people who have provided help, just in

time, on numerous occasions. I would like to thank all of the CalCOFI and LTER staff, especially Jim Wilkinson, Dave Wolgast, Jennifer Wolgast-Rogers, Dave Faber, Amy Hays, Dimitry Abremenkoff, Sue Manion, and Megan Roadman. They are fantastic.

Next, I would like to thank my fellow grad students who have sailed on numerous cruises with me. At sea, no man is an island, unless he falls overboard. In no particular order, I thank Mike Stukel, Pete Davison, Darcy Taniguchi, Moira Decima, Christian Briseño, Miriam Goldstein, Noelle Bowlin, Jenni Brandon, Cat Nickels, Ryan Rykaczewski, Alison Cawood, Andrew Taylor, and Meg Rippy. I also thank Mindi Summers, Miriam Goldstein, and Mike Stukel for their leadership as Chief Scientists on UC Ship Funds-funded Student Cruises.

I also thank the Ohman Lab, which has at one time or another included fellow graduate students Alison Cawood, Miriam Goldstein, Celli Hull, Kate Hanson, Cat Nickels, Jenni Brandon, Christian Briseño, and Jeff Ellen. I would especially like to thank the numerous undergraduates who have helped me collect samples, calibrate instruments, and scan and classify zooplankton samples. These include Todd Langland, Timbo Stillinger, and Jesse Scott Gordon. Finally, Robin Westlake-Storey is tremendous as the behind-the-scenes wizard who keeps the business of lab business running smoothly by compiling proposals, coordinating LTER-CCE events, and keeping us all on deadline.

None of this dissertation would have been possible without funding from the National Science Foundation and the California Current Ecosystem Long Term Ecological Research program. Glider observations were supported by the NOAA Ocean Climate Observation Program through the Consortium on the Ocean's Role in Climate, and by the US Integrated Ocean Observation System through the Southern California Coastal Ocean Observing System (SCCOOSs). I thank UC Ship funds for funding three student cruises I participated in. I also am grateful for support I received from the Wyer Family First Year Fellowship.

Finally, I would like to thank my family. Lene, my younger sister, has always been wiser and more mature than I. Now, I have finally proven that I am smarter! My father and mother, James and Ann Powell, have always wished the best for me, and supported me without fail. I will always be grateful for the family trips to the American Natural History Museum to see the dinosaur bones, the planetarium shows, and (most impressive to a small lad) the enormous Blue Whale that hung suspended in the Hall of Ocean Life. Mom and Dad, you are wonderful parents. Thank you for setting me on this road.

Chapter 2, in full, is a reprint of previously published material in *Journal of Plankton Research*, 2012, Powell, J.R., and Ohman, M.D. Copyright, 2012, by Oxford University Press. The dissertation author was the primary investigator and author of this paper.

Chapter 3, in part, is currently submitted for publication in Deep Sea Research II, 2013, Powell, J.R., Elsevier Press, 2013. The dissertation author was the primary investigator and author of this paper.

Chapter 4, in part, is being prepared for submission to Limnology and Oceanography, 2013, Powell, J.R., and Ohman, M.D., Association for the Sciences of Limnology and Oceanography, Inc., 2013. The dissertation author was the primary investigator and author of this paper.

VITA

- 1992 Bachelor of Arts in French Literature, University of California,
San Diego
- 1994 Bachelor of Science in General Biology, University of California,
San Diego
- 2001 Master of Science in Molecular Biology, San Diego State
University
- 2013 Doctor of Philosophy in Oceanography, University of California,
San Diego

PUBLICATIONS

Ohman, M.D., **Powell, J.R.**, Picheral, M., Jensen, D.W. (2012).

Mesozooplankton and particulate matter responses to a deep-water frontal system in the southern California Current System. *Journal of Plankton Research* 34, 815-827.

Powell, J.R., Ohman, M.D. (2012). Use of glider-class acoustic Doppler profilers for estimating zooplankton biomass. *Journal of Plankton Research* 34, 563-568.

ABSTRACT OF THE DISSERTATION

Ocean fronts in the Southern California Current System and their role in structuring zooplankton distributions, diel vertical migration, and size composition

by

Jesse Russell Powell

Doctor of Philosophy in Oceanography

University of California, San Diego, 2013

Professor Mark D. Ohman, Chair

Ocean fronts are dynamic gradients that divide waters with differing hydrographic properties. Fronts also play important ecological roles in structuring plankton distributions, modulating primary and secondary production, and delineating predator foraging areas. Here, I utilize autonomous “*Spray*” ocean gliders to describe the spatial and seasonal

distribution of deep-water fronts and their impact on the plankton within the Southern California Current System (SCCS).

To test the suitability of the *Spray's* 750 kHz acoustic doppler profilers (ADP) for mapping zooplankton distributions, I first present results from a seatruthing study in which I mounted an ADP on a Mocness plankton net. I show that the relative mean volume backscatter (rMVBS) measured by the ADP is correlated with the summed zooplankton cross-sectional area (a proxy for biomass). I also find that the relationship between rMVBS and zooplankton biomass is strongest for zooplankters with an estimated spherical diameter greater than 1.6 mm. Observed rMVBS was best explained by euphausiid and copepod biomass.

From *Spray* cross-shore sections between October, 2006 and December, 2011, I identified 154 distinct surface layer density fronts. The strongest and most numerous fronts occurred in spring, and were located closer to the coast, whereas summer and fall fronts were found further offshore. Fronts were weakest and least numerous in winter. Across all seasons, fronts structured plankton distributions. Horizontal gradients in physical variables (e.g., surface density, temperature, and salinity) co-varied with horizontal gradients in MVBS and Chl-*a* fluorescence, and the magnitude of biological gradients was higher at frontal areas compared with non-frontal areas. Frontal areas were also clearly associated with elevated Chl-*a* and zooplankton acoustic backscatter.

Fronts divided distinct plankton habitats and associated assemblages. Chlorophyll-a fluorescence maxima and euphotic zones were deeper offshore of fronts. The amplitude of diel vertical migration by zooplankton also increased offshore, in association with increased optical transparency in the upper ocean. Additionally, ADP data indicate that zooplankton assemblages change across fronts. I employ an inverse acoustic model to estimate zooplankton size spectra, inferring that larger-bodied zooplankters contributed a greater proportion to overall biomass inshore of these fronts. Vertically-stratified zooplankton samples from both inshore and offshore regions corroborated the model results.

CHAPTER 1:

Introduction

The mesozooplankton (ranging in size from 0.2 mm to 2 cm, and hereafter simply called “zooplankton”) play an important role in the world ocean both biogeochemically, in terms of carbon cycling, and ecologically, in their role as grazers of primary productivity and as prey for higher trophic levels. Understanding the dynamics of zooplankton production and temporal and spatial variations in the distribution of zooplankton is a fundamental concern of Biological Oceanography.

At large scales (1000 km and above), the distribution of zooplankton biomass and production broadly matches that of primary production in the world ocean – higher in coastal zones and upwelling areas that provide nutrients for phytoplankton growth, lower offshore where nutrients are scarce. This observation has led to the hypothesis that zooplankton distributions are controlled by bottom-up processes where productivity is ultimately determined by ocean physics and resource availability (Stromberg et al., 2009). Other studies suggest that zooplankton production is not food-limited, and that ocean temperature ultimately determines zooplankton productivity and distribution patterns (Huntley and Lopez, 1992) and also that top-down processes of predation and mortality may shape distribution and productivity patterns (Huntley and Lopez, 1992; Ohman and Wood, 1995; Gasol et al., 1997).

At the mesoscale (100-1000 km), the submesoscale (1-100 km), and smaller, zooplankton distributions are highly variable in space and time. While a significant proportion of primary production at these scales is determined by nutrient availability linked to coastal upwelling, or to wind-driven curl upwelling further offshore or in equatorial regions, or to transient vertical mixing at evolving frontal structures, the mechanisms that shape zooplankton distributions and production at these scales are unclear. Studies that have the resolution and breadth of sampling needed to examine mechanisms are rare or non-existent. While seasonal or annual averages may accurately estimate primary and secondary production within a region, a true mechanistic understanding of how a mosaic of a shifting productivity seascape at the mesoscale and submesoscale alters phytoplankton and zooplankton population dynamics and biomass distributions is lacking. Until a fuller understanding is developed of the role that dynamic ocean structures such as fronts, jets, eddies and filaments play in plankton production, we will never be sure whether ecosystem models are useful for predicting future zooplankton productivity and distributions.

This dissertation seeks to examine the biological response of zooplankton within the southern sector of the California Current System (CCS) to ocean fronts, and the role that ocean fronts play in structuring zooplankton distributions and behaviors. This introductory chapter provides a background to the basic physical and biological oceanography of the California Current System, with an emphasis on the southern sector, before turning to a

description of ocean fronts, the process of frontogenesis, and a review of current knowledge of zooplankton ecology at fronts. I also provide a review of past interdisciplinary studies of fronts within the CCS. Finally, I outline the research that is presented in the subsequent chapters.

Physical Oceanography of the California Current System

Major features

The California Current System (CCS) is one of the four great Eastern Boundary Currents (EBC) of the world ocean (Wooster and Reid, 1963). Eastern Boundary Currents are the equatorward-flowing currents of wind-driven, anticyclonic subtropical gyres, and are characterized by cooler sea surface temperatures (SST) and increased coastal upwelling due to prevailing wind patterns along the coastal margins. The CCS forms the eastern limb of the North Pacific Gyre, and flows southward along the coast of North America from about 47° N latitude to Southern Baja California before turning westward. The width of the CCS is not clearly defined, but is generally held to extend about 1000km offshore from the coast where the western boundary of the CCS increasingly mixes with gyre –associated waters (Hickey, 1979; Lynn and Simpson, 1987). The southern CCS comprises three major named currents, and one unnamed persistent flow. The California Current (CC) is often characterized as a broad and diffuse, equatorward, surface flow (0-300m). The core of the CC is typically found 300-400km offshore. Though current velocities within the CC are generally slow (0.1 m s⁻¹) there are often higher

velocity jets ($>0.5 \text{ m s}^{-1}$) embedded within the main flow. The California Undercurrent (CU) is a subsurface, slow ($\sim 0.05 \text{ m s}^{-1}$) poleward flow found within the Southern California Bight (SCB) and along the central Californian coast. The CU can vary in position within the water column between 50 and 400m depth (Lynn and Simpson, 1990). The Inshore Countercurrent (IC), also known as the Davidson Current when it surfaces north of Point Conception, is a seasonally varying, poleward surface current generally found within 50 km of the coast (Hickey, 1979; Lynn and Simpson, 1987). An additional subsurface poleward flow has recently been detected using both ship and glider data (Davis et al., 2008; Gay and Chereskin, 2009; Todd et al., 2011).

The CCS can be divided into three major latitudinal sections: the northern CCS extends from Vancouver Island to Cape Mendocino; the Central CCS extends from Cape Mendocino to Point Conception; and, the southern CCS extends from Point Conception to southern Baja California. This dissertation is concerned primarily with the SCCS, though the results are certainly influenced by processes in the central CCS due to its mean equatorward advection.

Water masses

The southern sector of the CCS contains four distinct water masses with varying hydrographic properties (Table 1) which can be used to track water origins of the major currents (Simpson, 1984). The CC carries relatively cool and fresh waters, reflecting its subarctic origins, though the western edge

of the CC becomes increasingly warm and salty as it mixes with North Pacific Gyre waters (Reid et al., 1958). The warm, salty, high nutrient and low oxygen properties of the CUC indicate its origins in the Equatorial Pacific (Pickard, 1964). Finally, the IC is marked by its cold, salty, high nutrient and low oxygen waters derived from coastal upwelling (Sverdrup, 1938; Reid et al., 1958).

Recurrent structures in the SCCS

In addition to the major currents, there are two recurrent hydrographic features that influence the physical and biological oceanography of the SCCS. One major feature is the Southern California Eddy (SCE): a large, cyclonic eddy, which is most prominent in the late summer (Schwartzlose, 1963; Di Lorenzo, 2003). The SCE may play a significant role in retention of larval fishes (Taylor et al., 2004) and invertebrates within the SCB. Another recurrent feature is the Ensenada front which marks the boundary between subarctic waters of the CC and subtropical waters offshore of Baja California, Mexico (Haury et al., 1993; Chereskin and Niiler, 1994). Other fronts may be found in the same region (Landry, Ohman et al. 2012).

Interannual and interdecadal variability

The CCS is a locally wind-forced current system. However, the CCS can also be remotely forced by large-scale atmospheric and oceanic changes occurring elsewhere within the basin. The largest source of interannual variation within the CCS is El Niño Southern Oscillation (ENSO). During El

Nino, coastally trapped Kelvin waves propagate poleward, depressing pycnoclines and increasing stratification along the west coast (Chelton and Davis, 1982). El Nino is characterized by a deeper nitracline, leading to less efficient transport of nitrate to the surface. El Nino has also been tied to weakened and delayed upwelling in the central sector of the CCS (Bograd et al., 2009). Equatorward advection is also weaker in the central and southern sectors of the CCS during El Nino, and subtropical water masses are more prevalent in the southern CCS (Lynn et al., 1998).

Lower frequency (i.e., interdecadal) forcing in the CCS can be tied to other large scale oceanic changes. The Pacific Decadal Oscillation (PDO) is associated with changes in SST within the CCS and in the position of the Aleutian low pressure center (Mantua et al., 1997). During the warm (cool) phase of the PDO, the Aleutian Low is strengthened (weakened) leading to decreased (increased) upwelling favorable winds along the coast and therefore higher (lower) SSTs (Chhak and Di Lorenzo, 2007). During the PDO warm phase, the southward advection of the CC is also diminished, which affects zooplankton distributions (Di Lorenzo and Ohman, 2013). The other mode of low-frequency variation is the North Pacific Gyre Oscillation, or NPGO (Di Lorenzo et al., 2008). The positive (negative) phase of the NPGO is correlated with positive (negative) Sea Surface Salinity anomalies, early (late) onset of upwelling favorable winds, and increased (decreased) nutrient levels (Chenillat et al., 2012). The NPGO has been shown to better track fluctuations in chlorophyll levels within the CCS than the PDO (Di Lorenzo et al., 2008).

Winds

As an Eastern Boundary Current, the CCS is characterized by strong coastal upwelling through much of the year. South of Cape Mendocino, winds blow predominantly equatorward, almost year-round, with the strongest winds occurring in spring and summer, setting up strong, Ekman-driven upwelling along much of the coast. The seasonal onset of upwelling favorable winds, i.e., the “Spring Transition” (Lynn et al., 2003), triggers stronger tilting of isopycnals at the coast and consequently contributes to the development of a strong equatorward jet. The strongest upwelling occurs in the central CCS, where the winds blow parallel to the coast, and diminished or absent coastal upwelling occurs south of Point Conception where the coastline turns eastward to form the Southern California Bight (SCB). Prevailing winds in the northern CCS turn poleward intermittently during the fall and winter months causing relaxation of upwelling, or even periods of downwelling (Bakun et al., 1974). Throughout much of the central and SCCS, the prevailing equatorward winds intensify with distance offshore, leading to increased wind stress curl-driven upwelling (Bakun and Nelson, 1991). Both coastal upwelling and wind-stress curl-driven upwelling are intensified during positive phases of the NPGO, and during La Nina years (Chenillat et al., 2012).

Mesoscale structure

Seasonal variations in the prevailing winds lead to changes in all three currents in the SCCS. Intensification of upwelling-favorable winds during spring alters the observed patterns of sea surface dynamic height and alters geostrophic flow patterns. A study of long term seasonal means of dynamic height measured by the California Cooperative Oceanic Fisheries Investigations (CalCOFI) program (Lynn and Simpson, 1987) found the largest cross-shore range in SSH occurring in late spring and early summer, corresponding to an intensification of the California Current jet, especially at the latitude of Point Conception. Lynn and Simpson's analysis of seasonal variation in dynamic height defined three zones: an oceanic zone, forced by large-scale air-sea processes; a coastal zone, forced by seasonal winds and changes in the inshore surface and subsurface currents; and, a transition zone, whose higher variability in dynamic height indicated that mesoscale activity (e.g., eddies and filaments) forced much of the observed variation. Further studies using satellite altimetry (Strub and James, 2000) inferred that eddy kinetic energy (EKE) increased during spring near the coast, and the zone of highest EKE moved progressively offshore through the summer and fall. The highest EKE occurred with wavelengths of 300 km, which corresponded to the wavelength of meanders in the CC jet, as well as to the distance between large eddies.

Several studies have successfully modeled the seasonal patterns of SSH and EKE as seen in observational data (Di Lorenzo, 2003; Marchesiello

et al., 2003; Kurian et al., 2011). The models point to baroclinic instability in alongshore currents leading to the formation of eddies and mesoscale frontal features. Kurian et al. (2011) found that surface eddies formed by this mechanism were predominantly cyclonic (i.e., cold-core), were between 25-100 km in diameter, propagated westward and slightly north at about 2 km per day and typically lasted less than a season. Subsurface eddies generated by the California Undercurrent, in contrast, were predominantly anticyclonic and propagated westward and slightly south (Kurian et al., 2011).

Biological oceanography of the CCS

Eastern boundary upwelling ecosystems

The four largest Eastern Boundary Upwelling Ecosystems (EBUE) are amongst the most productive ecosystems in the world, accounting for about 11% of global new primary productivity while covering less than 1% of the world's oceans (Messie et al., 2009). The high productivity of EBUEs is function of prevailing equatorward winds, coastline topography and Ekman dynamics (Sverdrup, 1938). While the CCS is the least productive of the four EBUEs, satellite-determine primary production is still very high at $479 \text{ gC m}^{-2} \text{ yr}^{-1}$ (mean annual production between 34° and 44° north latitude out to 150 km offshore) (Messie et al., 2009). EBUEs are generally thought to be controlled by bottom-up processes (Chavez and Messie, 2009), particularly due to the injection of new nitrate into the surface waters due to coastal upwelling by

Ekman transport (Sverdrup, 1938) and offshore Ekman pumping due to wind stress curl (Bakun and Nelson, 1991; Rykaczewski and Checkley, 2008).

Floristic and faunal provinces

Large-scale cross-shore gradients in near-surface nutrients (e.g., nitrate, silicic acid, and iron) contribute to the spatial structure the phytoplankton community. Within the SCCS, Venrick (2002) defines two floristic assemblages based on phytoplankton community analysis of CalCOFI samples, (the “inshore” and “offshore” communities) that are often separated by the sharp front between the inshore boundary of the California Current. The inshore group is dominated by diatoms, whereas the offshore group is a more diverse group dominated by coccolithophores and dinoflagellates found broadly throughout the North Pacific. Spatial patterning seems to be related to the availability of nutrients instead of other hydrographic properties (Venrick, 2009).

Faunal patterns within the SCCS are less well defined. Point Conception is often considered to be a faunal break between northern subarctic zooplankton species and southern (more tropical) species, although the waters of the SCCS are often a transition zone between these two biomes (Colebrook, 1977; Brinton and Townsend, 2003; Lavaniegos and Ohman, 2007). Years characterized by a greater influx of sub-tropical waters into the SCCS (i.e., during El Nino) are often notable for the greater abundance of

southern taxa (Rebstock, 2002; Brinton and Townsend, 2003; Lavaniegos and Ohman, 2007).

Sources and sinks – the generation of pattern

One might assume that the distribution of zooplankton biomass would be tightly coupled to areas of high primary productivity (e.g., coastal upwelling zones). However, within the SCCS, interannual variations in zooplankton displacement volumes have been suggested to be best explained by alongshore advection (Chelton et al., 1982) rather than interannual variations in upwelling favorable winds. A study of mean advective transport budgets (Bograd et al., 2001) within the SCCS showed that there is a net importation of nutrients and chlorophyll into the SCCS from the central CCS, with the highest net transport occurring in spring. Geostrophic volume flow into the region from the north was roughly matched by Ekman transport out of the region, primarily to the west and south. The study further found a significant correlation between the magnitude of transport and interannual ENSO-like forcing, corroborating the findings of Chelton et al. (1982). Taken together, these results suggest that the SCCS cannot be considered in isolation. Patterns in plankton productivity and standing stocks are a combination of local and remote processes.

Spring transition

The spring transition is defined as the day of the year when the Cumulative Upwelling Index (CUI) turns positive for a given stretch of coast (Schwing et al., 2006; Bograd et al., 2009). A seasonal intensification of equatorward, alongshore winds in late March through early April forces increases in coastal upwelling of cold nutrient rich waters, and strengthens the coastal jet which is often associated with strong frontal features. Although the spring transition is primarily associated with the California coast north of Point Conception (due to coastline topography), the ecological effects of the spring transition are clearly visible in the SCCS and SCB due to advection, including elevated chlorophyll concentrations (Lynn et al., 2003), copepod biomass (Chelton, 1982), and copepod egg production (Mullin, 1991). The phenology of the spring transition is important, and changes in the timing of events like the spring transition can result in mismatched production cycles between predators and prey (Cushing, 1990), leading to greatly increased mortality in planktivorous predators (Schwing et al., 2006; Sydeman et al., 2006).

Patterns in the zooplankton

At the mesoscale, phytoplankton can be considered passive tracers of advective flows (Strub et al., 1990; Denman and Abbott, 1994; d'Ovidio et al., 2010). The striking correspondence of mesoscale structures visible in satellite images of SST and chlorophyll a (as inferred from ocean color) emphasizes the tight physical-biological coupling for phytoplankton. The spatial distribution

of zooplankton is less predictable, however. Several studies have found that zooplankton exhibit significantly higher variance at all spatial scales compared with phytoplankton (Mackas and Boyd, 1979; Star and Mullin, 1981). There are many mechanisms that can generate spatial patterns in zooplankton distributions in addition to the purely physical mechanisms of advection and diffusion. These mechanisms include: spatial variations in zooplankton growth and reproduction rates (Mullin, 1991; Irigoien et al., 2005), spatial heterogeneity in mortality (Ohman and Hsieh, 2008), and spatially heterogeneity in diel vertical migration behavior (DVM) (Hays et al., 2001; Irigoien et al., 2004).

Long-term trends

Satellite studies suggest there is a secular trend of increasing net primary productivity (NPP) and phytoplankton biomass, and in the seasonal maximums of NPP and biomass, within the SCCS (Kahru et al., 2009). The reason for this trend is unclear, however. Increased NPP could be a result of increased wind-induced upwelling associated with global climate change (Bakun, 1990; Garcia-Reyes and Largier, 2010), or with decadal-scale forcing (Di Lorenzo et al., 2008; Chenillat et al., 2012). Unfortunately, the time series of satellite measurements is still too short to distinguish between climate change and inter-decadal forcing. Predicting how zooplankton will respond to a future of increased NPP is difficult. The present trends in zooplankton biomass are unclear. Roemmich and McGowan (1995) found a long-term

decrease in zooplankton displacement volume over the course of the CalCOFI timeseries (Roemmich and McGowan, 1995a, b), but subsequent studies have found that this was not a decline in zooplankton carbon biomass, but, a shift in assemblage wherein high-volume, low-carbon gelatinous zooplankton (particularly salps) decreased through time but overall carbon biomass did not change (Lavaniegos and Ohman, 2007).

In addition to long-term changes in NPP, there appears to be an long-term increase in the prevalence of thermal and chlorophyll fronts within the SCCS (Kahru et al., 2012). While this trend is not significantly correlated with either the PDO or the NPGO, it is possible that the climate change-associated increase in upwelling is forcing increased mesoscale activity and thus increasing frontal frequency within the region (Marchesiello et al., 2003). These results suggest that the effects of zooplankton-front interactions, whatever they may be, might be amplified in the future.

Fronts in the CCS region

Ocean fronts delineate boundaries between different water masses or parcels, and consequently can exhibit strong horizontal gradients in hydrographic properties such as density, temperature, or salinity (Legeckis, 1978). Fronts occur at variety of length scales, with along-front distances ranging from tens to hundreds of kilometers in length, and cross-front distances ranging from tens of meters to tens of kilometers in width (Belkin et al., 2009). Over the CCS region, the spatial and seasonal patterns of

frontogenesis are similar to the patterns of EKE and SSH variance. As with the zone of highest variability in SSH, the zone of highest probability for thermal fronts detected by satellite north of Point Conception is near to shore in early spring, and migrates westward through spring and summer to extend nearly 300 km offshore by September before collapsing again during fall and winter (Castelao et al., 2006). This suggests that fronts and frontogenesis is intrinsically tied to the mesoscale processes in the CCS.

Geostrophy and mesoscale features

At mesoscales and larger, frontal features can be stabilized by geostrophy whereby the pressure gradient force which otherwise would force less dense water to flow over the more dense water is counterbalanced by the Coriolis force, thus maintaining the observed gradients in temperature, salinity and chlorophyll. Geostrophic fronts often exhibit strong, cross-frontal gradients in current velocities, leading to horizontal shear. Horizontal shear, in turn, can lead to frontal meanders. If the meanderings of a jet become sufficiently energetic, the main flow of the frontal jet can pinch off to generate mesoscale eddies (Bernstein et al., 1977), or lead to the formation of submesoscale fronts (Wang, 1993; Capet et al., 2008b).

Submesoscale frontogenesis

The high EKE and strong gradients in dynamic height within the CCS transition zone directly contribute to increased submesoscale frontogenesis.

Submesoscale frontogenesis can be thought of as mechanism of dissipating the potential energy stored in larger, mesoscale fronts (D'Asaro et al., 2011). Geostrophic instability in mesoscale features induced by down-front wind effects, or horizontal or vertical shear result in ageostrophic secondary circulation which acts to restratify the mesoscale front (Lapeyre et al., 2006; D'Asaro et al., 2011) and also to generate smaller, submesoscale fronts and eddies (Wang, 1993; Capet et al., 2008b). Both mesoscale and submesoscale fronts can exhibit significant localized vertical water motions on the order of tens of meters per day (Pallas-Sanz et al., 2010; Johnston et al., 2011). The SCCS transition region (between nearshore coastal waters and the offshore subtropical waters) is notable for its mix of mesoscale and submesoscale frontal features which exhibit a range of vertical velocities. As the dynamic height gradients and EKE increases seasonally, the complexity of structure of the flow field increases as well.

Stirring and filament formation

At mesoscales and larger, mixing processes in the surface ocean can be considered to be two-dimensional. Higher eddy kinetic energy (EKE) leads to increased stirring and the creation of complex and filamentous patterns. Interactions between eddies, especially at eddy dipoles, aid in the formation of filaments. Filaments can increase the mixing rate of water properties (e.g., heat, salt) since filaments are long and thin and have inherently high surface area to volume ratios. Furthermore, cold (warm) filaments generated in the

stirring process can be associated with localized upwelling (downwelling) with vertical velocities approaching 20 m per day (Legal et al., 2007).

Barrier or blender? Cross-front exchange

An active area of research is whether fronts act primarily as effective barriers preventing exchange of material and properties across the front, or whether cross-frontal exchange processes facilitate the mixing of material and properties. Surface drifter studies, in the Gulf Stream, revealed that cross-frontal exchange does indeed occur (Shaw and Rossby, 1984; Bower and Rossby, 1989; McGrath et al., 2010) and suggested that cross-frontal exchange was related to meanders in the main jet (Bower, 1991). Model results reported by Bower (1991) implied that while most (90%) of the surface flow of a jet was retained in the jet, a significant portion (10%) was recirculated to waters flanking the jet. Cross-frontal exchange increased with depth, especially when along-jet velocities were lower. Cross-frontal exchange can also be initiated by baroclinic instability leading to ageostrophic flows and subduction (Spall, 1995).

Modeling

At the mesoscale, moderately high-resolution (<3.5 km) ROMS studies of the CCS region have confirmed that strong fronts are associated with mesoscale eddies generated by baroclinic instabilities in upwelling-forced, alongshore currents. Interactions between near-shore currents and orographic

features (e.g., capes and promontories) also create a variety of frontal structures (Marchesiello et al., 2003).

Submesoscale processes, on the other hand, only become clear when model resolutions are improved to 1 km (Capet et al., 2008a; Capet et al., 2008b, c). Model results show that local wind stress can destroy the geostrophic balance of a front within submesoscale subsections, leading to ageostrophic secondary circulation (ASC) and frontogenesis. Large vertical motions (10-20m per day) are often associated with ASC and frontogenesis

Fronts and zooplankton ecology

Fronts have long been considered to be locations of special ecological significance (Lefevre, 1986). Several studies have shown increased phytoplankton and zooplankton abundances at fronts of all kinds around the world. Given the localized upwelling that occurs at some fronts (discussed above) it may be plausible that fronts would be hotspots for both primary and secondary production, if growth rates permit plankton accumulation faster than advection removes the plankton (Kierstead and Slobodkin, 1953). However, fronts often have lifespans (days to weeks) that are shorter than zooplankton (weeks to months), so in some cases there must be additional mechanisms which contribute to the high zooplankton biomass gradients observed at fronts. One mechanism is the simple increase in apparent concentration due to convergent flows at a front (Franks, 1992). Another mechanism is simply the advection of a high zooplankton abundance water parcel along a frontal jet,

adjacent to a low zooplankton abundance water parcel. Finally, zooplankton swimming behavior can combine with frontal convergent or divergent flows to alternatively aggregate or disperse plankton (Franks, 1992). Thus, one can expect that there will be a variety of zooplankton-front interactions contributing to observed patterns of zooplankton at fronts in the CCS.

Distributions and assemblages across fronts

Zooplankton abundances or biomass concentrations often change across fronts (Boucher, 1984; Sournia, 1994; Thibault et al., 1994; Youssara and Gaudy, 2001; Riandey et al., 2005). In all these cases, biomass cases are higher on the colder, denser sides of fronts.

Several studies have also shown cross-frontal changes in zooplankton assemblages at a variety of front types: across coastal filaments (Mackas et al., 1991); buoyancy plume fronts in the Aegean (Zervoudaki et al., 2006); the seasonal Ligurian front in the western Mediterranean (Boucher, 1984); a front associated with the recurrent Southern California Eddy (Haury, 1984); shelf-break fronts in West Greenland (Munk et al., 2003); and a deep-water front in the SCCS (Ohman et al., 2012). It is clear that fronts in these cases are acting as barriers to zooplankton transport, despite established mechanisms for cross-frontal exchange. Furthermore, the barrier nature of fronts can also enhance larval retention and settlement success rates. In the central CCS nearshore region, the number of upwelling fronts was positively correlated with barnacle and mussel recruitment, and also with rockfish recruitment (Woodson

et al., 2012). Zooplankton abundances or biomass concentrations often change across fronts (Boucher, 1984; Sournia, 1994; Thibault et al., 1994; Youssara and Gaudy, 2001; Riandey et al., 2005). In all these cases, biomass cases are higher on the colder, denser sides of fronts.

Fronts and Diel Vertical Migration

Because fronts can separate waters with greatly different environmental characteristics (e.g., light, temperature, salinity, food availability, predators, etc.), mesozooplankton on either side of a front may display different behaviors even if the assemblage does not change across the front. Diel Vertical Migration (DVM) by zooplankton may be cued differentially across fronts. Several studies have shown zooplankton can exhibit altered DVM behavior in response to changing conditions such as light levels at depth (Backus et al., 1965; De Robertis et al., 2000), predator density (Ohman et al., 1983) and food availability. Few studies, however, have directly examined cross-frontal changes in DVM behavior since sampling requires specialized plankton nets capable of discretely sampling target depth strata. A study in the Almeria-Oran frontal zone in the Mediterranean showed clear changes in DVM behavior across the front for some zooplankton taxa, but not for others (Andersen et al., 2004). For taxa that changed their DVM behavior, there was a clear correlation between daytime mean depths and the depth of enhanced chlorophyll. The amplitude of migration was lowest in chlorophyll-rich waters and highest in the chlorophyll-poor waters.

Predator-prey interactions

Abundances of highly mobile predators like large fish (Fiedler and Bernard, 1987; Podesta et al., 1993), marine mammals (Bost et al., 2009; Tynan et al., 2005) and seabirds (Ainley et al., 2009) can be elevated at fronts. There is some indication that mobile predators target submesoscale features that have high prey density. The formation of filaments at eddy-eddy interfaces creates long convergent flow filaments along which a predator can travel. Great-frigate birds, for example, have been shown to target these submesoscale structures in the Mozambique Channel (Kai et al., 2009).

Depth-targeting planktonic predators can also be found in increased abundances at fronts due to convergent flows. A recent study of a thermal front in the SCCS revealed elevated abundances of narcomedusae (McClatchie et al., 2012).

The effect of fronts on the population dynamics of prey species is complex and unknown. Simple conceptual models (Bakun, 2006), however, tell us that predation will be minimized at stable convergent features when either prey abundance is too low to sustain predator foraging, or if the prey production rate within the feature (due to convergent flow, population growth within the feature, or a combination of flow and growth) is greater than the predation rate. Between these two scenarios lies the “Predation Pit” in which prey abundance decreases dramatically.

Example Fronts in the CCS

Coastal Transition Zone (CTZ) Program

The CTZ program in the mid to late 1980s intensively sampled a semi-permanent coastal cold water filament that separated from Point Arena in central California (Brink and Cowles, 1991). For the CTZ program, the filament divided the offshore waters (i.e., warmer and fresher) north and west of the frontal jet from the inshore waters (colder and saltier) located to the east and south. Coastal filaments are relatively long-lived structures that occur in coastal upwelling regions, particularly at prominent capes and headlands, and can extend offshore for several hundred kilometers as narrow (<100 km) features. Filaments can facilitate cross-shore exchange of nutrients and biomass into more oligotrophic waters offshore. Maximum velocities in the jet ($\sim 0.6 \text{ m s}^{-1}$) occurred during summer in response to upwelling favorable winds (Brink and Cowles, 1991).

Biological responses to this front were varied. Zooplankton assemblages clearly changed across the front (Mackas et al., 1991). On the offshore, less dense side of the front the assemblage was characterized by doliolids, chaetognaths, and small copepods. Abundances of the copepod *Eucalanus californicus* were elevated within the jet. On the inshore, more dense side of the front, abundances of the euphausiid *Euphausia pacifica* were highest. Egg production by *Eucalanus californicus* was highest in the jet ($>100 \text{ eggs female}^{-1} \text{ d}^{-1}$), whereas egg production directly adjacent to the jet was minimal or non-existent (Smith and Lane, 1991). Egg production rates

were positively correlated with lipid sac size, implying that the females were not using stored reserves for egg production, but relied on food available within the jet.

The Ensenada Front

The Ensenada front is a persistent feature in the SCCS formed where the cooler and fresher surface flows from the CC meet warm and salty subtropical waters from the south (Haury et al., 1993). The southward flowing CC turns onshore around 32° N latitude to flow eastward for approximately 200 km before bifurcating into a poleward component, which becomes entrained in the Southern California Eddy, and equatorward component that continues southward along the coast of Baja California, Mexico (Chereskin and Niiler, 1994). Zooplankton biomass, as inferred from zooplankton displacement volume, increased across the front towards the north. Zooplankton displacement volumes north of the front were 3-4 fold higher compared with those south of the front (Haury et al., 1993). The front also delineated a transition from northern subarctic/transitional associated fish larvae to larvae associated with the Eastern Tropical Pacific (Moser and Smith, 1993). In cases where the same species of fish larvae were present on both sides of the front, Moser noted distinctly deeper daytime depths of migrating fish indicating increased DVM amplitude. Previous studies have shown that the area around the Ensenada Front is a transitional region between southern, Eastern Tropical Pacific-associated zooplankton taxa and

northern-associated taxa (Brinton, 1976). While integrated chlorophyll-a (0-250 m) did not change significantly across the front (Haury et al., 1993), the vertical distribution of chlorophyll-a did change from a deep chlorophyll maximum layer south of the front to surface layer north of the front. Interestingly, the frontal zone was associated with change in southern to northern-associated phytoplankton groups. Instead, Central Pacific-associated flora dominated both sides of the front (Venrick, 2000).

The A-Front

The A-front study was the result of a brief, intensive and multi-disciplinary sampling effort across a sharp east-west running front 330 km due west of San Diego California (Landry, Ohman, et al. 2012). While located in the same general area as the Ensenada Front, the A-front appeared to be a separate, distinct front that exhibited much stronger cross-front gradients in temperature, salinity and chlorophyll, and separated previously upwelled coastal water from mixed CC and subtropical waters. The study found strong cross-frontal variations in phytoplankton community with surface expressions of chlorophyll 3-4 fold higher north of the front compared to south, and a shift from *Prochlorococcus* and blue-water associated *Synechococcus* to a mix of blue and green-water associated *Synechococcus* (Chekalyuk et al., 2012; Taylor et al., 2012). Fauna south of the front were dominated by poecilostomatoid copepods, ostracods, chaetognaths and radiolaria, whereas calanoid copepods, Oithona-like copepods, and euphausiids were elevated at

and north of the front compared to the south (Ohman et al., 2012). The front itself was associated with increased nitrate supply (Li et al., 2012) and increased autotrophic biomass, dominated by chain-forming diatoms (Taylor et al., 2012). The center of the front was also associated with maximal total zooplankton levels (and maximal levels of all enumerated mesozooplankton taxa except ostracods and radiolarian), and elevated copepod nauplii (Ohman et al., 2012). Taken together, these results indicate that increased abundances and production rates at the front could be triggered by a combination of frontal convergence and/or localized nitrate injection into the surface waters, though the complete 3-D picture of the frontal system is not yet sufficient to identify the mechanism definitively (Landry, Ohman, et al., 2012).

Research questions

My research is motivated primarily by a broader desire to understand the ecological significance of dynamic, evolving frontal structures within the CCS. How much of a role do fronts play in shaping zooplankton distributions? Are fronts generally sites of biomass accumulation that can be targeted by foraging mobile predators? For the zooplankton, what is the balance of reproduction, growth and mortality rates? Do fronts increase or decrease overall secondary production with the CCS? Do most fronts act as boundaries separating zooplankton assemblages, or if not, does the same assemblage behave differently when exposed to different environments present on either side of a front?

These motivating questions are too broad for the scope of a single dissertation and would require enormous resources to study given the spatial and temporal variability of the CCS. However, I will focus on a subset of them, including how fronts shape zooplankton biomass distributions in the SCCS, under what conditions fronts are zones of zooplankton biomass accumulation, and how fronts modulate zooplankton vertical migration behavior and may act to structure zooplankton assemblages.

Research approach

To date, almost all studies examining the physical-biological interactions and ecology at fronts have involved limited duration ship-based sampling efforts. These studies are useful in the breadth and depth of measurements and sampling that can be performed during the course of a study. Ship-based studies can provide a detailed look at the physical dynamics and biological processes occurring during a small window in time.

However, an important characteristic of fronts is their inherent variability. The physical and biological character of fronts varies greatly within the CCS across space and time. Furthermore, along the length of a single front, one can find upwelling zones, downwelling zones, convergent or divergent surface flows, complex outcroppings due to ageostrophic secondary circulation, all embedded within regions with varying plankton assemblages.

Thus, in order to understand the ecological significance of fronts, it is necessary to observe a large number of fronts across a wide geographic area

over timescales sufficient to capture frontal variability. This is an impossible task using ship-based methods alone, due to the expense and the labor involved. Satellites are very useful for observing fronts over space and time, but they are also of limited use in the study of subsurface hydrography and plankton distributions. Unfortunately, there is no zooplankton-sensing satellite.

Consequently, to address my specific research questions, I have relied on data acquired by *Spray* autonomous ocean gliders. *Spray* gliders are a class of Autonomous Underwater Vehicles (AUV) that combine buoyancy control, a controllable center of gravity, and lift generating surfaces to translate gravitational potential into steerable, forward motion (Sherman et al., 2001). Since they do not require active propulsion, gliders use very little energy to conduct profiles of the water column. With regard to the *Spray* gliders used in this dissertation, each glider carried a pumped Seabird CTD and chlorophyll a fluorometer to profile water column properties, as well as a compact 750kHz Acoustic Doppler Profiler (ADP) to measure current velocities and acoustic backscatter (ABS). The ABS measured by *Spray* is proportional to zooplankton biomass (Powell and Ohman, 2012). Preliminary results from a few glider missions showed strong covariability of density fronts with elevated horizontal gradients in fluorescence and ABS (Davis et al., 2008). However, the Davis study did not examine the strength and variability of the relationship between physical fronts and biological structure as visible in the glider data in a statistical manner. This dissertation examines a longer time series of glider data from 2006 through 2011 to examine the physical-biological coupling of

fronts, the seasonality and spatial distribution of fronts along CalCOFI lines 80 and 90 over this time period, and the biological responses to fronts as visible in the glider data.

Description of chapters

First, in chapter 2, I examine the applicability of the *Spray* glider-based ADP to measure biomass. This methods-focused chapter presents an analysis of data and samples collected in October 2010 in the Santa Barbara Basin using an ADP mounted on a Mocness (Wiebe et al., 1985). This co-location of instruments permitted me to collect acoustic data and plankton samples simultaneously within discrete depth strata. My analysis of these data and samples shows that ABS is significantly correlated with bulk zooplankton biomass, though there are wide confidence intervals on any individual biomass estimate. I also determined that ABS is most strongly correlated with zooplankters with an Equivalent Circular Diameter (ECD) greater than 1.6 mm and that the presence of rare, but strongly scattering taxa such pteropods and siphonophores (Stanton et al., 1994), did not alter the observed relationship between observed ABS and total net-collected biomass. These results were published (Powell and Ohman, 2012) and the manuscript is presented here.

In chapter 3, I examine the relationship between physical and biological fronts through the comparison of horizontal gradients of physical properties (e.g., density gradient) with horizontal gradients in ABS and chlorophyll a fluorescence. Specifically, I test the hypotheses that fronts exhibit a non-

random spatial and seasonal distribution in the SCCS, that biotic gradients in acoustic backscatter and Chl-a fluorescence co-vary with physical gradients, and that fronts are zones of plankton accumulation. I define criteria for a physical front and then examine which of these fronts are associated with elevated ABS and fluorescence. Using this approach, I find not only that fronts are significantly associated with stronger horizontal gradients of ABS and fluorescence, but also that there is evidence supporting the hypothesis of zooplankton and phytoplankton accumulation at fronts. I also examine the spatial and seasonal distribution of fronts over the five-year time series, relating the observed distribution patterns to the physical circulation of the SCCS (including seasonal and interannual variation within the CCS) as well as to reported frontal distributions determined from satellite-based studies (Castelao et al., 2006).

In chapter 4, I examine some biological responses to physical fronts as seen in the glider data. First, I test the hypothesis that the depth of the chlorophyll maximum and euphotic zone increases across fronts. Next, I examine changes in zooplankton DVM behavior across fronts by tracking daytime versus nighttime vertical distributions of ABS across fronts and relate these changes in DVM amplitude to modeled light penetration depths, and find that DVM amplitude is increased offshore of fronts. Finally, I present data supporting cross-frontal changes in the size-structure of the zooplankton assemblage based upon interbeam differences in ABS measured by the ADP.

These acoustically-based results were corroborated by vertically-stratified Moccness sampling and subsequent ZooScan digital analysis.

I finish in chapter 5 with a summary of results and a discussion of the broader implications of this dissertation. I also recommend some next steps necessary to advance research in frontal ecology. Finally, I present a call to arms to ocean scientists to better utilize the new tools of autonomous vehicles and high-resolution ocean modeling. A bright future lays ahead for ocean research, if we choose to grasp it.

References

- Ainley, D. G., K. D. Dugger, R. G. Ford, S. D. Pierce, D. C. Reese, R. D. Brodeur, C. T. Tynan, and J. A. Barth. 2009. Association of predators and prey at frontal features in the California Current: competition, facilitation, and co-occurrence. *Marine Ecology Progress Series* **389**:271-294.
- Andersen, V., C. Devey, A. Gubanova, M. Picheral, V. Melnikov, S. Tsarin, and L. Prieur. 2004. Vertical distributions of zooplankton across the Almeria-Oran frontal zone (Mediterranean Sea). *Journal of Plankton Research* **26**:275-293.
- Backus, R. H., R. C. Clark, and A. S. Wing. 1965. Behaviour of certain marine organisms during solar eclipse of July 20, 1963. *Nature* **205**:989-991.
- Bakun, A. 1990. Global climate change and intensification of coastal ocean upwelling. *Science* **247**:198-201.
- Bakun, A. 2006. Fronts and eddies as key structures in the habitat of marine fish larvae: opportunity, adaptive response and competitive advantage. *Scientia Marina* **70**:105-122.

- Bakun, A., D. R. McLain, and F. V. Mayo. 1974. Mean annual cycle of coastal upwelling off western North-America as observed from surface measurements. *Fishery Bulletin* **72**:843-844.
- Bakun, A. and C. S. Nelson. 1991. The seasonal cycle of wind-stress curl in subtropical eastern boundary current regions.. *Journal of Physical Oceanography* **21**:1815-1834.
- Belkin, I. M., P. C. Cornillon, and K. Sherman. 2009. Fronts in large marine ecosystems. *Progress in Oceanography* **81**:223-236.
- Bernstein, R. L., L. Breaker, and R. Whritner. 1977. California Current eddy formation - ship, air, and satellite results. *Science* **195**:353-359.
- Bograd, S. J., T. K. Chereskin, and D. Roemmich. 2001. Transport of mass, heat, salt, and nutrients in the southern California Current System: annual cycle and interannual variability. *Journal of Geophysical Research-Oceans* **106**:9255-9275.
- Bograd, S. J., I. Schroeder, N. Sarkar, X. Qiu, W. J. Sydeman, and F. B. Schwing (2009), Phenology of coastal upwelling in the California Current, *Geophysical Research Letters* **36**: L01602, doi:10.1029/2008GL035933..
- Bost, C. A., C. Cotte, F. Bailleul, Y. Cherel, J. B. Charrassin, C. Guinet, D. G. Ainley, and H. Weimerskirch. 2009. The importance of oceanographic fronts to marine birds and mammals of the southern oceans. *Journal of Marine Systems* **78**:363-376.
- Boucher, J. 1984. Localization of Zooplankton Populations in the Ligurian Marine Front - Role of Ontogenic Migration. *Deep-Sea Research Part a-Oceanographic Research Papers* **31**:469-484.
- Bower, A. S. 1991. A simple kinematic mechanism for mixing fluid parcels across a meandering jet. *Journal of Physical Oceanography* **21**:173-180.

- Bower, A. S. and T. Rossby. 1989. Evidence of cross-frontal exchange processes in the gulf-stream based on isopycnal RAFOS float data. *Journal of Physical Oceanography* **19**:1177-1190.
- Brink, K. H. and T. J. Cowles. 1991. The Coastal Transition Zone Program. *Journal of Geophysical Research-Oceans* **96**:14637-14647.
- Brinton, E. 1976. Population biology of *Euphausia pacifica* off Southern California. *Fishery Bulletin* **74**:733-762.
- Brinton, E. and A. Townsend. 2003. Decadal variability in abundances of the dominant euphausiid species in southern sectors of the California Current. *Deep-Sea Research Part II-Topical Studies in Oceanography* **50**:2449-2472.
- Capet, X., J. C. McWilliams, M. J. Molemaker, and A. F. Shchepetkin. 2008a. Mesoscale to submesoscale transition in the California current system. Part I: Flow structure, eddy flux, and observational tests. *Journal of Physical Oceanography* **38**:29-43.
- Capet, X., J. C. McWilliams, M. J. Molemaker, and A. F. Shchepetkin. 2008b. Mesoscale to submesoscale transition in the California current system. Part II: Frontal processes. *Journal of Physical Oceanography* **38**:44-64.
- Capet, X., J. C. McWilliams, M. J. Molemaker, and A. F. Shchepetkin. 2008c. Mesoscale to submesoscale transition in the California current system. Part III: Energy balance and flux. *Journal of Physical Oceanography* **38**:2256-2269.
- Castelao, R. M., T. P. Mavor, J. A. Barth, and L. C. Breker (2006), Sea surface temperature fronts in the California Current System from geostationary satellite observations, *Journal of Geophysical Research*, 111: C09026, doi:10.1029/2006JC003541.
- Chavez, F. P. and M. Messie. 2009. A comparison of Eastern Boundary Upwelling Ecosystems. *Progress in Oceanography* **83**:80-96.

- Chekalyuk, A. M., M. R. Landry, R. Goericke, A. G. Taylor, and M. A. Hafez. 2012. Laser fluorescence analysis of phytoplankton across a frontal zone in the California Current ecosystem. *Journal of Plankton Research* **34**: 761-777
- Chelton, D. B. 1982. Large-scale response of the California Current to forcing by the wind stress curl. *Calif. Coop. Oceanic Fish. Invest. Rep* **23**:130-148.
- Chelton, D. B., P. A. Bernal, and J. A. McGowan. 1982. Large-Scale Interannual Physical and Biological Interaction in the California Current. *Journal of Marine Research* **40**:1095-1125.
- Chelton, D. B. and R. E. Davis. 1982. Monthly Mean Sea-Level Variability Along the West-Coast of North-America. *Journal of Physical Oceanography* **12**:757-784.
- Chenillat, F., P. Rivière, X. Capet, E. Di Lorenzo, and B. Blanke. 2012. North Pacific Gyre Oscillation modulates seasonal timing and ecosystem functioning in the California Current upwelling system. *Geophysical Research Letters* **39**: L01606, doi:10.1029/2011GL049966.
- Chereskin, T. K. and P. P. Niiler. 1994. Circulation in the Ensenada Front - September 1988. *Deep-Sea Research Part I-Oceanographic Research Papers* **41**:1251-1287.
- Chhak, K. and E. Di Lorenzo. 2007. Decadal variations in the California Current upwelling cells. *Geophysical Research Letters* **34**: L14604, doi:10.1029/2007GL030203.
- Colebrook, J. M. 1977. Annual Fluctuations in Biomass of Taxonomic Groups of Zooplankton in California Current, 1955-1959. *Fishery Bulletin* **75**:357-368.
- Cushing, D. H. 1990. Plankton production and year-class strength in fish populations: an update of the match/mismatch hypothesis. *Advances in Marine Biology* **26**:249-293.

- d'Ovidio, F., S. De Monte, S. Alvain, Y. Dandonneau, and M. Lévy. 2010. Fluid dynamical niches of phytoplankton types. *Proceedings of the National Academy of Sciences* **107**:18366-18370.
- Davis, R. E., M. D. Ohman, D. L. Rudnick, J. T. Sherman, and B. Hodges. 2008. Glider surveillance of physics and biology in the southern California Current System. *Limnology and Oceanography* **53**:2151-2168.
- De Robertis, A., J. S. Jaffe, and M. D. Ohman. 2000. Size-dependent visual predation risk and the timing of vertical migration in zooplankton. *Limnology and Oceanography* **45**:1838-1844.
- Denman, K. L. and M. R. Abbott. 1994. Time Scales of Pattern Evolution from Cross-Spectrum Analysis of Advanced Very High-Resolution Radiometer and Coastal Zone Color Scanner Imagery. *Journal of Geophysical Research-Oceans* **99**:7433-7442.
- Di Lorenzo, E. 2003. Seasonal dynamics of the surface circulation in the Southern California Current System. *Deep-Sea Research Part II-Topical Studies in Oceanography* **50**:2371-2388.
- Di Lorenzo, E. and M. D. Ohman. 2013. A double-integration hypothesis to explain ocean ecosystem response to climate forcing. *Proceedings of the National Academy of Sciences of the United States of America* **110**:2496-2499.
- Di Lorenzo, E., N. Schneider, K. M. Cobb, P. J. S. Franks, K. Chhak, A. J. Miller, J. C. McWilliams, S. J. Bograd, H. Arango, E. Curchitser, T. M. Powell, and P. Riviere. 2008. North Pacific Gyre Oscillation links ocean climate and ecosystem change. *Geophysical Research Letters* **35**.
- Fiedler, P. C. and H. J. Bernard. 1987. Tuna aggregation and feeding near fronts observed in satellite imagery. *Continental Shelf Research* **7**:871-881.
- Franks, P. J. S. 1992. Sink or Swim - Accumulation of Biomass at Fronts. *Marine Ecology Progress Series* **82**:1-12.

- Garcia-Reyes, M. and J. Largier. 2010. Observations of increased wind-driven coastal upwelling off central California. *Journal of Geophysical Research: Oceans* **115**.
- Gasol, J. M., P. A. del Giorgio, and C. M. Duarte. 1997. Biomass distribution in marine planktonic communities. *Limnology and Oceanography* **42**:1353-1363.
- Gay, P. S. and T. K. Chereskin. 2009. Mean structure and seasonal variability of the poleward undercurrent off southern California. *Journal of Geophysical Research-Oceans* **114**: C02007, doi:10.1029/2008JC004886.
- Haury, L. R., E. L. Venrick, C. L. Fey, J. A. McGowan, and P. P. Niiler. 1993. The Ensenada Front: July 1995. *California Cooperative Oceanic Fisheries Investigations Reports* **34**:69-88.
- Hays, G. C., H. Kennedy, and B. W. Frost. 2001. Individual variability in diel vertical migration of a marine copepod: Why some individuals remain at depth when others migrate. *Limnology and Oceanography* **46**:2050-2054.
- Hickey, B. M. 1979. The California current system—hypotheses and facts. *Progress in Oceanography* **8**:191-279.
- Huntley, M. E. and M. D. G. Lopez. 1992. Temperature-Dependent Production of Marine Copepods: A Global Synthesis. *The American Naturalist* **140**:201-242.
- Irigoiien, X., D. V. P. Conway, and R. P. Harris. 2004. Flexible diel vertical migration behaviour of zooplankton in the Irish Sea. *Marine Ecology-Progress Series* **267**:85-97.
- Irigoiien, X., H. M. Verheye, R. P. Harris, and D. Harbour. 2005. Effect of food composition on egg production and hatching success rate of two copepod species (*Calanoides carinatus* and *Rhincalanus nasutus*) in the Benguela upwelling system. *Journal of Plankton Research* **27**:735-742.

- Kahru, M., E. Di Lorenzo, M. Manzano-Sarabia, and B. G. Mitchell. 2012. Spatial and temporal statistics of sea surface temperature and chlorophyll fronts in the California Current. *Journal of Plankton Research* **34**:749-760.
- Kahru, M., R. Kudela, M. Manzano-Sarabia, and B. G. Mitchell. 2009. Trends in primary production in the California Current detected with satellite data. *Journal of Geophysical Research-Oceans* **114**: C02004, doi:10.1029/2008JC004979.
- Kai, E. T., V. Rossi, J. Sudre, H. Weimerskirch, C. Lopez, E. Hernandez-Garcia, F. Marsac, and V. Garcon. 2009. Top marine predators track Lagrangian coherent structures. *Proceedings of the National Academy of Sciences of the United States of America* **106**:8245-8250.
- Kierstead, H. and L. B. Slobodkin. 1953. The Size of Water Masses Containing Plankton Blooms. *Journal of Marine Research* **12**:141-147.
- Kurian, J., F. Colas, X. Capet, J. C. McWilliams, and D. B. Chelton. 2011. Eddy properties in the California Current System. *Journal of Geophysical Research-Oceans* **116**: C08027, doi:10.1029/2010JC006895.
- Landry, M. R., M. D. Ohman, R. Goericke, M. R. Stukel, K. A. Barbeau, R. Bundy, and M. Kahru. 2012. Pelagic community responses to a deep-water front in the California Current Ecosystem: overview of the A-Front Study. *Journal of Plankton Research* **34**:739-748.
- Lavaniegos, B. E. and M. D. Ohman. 2007. Coherence of long-term variations of zooplankton in two sectors of the California Current System. *Progress in Oceanography* **75**:42-69.
- Lefevre, J. 1986. Aspects of the Biology of Frontal Systems. *Advances in Marine Biology* **23**:163-299.
- Legeckis, R. 1978. Survey of worldwide sea-surface temperature fronts detected by environmental satellites. *Journal of Geophysical Research-Oceans and Atmospheres* **83**:4501-4522.

- Li, Q. P., P. J. S. Franks, M. D. Ohman, and M. R. Landry. 2012. Enhanced nitrate fluxes and biological processes at a frontal zone in the southern California current system. *Journal of Plankton Research* **34**:790-801.
- Lynn, R. J., T. Baumgartner, J. Garcia, C. A. Collins, T. L. Hayward, K. D. Hyrenbach, A. W. Mantyla, T. Murphree, A. Shankle, F. B. Schwing, K. M. Sakuma, and M. J. Tegner. 1998. The state of the California current, 1997-1998: Transition to El Nino conditions. *California Cooperative Oceanic Fisheries Investigations Reports* **39**:25-49.
- Lynn, R. J., S. J. Bograd, T. K. Chereskin, and A. Huyer. 2003. Seasonal renewal of the California Current: the spring transition off California. *Journal of Geophysical Research* **108**: 3279, doi:10.1029/2003JC001787, C8.
- Lynn, R. J. and J. J. Simpson. 1987. The California Current System - the Seasonal Variability of Its Physical Characteristics. *Journal of Geophysical Research: Oceans* **92**:12947-12966.
- Lynn, R. J. and J. J. Simpson. 1990. The Flow of the Undercurrent over the Continental Borderland Off Southern California. *Journal of Geophysical Research-Oceans* **95**:12995-13008.
- Mackas, D. L. and C. M. Boyd. 1979. Spectral Analysis of Zooplankton Spatial Heterogeneity. *Science* **204**:62-64.
- Mackas, D. L., L. Washburn, and S. L. Smith. 1991. Zooplankton Community Pattern Associated with a California Current Cold Filament. *Journal of Geophysical Research-Oceans* **96**:14781-14797.
- Mantua, N. J., S. R. Hare, Y. Zhang, J. M. Wallace, and R. C. Francis. 1997. A Pacific interdecadal climate oscillation with impacts on salmon production. *Bulletin of the American Meteorological Society* **78**:1069-1079.
- Marchesiello, P., J. C. McWilliams, and A. Shchepetkin. 2003. Equilibrium structure and dynamics of the California Current System. *Journal of Physical Oceanography* **33**:753-783.

- McClatchie, S., R. Cowen, K. Nieto, A. Greer, J. Y. Luo, C. Guigand, D. Demer, D. Griffith, and D. Rudnick. 2012. Resolution of fine biological structure including small narcomedusae across a front in the Southern California Bight. *Journal of Geophysical Research-Oceans* **117**: C04020, doi:10.1029/2011JC007565.
- McGrath, G. G., T. Rossby, and J. T. Merrill. 2010. Drifters in the Gulf Stream. *Journal of Marine Research* **68**:699-721.
- Messie, M., J. Ledesma, D. D. Kolber, R. P. Michisaki, D. G. Foley, and F. P. Chavez. 2009. Potential new production estimates in four eastern boundary upwelling ecosystems. *Progress in Oceanography* **83**:151-158.
- Moser, H. G. and P. E. Smith. 1993. Larval fish assemblages of the California Current region and their horizontal and vertical distributions across a front. *Bulletin of Marine Science* **53**:645-691.
- Mullin, M. M. 1991. Production of eggs by the copepod *Calanus pacificus* in the Southern California sector of the California Current System. *California Cooperative Oceanic Fisheries Investigations Reports* **32**:65-90.
- Ohman, M. D., B. W. Frost, and E. B. Cohen. 1983. Reverse Diel Vertical Migration - an Escape from Invertebrate Predators. *Science* **220**:1404-1407.
- Ohman, M. D. and C. H. Hsieh. 2008. Spatial differences in mortality of *Calanus pacificus* within the California Current System. *Journal of Plankton Research* **30**:359-366.
- Ohman, M. D., J. R. Powell, M. Picheral, and D. W. Jensen. 2012. Mesozooplankton and particulate matter responses to a deep-water frontal system in the southern California Current System. *Journal of Plankton Research* **34**:815-827.
- Ohman, M. D. and S. N. Wood. 1995. The inevitability of mortality. *ICES Journal of Marine Science: Journal du Conseil* **52**:517-522.

- Pickard, G. L. 1964. Descriptive physical oceanography, an introduction. Pergamon Press; [distributed in the Western Hemisphere by Macmillan, New York], Oxford, New York.
- Podesta, G. P., J. A. Browder, and J. J. Hoey. 1993. exploring the association between swordfish catch rates and thermal fronts on United States longline grounds in the western North Atlantic. *Continental Shelf Research* **13**:253-277.
- Powell, J. R. and M. D. Ohman. 2012. Use of glider-class acoustic Doppler profilers for estimating zooplankton biomass. *Journal of Plankton Research* **34**:563-568.
- Rebstock, G. A. 2002. Climatic regime shifts and decadal-scale variability in calanoid copepod populations off southern California. *Global Change Biology* **8**:71-89.
- Reid, J. L., Jr., G. I. Roden, and J. G. Wyllie. 1958. Studies of the California Current System. California Cooperative Oceanic Fisheries Investigations, La Jolla.
- Riandey, V., G. Champalbert, F. Carlotti, I. Taupier-Letage, and D. Thibault-Botha. 2005. Zooplankton distribution related to the hydrodynamic features in the Algerian Basin (western Mediterranean Sea) in summer 1997. *Deep-Sea Research Part I-Oceanographic Research Papers* **52**:2029-2048.
- Roemmich, D. and J. McGowan. 1995a. Climatic Warming and the Decline of Zooplankton in the California Current. *Science* **267**:1324-1326.
- Roemmich, D. and J. McGowan. 1995b. Climatic warming and the decline of zooplankton in the California Current (vol 267, pg 1324, 1995). *Science* **268**:352-353.
- Rykaczewski, R. R. and D. M. Checkley. 2008. Influence of ocean winds on the pelagic ecosystem in upwelling regions. *Proceedings of the National Academy of Sciences of the United States of America* **105**:1965-1970.

- Schwartzlose, R. A. 1963. Nearshore currents of the western United States and Baja California as measured by drift bottles. Calif Coop Oceanic Fish Invest Rept **9**:15-22.
- Schwing, F. B., N. A. Bond, S. J. Bograd, T. Mitchell, M. A. Alexander, and N. Mantua. 2006. Delayed coastal upwelling along the U.S. West Coast in 2005: a historical perspective. Geophysical Research Letters **33**.
- Shaw, P. T. and H. T. Rossby. 1984. Towards a Lagrangian description of the Gulf Stream. Journal of Physical Oceanography **14**:528-540.
- Sherman, J., R. E. Davis, W. B. Owens, and J. Valdes. 2001. The autonomous underwater glider "spray". IEEE Journal of Oceanic Engineering **26**:437-446.
- Simpson, J. J. 1984. El Nino-induced onshore transport in the California Current during 1982-3. Geophysical Research Letters **11**:233-236.
- Smith, S. L. and P. V. Z. Lane. 1991. The jet off Point Arena, California: its role in aspects of secondary production in the copepod *Eucalanus californicus johnson*. Journal of Geophysical Research: Oceans **96**:14849-14858.
- Sournia, A. 1994. Pelagic Biogeography and Fronts. Progress in Oceanography **34**:109-120.
- Spall, M. A. 1995. Frontogenesis, Subduction, and Cross-Front Exchange at Upper Ocean Fronts. Journal of Geophysical Research-Oceans **100**:2543-2557.
- Stanton, T. K., P. H. Wiebe, D. Z. Chu, M. C. Benfield, L. Scanlon, L. Martin, and R. L. Eastwood. 1994. On Acoustic Estimates of Zooplankton Biomass. Ices Journal of Marine Science **51**:505-512.
- Star, J. L. and M. M. Mullin. 1981. Zooplanktonic Assemblages in 3 Areas of the North Pacific as Revealed by Continuous Horizontal Transects. Deep-Sea Research Part a-Oceanographic Research Papers **28**:1303-1322.

- Stromberg, K. H. P., T. J. Smyth, J. I. Allen, S. Pitois, and T. D. O'Brien. 2009. Estimation of global zooplankton biomass from satellite ocean colour. *Journal of Marine Systems* **78**:18-27.
- Strub, P. T. and C. James. 2000. Altimeter-derived variability of surface velocities in the California Current System: 2. Seasonal circulation and eddy statistics. *Deep-Sea Research II* **47**:831-870.
- Strub, P. T., C. James, A. C. Thomas, and M. R. Abbott. 1990. Seasonal and nonseasonal variability of satellite-derived surface pigment concentration in the California Current. *Journal of Geophysical Research-Oceans* **95**:11501-11530.
- Sverdrup, H. U. 1938. On the process of upwelling. *Journal of Marine Research* **1**:155-164.
- Sydeman, W. J., R. W. Bradley, P. Warzybok, C. L. Abraham, J. Jahncke, K. D. Hyrenbach, V. Kousky, J. M. Hipfner, and M. D. Ohman. 2006. Planktivorous auklet *Ptychoramphus aleuticus* responses to ocean climate, 2005: Unusual atmospheric blocking? *Geophysical Research Letters* **33**: L22S09, doi:10.1029/2006GL026736.
- Taylor, A. G., R. Goericke, M. R. Landry, K. E. Selph, D. A. Wick, and M. J. Roadman. 2012. Sharp gradients in phytoplankton community structure across a frontal zone in the California Current Ecosystem. *Journal of Plankton Research* **34**:778-789.
- Taylor, C. A., W. Watson, T. Chereskin, J. Hyde, and R. Vetter. 2004. Retention of larval rockfishes, *Sebastes*, near natal habitat in the Southern California Bight, as indicated by molecular identification methods. *California Cooperative Oceanic Fisheries Investigations Reports* **45**:152-166.
- Thibault, D., R. Gaudy, and J. Lefevre. 1994. Zooplankton biomass, feeding and metabolism in a geostrophic frontal area (Almeria-Oran Front, western Mediterranean). Significance to pelagic food webs. *Journal of Marine Systems* **5**:297-311.

- Todd, R. E., D. L. Rudnick, M. R. Mazloff, R. E. Davis, and B. D. Cornuelle. 2011. Poleward flows in the southern California Current System: Glider observations and numerical simulation. *Journal of Geophysical Research-Oceans* **116**: C02026, doi:10.1029/2010JC006536.
- Tynan, C. T., D. G. Ainley, J. A. Barth, T. J. Cowles, S. D. Pierce, and L. B. Spear. 2005. Cetacean distributions relative to ocean processes in the northern California Current System. *Deep-Sea Research Part II* **52**:145-167.
- Venrick, E. L. 2000. Summer in the Ensenada Front: The distribution of phytoplankton species, July 1985 and September 1988. *Journal of Plankton Research* **22**:813-841.
- Venrick, E. L. 2002. Floral patterns in the California current system off southern California: 1990-1996. *Journal of Marine Research* **60**:171-189.
- Venrick, E. L. 2009. Floral patterns in the California Current: The coastal-offshore boundary zone. *Journal of Marine Research* **67**:89-111.
- Wang, D. P. 1993. Model of Frontogenesis - Subduction and Upwelling. *Journal of Marine Research* **51**:497-513.
- Wiebe, P. H., A. W. Morton, A. M. Bradley, R. H. Backus, J. E. Craddock, V. Barber, T. J. Cowles, and G. R. Flierl. 1985. New Developments in the MOCNESS, an Apparatus for Sampling Zooplankton and Micronekton. *Marine Biology* **87**:313-323.
- Wooster, W. S. and J. L. Reid, Jr. 1963. Eastern boundary currents. *in* M. N. Hill, editor. *The composition of sea-water: comparative and descriptive oceanography*. Interscience.
- Youssara, F. and R. Gaudy. 2001. Variations of zooplankton in the frontal area of the Alboran sea (Mediterranean sea) in winter 1997. *Oceanologica Acta* **24**:361-376.

Table 1.1: Water masses of the California Current System (L= Low; H = High). After Simpson, 1984

| | T | S | O ₂ | Nutrients |
|--|---|---|----------------|-----------|
| Surface Water Masses (0-200m) | | | | |
| Pacific Subarctic | L | L | H | H |
| N. Pacific Central | H | H | L | L |
| Coastal Upwelled | L | H | L | H |
| Surface Water Masses (200-500m) | | | | |
| Equatorial Pacific | H | H | L | H |

Chapter 2:

JOURNAL OF PLANKTON RESEARCH | VOLUME 34 | NUMBER 6 | PAGES 563–568 | 2012

SHORT COMMUNICATION

Use of glider-class acoustic Doppler profilers for estimating zooplankton biomass

JESSE R. POWELL* AND MARK D. OHMAN

CALIFORNIA CURRENT ECOSYSTEM LTER SITE, SCRIPPS INSTITUTION OF OCEANOGRAPHY, UNIVERSITY OF CALIFORNIA, SAN DIEGO, LA JOLLA, CA 92093-0218, USA

*CORRESPONDING AUTHOR: jrpowell@ucsd.edu

Received August 30, 2011; accepted in principle March 5, 2012; accepted for publication March 8, 2012

Corresponding editor: Roger Harris

We evaluate the feasibility of estimating zooplankton biomass using acoustic Doppler profilers (ADP) as deployed on autonomous ocean gliders. A Sontek *Spray* ADP mounted on a Moccness net was used for simultaneous collection of zooplankton and measurement of acoustic backscatter (ABS). Zooplankton biomass was estimated from optically scanned plankton samples. We found a direct proportionality between ABS and the summed cross-sectional area of the zooplankton as well as with the estimated zooplankton carbon biomass. ABS at 750 kHz was most closely related to the summed cross-sectional area of zooplankton and micronekton greater than 1.6 mm equivalent circular diameter.

KEYWORDS: bioacoustics; zooplankton; acoustic Doppler profiler; Zooscan

Acoustic backscatter (ABS) from acoustic Doppler profilers (ADPs) or acoustic Doppler current profilers (ADCPs) has been used to estimate zooplankton biomass (e.g. Flagg and Smith, 1989). Ship-mounted (Lynn, 2003), mooring-mounted (Batchelder *et al.*, 1995) and lowered platform-mounted (Postel *et al.*, 2007) ADCPs have also been employed for biomass estimation. Scientific echosounders have been used on larger autonomous underwater vehicles such as the Autosub (Brierley *et al.*, 2002). Scientific echosounders are generally preferable for estimating biomass for many reasons, including the use of multiple frequencies, ease of calibration and better defined instrument parameters. However, studies have shown that simultaneously collected ADCP and

scientific echosounder backscatter data are well correlated (Griffiths and Diaz, 1996). The advent of long-duration autonomous gliders (Sherman *et al.*, 2001; Rudnick *et al.*, 2004) provides a new opportunity for sustained measurement of acoustically determined zooplankton biomass distributions concurrently with environmental variables (Davis *et al.*, 2008). Gliders can be deployed for months and observe thousands of kilometers of trackline at high spatial resolution, but require physically smaller sensors that are power efficient. As some ocean gliders now include small ADPs in their instrument payload (e.g. Davis *et al.*, 2008), examining the applicability of glider-class ADPs to estimating zooplankton biomass is important to future research efforts.

doi:10.1093/plankt/fbs023, available online at www.plankt.oxfordjournals.org. Advance Access publication April 6, 2012

© The Author 2012. Published by Oxford University Press. All rights reserved. For permissions, please email: journals.permissions@oup.com

To date, there have been no published reports verifying a relationship between zooplankton biomass and ABS from small glider-class ADPs. The *Spray* glider (Sherman *et al.*, 2001; Davis *et al.*, 2008) uses a compact, low-power, narrow-band 3-beam Sontek ADP with a center frequency of 750 kHz. Here, we report a comparison of ABS with zooplankton biomass using a stand-alone *Spray* ADP mounted to a 1-m² Mocness net system (Wiebe *et al.*, 1985), allowing the simultaneous collection of zooplankton and ADP data from specific depth ranges. These data were obtained from the Santa Barbara Basin (34°18'N, 120°01'W) aboard the R/V *Melville* in October 2010. A total of 5 Mocness tows comprising 43 individual net samples are analyzed here. All tows were conducted within 5 km of each other. A primary advantage of this sampling strategy is that zooplankton and ABS were obtained from a range of strata varying from a deep (>500 m), low biomass, anoxic zone to the zooplankton-rich surface layer.

For each of its three beams, the *Spray* ADP measures current velocities and ABS within five sequential 5 m range cells from 2 to 26 m. The *Spray* ADP uses a log amplifier that is log-linear in its response across 90 dB of received acoustic energy. The average ABS during each 10 s integration period was recorded for each cell of all three beams, although due to the geometry of the ADP transducers, only data from the two beams that were horizontally aligned to ensnify the depth strata simultaneously sampled by the Mocness are used in this analysis (Supplementary data, Fig. S1). For each beam, data from the first and last range cells were discarded due to unacceptable noise levels. For each minute of sampling, 36 individual measurements of ABS were recorded from waters close to the Mocness net mouth. The recorded raw ABS, or echo level (EL), for each cell was first converted into decibels by multiplication by a constant as per instrument specifications (Sontek-YSI, Inc., 1997). EL was then converted into relative volume backscatter using a rearrangement of the sonar equation (equation (1)) (Deines, 1999; Sontek-YSI, Inc., 1997)

$$S_v = EL - NL - SL - RS - 10 \log_{10}(PL) - 2TL \quad (1)$$

where S_v is volume backscattering strength (dB), NL the noise level (dB) recorded by the instrument, SL the source level of the instrument, RS the receiver sensitivity, PL the acoustic pulse length (1 m) and TL equals the one-way transmission loss, which is equal to $10 \log_{10} R + \alpha R$ [where R is range in meters to the cell midpoint and α is the frequency-specific absorption coefficient in seawater (0.22 dB/m at 750 kHz)]. Since SL and RS could not be accurately measured during sampling, they were set to zero and thus S_v here actually represents

relative volume backscatter. All estimates of S_v recorded by beams 1 and 3 while a Mocness net was open were then converted to linear values, averaged and then converted back to log values to generate the relative mean volume backscatter (RMVBS), to compare with net-collected zooplankton.

Zooplankton were sampled with a 1 m², 202 μ m mesh Mocness and preserved in 1.8% buffered formaldehyde. Ashore, each net sample was analyzed using Zooscan (Gorsky *et al.*, 2010), a specialized flatbed scanner and image analysis system. Briefly, the preserved sample was passed through a series of three increasingly fine meshes (5 mm, 1 mm, 0.2 mm). Plankton retained on each mesh were then resuspended in a fixed volume of seawater, and a number of aliquots from each of these subsamples scanned by the Zooscan system. Typically, 1/100th of the small size fraction, 1/20th of the medium size fraction and often all of the large size fraction were scanned. This fractionation approach ensured that large zooplankters which can often contribute greatly to the measured ABS were not undersampled in the scanning process due to their relative scarcity. After scanning, each of the individual plankters was measured by the Zooscan software that has been validated independently (Gorsky *et al.*, 2010). Relevant measurements used in this analysis include cross-sectional area of the plankter and equivalent circular diameter (ECD) (i.e. the diameter of the circle which would result if all the image pixels composing an organism's area were formed into a circle). The linear resolution of the scanned images is 10.6 μ m per pixel. Finally, each segmented plankter image was classified into 1 of the 23 taxonomic categories (Supplementary data, Table S1). The results of machine classification were visually checked, and, if needed, corrected manually.

This study uses the cross-sectional area of scanned plankton (in mm²) adjusted for the aliquot scanned and the volume filtered (m³) by the net as a proxy for biomass concentration. This quantity is termed the summed area concentration (SAC, mm² m⁻³). Previous studies have shown that it is possible to estimate biomass concentrations with length-carbon relationships (Lavaniegos and Ohman, 2007), or with biovolume estimated by image analysis (Alcaraz *et al.*, 2003). However, we found that RMVBS measured by the ADP showed stronger correlation with \log_{10} SAC ($r^2 = 0.55$, Fig. 1) than with \log_{10} C biomass ($r^2 = 0.47$, Supplementary data, Fig. S3). Thus, the cross-sectional area measurement SAC used in Figs 1–3 is a somewhat more robust measurement with which to evaluate the performance of the ADP. Further discussion of the relationship between RMVBS and carbon biomass can be found in the Online Supplement. Observed

zooplankton assemblages varied with depth, ranging from mostly amphipods in the anoxic zone, to layers of increased abundance of calanoid copepods found just above the anoxic layer typical of the Santa Barbara Basin (Johnson and Checkley, 2004), to mid-profile abundance of chaetognaths, to a night time surface layer composed of many taxa but dominated by copepods and euphausiids.

Comparison of RMVBS measured by the ADP with \log_{10} SAC of zooplankton shows the two can be described by a linear relationship (Fig. 1, $P < 0.001$,

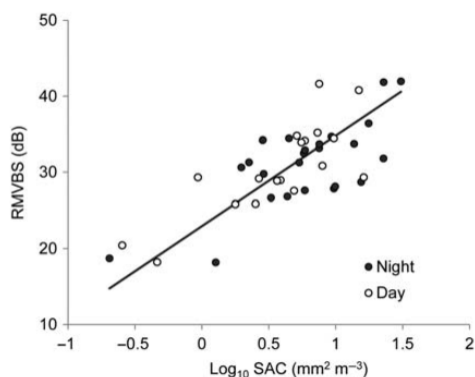


Fig. 1. RMVBS measured by the ADP versus \log_{10} SAC ($\text{mm}^2 \text{m}^{-3}$). The line depicts a Model II regression ($y = 11.87x + 22.93$, $r^2 = 0.55$) fitted using a reduced major axis algorithm.

$r^2 = 0.55$). Although the sample size is modest ($n = 43$), the samples themselves cover the wide range of biomass concentrations typically found in the study area and include a depth-varying assemblage of zooplankters that are representative of organisms found in much of the southern California Current system (Lavaniegos and Ohman, 2007). While strongly scattering taxa such as physonect siphonophores (Stanton *et al.*, 1998; Lavery *et al.*, 2007) were present in low abundance in most of the samples, their presence did not alter the underlying empirical relationship between RMVBS and \log_{10} SAC. There was no significant correlation ($P = 0.25$, $r^2 = 0.04$, $n = 37$) between residuals of the RMVBS- \log_{10} SAC regression and the proportion of SAC comprised by the pneumatophores of physonect siphonophores. Thecosome pteropods were quite rare in the samples.

The enumeration, classification and detailed measurements of zooplankton made possible by Zooscan analysis permit a closer examination of which components of the plankton field likely contributed most to the observed RMVBS. For each net sample, a sliding size window consisting of an upper and lower ECD limit was used to select a subset of the plankton sample. The \log_{10} SAC of the subset was then recalculated for each net sample and correlated with the observed RMVBS, and the resulting r^2 and P -values were then analyzed to determine which size fraction of the plankton field contributed most to RMVBS. A dramatic improvement in correlation is observed when a lower limit ECD

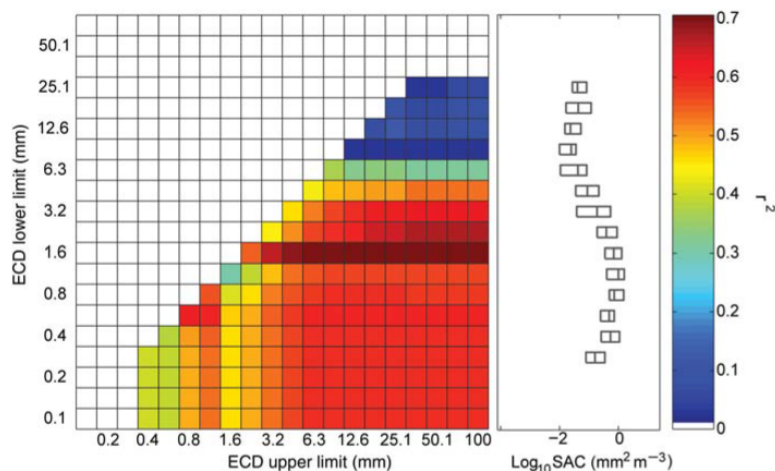


Fig. 2. (Left) Coefficient of determination, r^2 , for correlation of RMVBS with \log_{10} SAC of zooplankton of different size classes. The ordinate of the heatmap depicts the lower size limit of ECD and the abscissa the ECD upper size limit of zooplankton included in each correlation of \log_{10} SAC with RMVBS. White space indicates no data. (Right) Boxplots show the \log_{10} SAC of zooplankton in the size bins shown along the diagonal edge of the heatmap. Boxplot boundaries illustrate the 25th and 75th percentile range of measured \log_{10} SAC and the vertical line within each box depicts the median value.

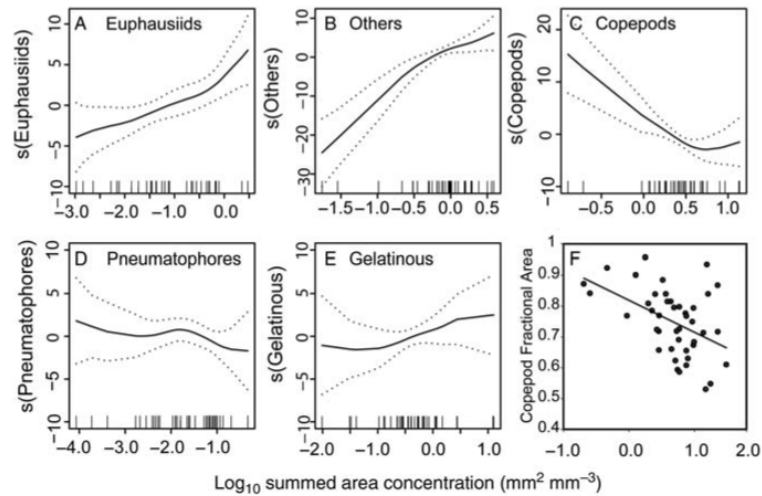


Fig. 3. (A–E) Partial response functions for \log_{10} SAC for each of the five explanatory variables used by the GAM. In each panel, the relative weighting of the smoothing function (ordinate) is plotted against \log_{10} SAC ($\text{mm}^2 \text{m}^{-3}$; abscissa). Vertical ticks along the abscissa indicate measured \log_{10} SAC values of the explanatory variable. (F) Fractional area of copepods (\log_{10} SAC of copepods divided by the sum of \log_{10} SAC of copepods, euphausiids and “others”) plotted against the \log_{10} SAC of total zooplankton.

threshold of 1.6 mm is crossed (Fig. 2). Interestingly, an equivalent volume plankter with a 3-to-1 aspect ratio would have a cross-sectional radius of ~ 0.5 mm, which approaches the size threshold below which Rayleigh scattering processes begin to dominate backscatter at 750 kHz ($ka = 1$ at 0.3 mm, where k is the wavenumber and a is the cross-sectional radius), and consequently echo amplitudes and r^2 values decrease markedly. Conversely, as the lower limit of the size window rises past 4.5 mm, r^2 values decrease markedly because the number of particles within the size window decreases exponentially and stochastic effects dominate the regression. It is clear that the size threshold for increased r^2 values is not caused merely by increased biomass within that particular size bin since biomass concentrations are actually higher in the smaller size bins (Fig. 2).

Similar correlation analyses were performed with individual taxa to explore whether any particular taxon and size window combination yielded better predictive power than the combination of all taxa, although none did. The effect of specific taxonomic groups within the plankton assemblage upon the observed RMVBS was further explored using generalized additive models (GAMs) (Hastie and Tibshirani, 1987). GAMs can be useful for generating predictive models of a response variable (e.g. RMVBS), and are also useful for exploring the relative importance of explanatory variables and uncovering non-linearity in the relationship between explanatory and response variables. Plankters were grouped into one of the five categories: euphausiids,

copepods, pneumatophores, gelatinous (including salps, doliolids, ctenophores and eggs), and “others” (including amphipods, appendicularians, chaetognaths, ostracods, polychaetes, among others). These five categories were used in the GAM as explanatory variables instead of a total possible 23 categories because the GAM procedure discards samples in which any of the variables contain no data. Using all 23 categories would have reduced unacceptably the number of samples available for the analysis. The \log_{10} SAC for each of these five groups were then entered as explanatory variables into a GAM. The resulting GAM (Gaussian identity link function, dispersion = 7.75, null deviance = 1122.64 on 35 df, residual deviance = 116.1947 on 15 df, AIC = 188.3, number of scoring iterations = 9) had a pseudo- r^2 of 0.90. Trends in the partial response functions for each explanatory variable (Fig. 3A–E) show that higher values of RMVBS are associated with high values of \log_{10} SAC for euphausiid and “other” organisms. In contrast, copepod \log_{10} SAC exhibits a negative relationship with RMVBS. The pneumatophore and gelatinous variables did not offer much explanatory power since the relative weighting of their respective partial response functions was close to zero throughout the range of observed biomasses. A multiple linear regression of logged SAC with RMVBS of the same categories yielded complimentary results: the coefficients for the partial regressions of Euphausiids, Others, Copepods, Pneumatophores and Gelatinous variables were 2.17, 4.96, -2.79 , -0.36 and 2.69, respectively.

However, only the Euphausiid partial regression was significant at $P < 0.05$. The adjusted r^2 for the multiple regression of 0.60 was only marginally better than the simple linear regression of \log_{10} SAC on RMVBS.

The apparent negative relationship between copepod biomass and RMVBS (Fig. 3C) does not imply that increased numbers of copepods lead to less acoustic energy being reflected. Rather, as total biomass increases in the sample volume, the relative contribution of copepods compared with other strong scatterers becomes less and less important (Fig. 3F and Supplementary data, Fig. S2). It is important to recall that observed RMVBS is not only a function of acoustic reflectivity of the animals in each category, but also a function of numerical density of the animals. At low densities, even strongly scattering individual plankters (such as euphausiids and pneumatophores) are unlikely to contribute much to RMVBS not only because they are few in number, but also because it is more likely that rare plankters, in general, will be located in the periphery of the ADP beam where observed ABS is greatly diminished. Thus, at low densities, euphausiids and pneumatophores are likely to contribute only a fraction of their potential backscatter to the overall RMVBS. Similarly, at the lowest observed RMVBS values, it is likely that only copepods are present in densities high enough to contribute much to the scattering signal (Supplementary data, Fig. S2).

Previous studies have demonstrated that observed ABS often does not correlate well with predicted ABS based on forward acoustic models of the sampled zooplankton (Greene *et al.*, 1998; Fielding *et al.*, 2004), and concluded that single frequency, narrowband acoustic systems can only poorly estimate biomass in mixed zooplankton populations. Analytical work and numerical simulations, however, have shown that incorporating beam pattern effects can significantly reduce the contribution of strong, but rare, scatterers to the observed ABS (Chu and Stanton, 2010). The empirical results presented here support this conclusion and suggest that the high variance seen in the RMVBS-biomass relationship represents a stochasticity inherent to the narrow beam, narrow band nature of the instrument, rather than solely the composition of the plankton field. Further studies, including numerical simulations, specific to a particular ADP's physical parameters (e.g. frequency, beam-width, dynamic range, etc.) could lead to better statistical models of zooplankton biomass in the future.

SUPPLEMENTARY DATA

Supplementary data can be found online at <http://plankt.oxfordjournals.org>

ACKNOWLEDGEMENTS

We thank R. E. Davis for creating the opportunity for collaborative work with *Spray* gliders, C. Briseno for assistance with image classification and the anonymous reviewers for their constructive comments.

FUNDING

This work was supported by the Gordon and Betty Moore Foundation, the U.S. National Science Foundation via the California Current Ecosystem Long Term Ecological Research site, and by UC Ship Funds.

REFERENCES

- Alcaraz, M., Saiz, E., Calbet, A. *et al.* (2003) Estimating zooplankton biomass through image analysis. *Mar. Biol.*, **143**, 307–315.
- Batchelder, H. P., Vankeuren, J. R., Vaillancourt, R. *et al.* (1995) Spatial and temporal distributions of acoustically estimated zooplankton biomass near the marine light-mixed layers station (59° 30' N, 21° 00' W) in the North Atlantic in May 1991. *J. Geophys. Res. Oceans*, **100**, 6549–6563.
- Brierley, A. S., Fernandes, P. G., Brandon, M. A. *et al.* (2002) Antarctic krill under sea ice: elevated abundance in a narrow band just south of ice edge. *Science*, **295**, 1890–1892.
- Chu, D. Z. and Stanton, T. K. (2010) Statistics of echoes from a directional sonar beam insonifying finite numbers of single scatterers and patches of scatterers. *IEEE J. Ocean Eng.*, **35**, 267–277.
- Davis, R. E., Ohman, M. D., Rudnick, D. L. *et al.* (2008) Glider surveillance of physics and biology in the southern California Current System. *Limnol. Oceanogr.*, **53**, 2151–2168.
- Deines, K. L. (1999) Backscatter estimation using broadband acoustic doppler current profilers. In Anderson, S. P., Terray, E. A., Rizoli White, J. A. and Williams, A. J. (eds), *Proceedings of the IEEE Sixth Working Conference on Current Measurement*. IEEE, pp. 249–253.
- Fielding, S., Griffiths, G. and Roc, H. S. J. (2004) The biological validation of ADCP acoustic backscatter through direct comparison with net samples and model predictions based on acoustic-scattering models. *ICES J. Mar. Sci.*, **61**, 184–200.
- Flagg, C. N. and Smith, S. L. (1989) On the use of the acoustic doppler current profiler to measure zooplankton abundance. *Deep-Sea Res.*, **36**, 455–474.
- Gorsky, G., Ohman, M. D., Picheral, M. *et al.* (2010) Digital zooplankton image analysis using the ZooScan integrated system. *J. Plankton Res.*, **32**, 285–303.
- Greene, C. H., Weibe, P. H., Pershing, A. J. *et al.* (1998) Assessing the distribution and abundance of zooplankton: a comparison of acoustic and net-sampling methods with D-BAD MOCNESS. *Deep-Sea Res. II*, **45**, 1219–1237.
- Griffiths, G. and Diaz, J. I. (1996) Comparison of acoustic backscatter measurements from a ship-mounted Acoustic Doppler Current Profiler and an EK500 scientific echo-sounder. *ICES J. Mar. Sci.*, **53**, 487–491.

- Hastie, T. and Tibshirani, R. (1987) Generalized additive models – some applications. *J. Am. Stat. Assoc.*, **82**, 371–386.
- Johnson, C. L. and Checkley, D. M. (2004) Vertical distribution of diapausing *Calanus pacificus* (Copepoda) and implications for transport in the California undercurrent. *Prog. Oceanogr.*, **62**, 1–13.
- Lavaniegos, B. E. and Ohman, M. D. (2007) Coherence of long-term variations of zooplankton in two sectors of the California Current System. *Prog. Oceanogr.*, **75**, 42–69.
- Lavery, A. C., Wiebe, P. H., Stanton, T. K. *et al.* (2007) Determining dominant scatterers of sound in mixed zooplankton populations. *J. Acoustic Soc. Am.*, **122**, 3304–3326.
- Lynn, R. J. (2003) Variability in spawning habitat of Pacific sardine (*Sardinops sagax*) off southern and central California. *Fish. Oceanogr.*, **12**, 541–553.
- Postel, L., da Silva, A. J., Mohrholz, V. *et al.* (2007) Zooplankton biomass variability off Angola and Namibia investigated by a lowered ADCP and net sampling. *J. Mar. Syst.*, **68**, 143–166.
- Rudnick, D. L., Davis, R. E., Ericksen, C. C. *et al.* (2004) Underwater gliders for ocean research. *Mar. Technol. Soc. J.*, **38**, 73–84.
- Sherman, J., Davis, R. E., Owens, W. B. *et al.* (2001) The autonomous underwater glider “Spray”. *IEEE J. Oceanic Eng.*, **26**, 437–446.
- Sontek-YSI, Inc. (1997) SonTek doppler current meters-using signal strength data to monitor suspended sediment concentration. *Application Note*, **7**.
- Stanton, T. K., Chu, D. Z. and Wiebe, P. H. (1998) Sound scattering by several zooplankton groups. II. Scattering Models. *J. Acoust. Soc. Am.*, **103**, 236–253.
- Wiebe, P. H., Morton, A. W., Bradley, A. M. *et al.* (1985) New developments in the MOCNESS, an apparatus for sampling zooplankton and micronekton. *Mar. Biol.*, **87**, 313–323.

Acknowledgements

Chapter 2, in full, is a reprint of previously published material in Journal of Plankton Research, 2012, Powell, J.R., and Ohman, M.D. Copyright, 2012, by Oxford University Press. The dissertation author was the primary investigator and author of this paper.

Chapter 3:

Co-variability of zooplankton gradients with glider-detected density fronts in the Southern California Current System

Abstract

Fronts represent sharp boundaries in ocean conditions. However, seasonal and interannual variation in their occurrence and effects on the distributions of pelagic organisms are poorly understood. Here I report the results from six years of ocean front observations (2006 to 2011) along two transects across the Southern California Current System (SCCS) using autonomous *Spray* ocean gliders. I identified 154 near-surface density fronts along 124 transects consisting of 22,942 vertical profiles. The incidence of surface density fronts showed distinct seasonality, with fewer fronts occurring during winter months and more numerous and stronger fronts in the nearshore during spring. Summer and fall fronts were also more numerous than winter fronts, and located farther offshore than spring fronts. Horizontal density gradients in the surface layer (0-50 m) were significantly correlated with horizontal gradients in surface layer chlorophyll-*a* (Chl-*a*) fluorescence as well as with mean volume backscatter (MVBS) recorded by a 750 kHz acoustic Doppler profiler, suggesting that density fronts were zones of rapidly changing phytoplankton and zooplankton biomass concentrations. Surface density fronts were also more likely to be zones of enhanced MVBS and Chl-*a* fluorescence compared to regions flanking the fronts, indicating that zooplankton and phytoplankton biomass tended to be

concentrated at fronts. MVBS and Chl-a fluorescence gradients were significantly correlated with gradients in other hydrographic variables such as temperature, salinity, and in some cases spiciness, though density gradients remained the single best predictor of strong MVBS and fluorescence gradients. I also examine the implications of observed patterns in front occurrence for prey foraging by mobile predators such as birds, marine mammals, and larger fish, and discuss the implications of the results in the context of long-term trends in ocean fronts in the SCCS.

Introduction

Fronts delineate boundaries between different water masses or parcels, and consequently are often areas characterized by strong horizontal gradients in hydrographic properties such as density, temperature, or salinity (Legeckis 1978, Sournia 1994). While there are several categories of fronts, generated under a variety of conditions (e.g., estuarine fronts, river plume fronts, tidal fronts, shelf-break fronts, among others), this paper examines open ocean fronts in the Southern California Current System (SCCS) and their role in shaping zooplankton and phytoplankton distributions.

Fronts have long been considered to be locations of special ecological significance for zooplankton (Lefevre 1986, Boucher et al. 1987). Both modeling studies and field observations have demonstrated that primary productivity can be significantly elevated at fronts due to transient vertical mixing events (Claustre

et al. 1994, Franks and Walstad 1997). Enhanced nutrient availability can enable growth of larger phytoplankton such as diatoms (Claustre et al. 1994, Landry et al. 2012, Taylor et al. 2012) which are more readily grazed by mesozooplankton, as compared to picophytoplankton which often dominate in oligotrophic conditions. Both the composition of zooplankton assemblages and the total biomass concentrations of zooplankton can change abruptly across fronts (Mackas et al. 1991, Ohman et al. 2012). Increased egg production rates by mesozooplankton have been observed at phytoplankton-rich fronts (Smith and Lane 1991). Fronts have also been observed to have elevated abundances of highly mobile predators such as large fish (Fiedler and Bernard 1987, Podesta et al. 1993), marine mammals (Tynan et al. 2005, Bost et al. 2009), and seabirds (Ainley et al. 2009, Kai et al. 2009). GPS-tracking studies have confirmed that seabirds can actively target and follow open ocean fronts (Kai et al. 2009).

Our understanding of zooplankton ecology at fronts is limited, however, because fronts are dynamic and often inadequately sampled in field studies. In addition, advection along the length of a single front can vary rapidly from convergent to divergent, and from upwelling to downwelling in response to local winds (Franks and Walstad 1997, D'Asaro et al. 2011), frontal meanders (Bower 1991), or secondary circulation (D'Asaro et al. 2011), leading to changes in nutrient supply, light penetration, and localized accumulation and dispersal of plankton. Fronts can persist on timescales varying from days to weeks, making prediction of zooplankton and phytoplankton responses to altered environmental

conditions at fronts difficult. Furthermore, zooplankton are not passive particles and can alter their swimming or vertical migration behavior in response to changing physical conditions. Varying vertical migration behavior can lead to markedly different zooplankton densities at both convergent and divergent flows (Franks 1992).

Most studies of plankton responses to fronts have focused on predictable, recurrent shallow-water fronts such as tidal and estuarine fronts (Pingree et al. 1975), or semi-permanent deep ocean fronts such as the Ligurian Front in the Mediterranean Sea (Boucher et al. 1987). In contrast, the Southern California Current System (SCCS) is characterized by complex and varying mesoscale structures including fronts, jets, and eddies, especially within a transitional zone centered approximately 200 km offshore that separates the nearshore, coastally-upwelled waters from both the core California Current and the subtropical-influenced waters further offshore (Lynn and Simpson 1987). Modeling studies have suggested that intensification of equatorward winds, especially off central California, in spring and summer increase baroclinic instabilities in the wind-forced alongshore currents and consequently lead to an increase in frontogenesis with increased formation of meanders, jets and mesoscale eddies (Marchesiello et al. 2003, Capet et al. 2008). Submesoscale and fine-scale frontal features can also be spawned from instabilities in the mesoscale features via ageostrophic secondary circulation (Johnston et al. 2011).

Zooplankton within the SCCS, are therefore subject to continually varying environments where they may be carried into convergent features, entrained within eddies or fast-moving jets, or maintained within quiescent waters. Each of these environments presents zooplankton with different conditions of food availability, predation pressure, dispersal potential, and potential for reproductive success. Consequently, these varying conditions can lead to spatially variable zooplankton and phytoplankton densities, leading to plankton fronts or accumulation zones.

Mechanisms leading to the development of plankton gradients or localized accumulation zones can be divided into four general categories. Plankton can accumulate due to convergent flows. Horizontal shear or stirring can bring two water parcels containing different plankton concentrations in close proximity. Altered *in situ* plankton growth or predation can increase or decrease local densities. Lastly, changes in zooplankton swimming and vertical migration behavior can interact with local advection patterns, leading to the local accumulation or dispersal of zooplankton. Regardless of which mechanism dominates in specific cases, however, the front-seeking behavior observed in highly-mobile predators (Kai et al. 2009) suggests that zooplankton accumulation at fronts is not uncommon, and that fronts, while limited in areal extent, may play a disproportionate role in predator behavior as well as zooplankton reproduction, growth and mortality.

In a previous study of zooplankton in fronts extending from Point Arena in northern California, Mackas *et al.* (1991) found that zooplankton biomass was 4-fold higher on the cool, dense side of a filament compared to the warm, fresh side of the filament. These authors also found that zooplankton assemblages changed strongly across the filament from a euphausiid and doliolid-dominated assemblage on the cool side to a small-copepod, chaetognath and heteropod-dominated assemblage on the warm side. Smith and Lane (1991), studying the same filament, found that egg production by *Eucalanus californicus* was enhanced within the southern (cold) edge of the jet and in the cool waters adjacent to the jet, and concluded that elevated food supply in these areas permitted increased egg production.

A study of the Ensenada Front (Haury *et al.* 1993), a semi-recurrent frontal feature west of San Diego, also found 3-4 fold higher zooplankton displacement volumes on the cool (North) side of the front where primary productivity was also elevated. Interestingly, despite relatively weak cross-front gradients in physical variables, the increase in zooplankton displacement volumes occurred over an abrupt transition of only 15 km. Moser and Smith (1993) found distinct assemblages of fish larvae on either side of the Ensenada Front, and distinct vertical migration behaviors in species of fish that were found on both sides of the front.

Another front study within the SCCS near the Ensenada Front, the A-Front study, found 2-3 fold increases in zooplankton and phytoplankton biomass on the

northern (cool) side of the front (Ohman et al. 2012, Taylor et al. 2012). Within the core of the front itself, diatom biomass, as well as bacterial production, was greatly enhanced (Samo et al. 2012, Taylor et al. 2012). Zooplankton assemblages changed from a particle-grazer dominated assemblage north of the front (mostly calanoid and *Oithona*-like copepods, euphausiids, and appendicularians) to a carnivore-dominated assemblage to the south (poecilostomatoid copepods, ostracods, chaetognaths and radiolarians; Ohman *et al.*, 2012). Increased calanoid copepod and copepod nauplii biomass within the front itself suggested that secondary production was elevated within the front, perhaps due to increased food availability.

Taken together, these previous studies suggest that fronts may be important in structuring the distribution, productivity and behavior of zooplankton within the CCS. However, each study based its conclusions on observations of limited duration of a single front for which shipboard sampling was possible. To assess the importance of fronts more generally, it is necessary to observe a variety of fronts over an extended period, throughout different seasons, and across a broad area.

Autonomous ocean gliders represent a means to extend our observational capabilities when studying ocean fronts. Since 2006, *Spray* gliders (Davis et al. 2008) have been deployed nearly continuously along two cross-shore ocean transects, Line 80 and Line 90 within the SCCS (Fig. 1). Lines 80 and 90 are part of the CalCOFI sampling grid that has been sampled by ship for more than sixty

years, and since 2004 have been sampled as part of the California Current Ecosystem – Long Term Ecological Research (CCE-LTER) program (<http://cce.lternet.edu>). Together, Lines 80 and 90 span the range of oceanographic conditions found within the SCCS. Line 80, extending west-southwest from Point Conception, is often marked by cold, upwelled waters close to the coast, and is bounded to the west by the fresher and somewhat warmer core of the equatorward-flowing California Current (CC) proper, which typically becomes progressively warmer and saltier towards the west. The major currents, including the CC, the California Undercurrent (CUC), and the Inshore Countercurrent (ICC) crossing line 80 are often intensified compared to Line 90, with more compact, faster flowing cores. In contrast, Line 90 is often influenced by warmer, more subtropical waters intruding from the south and west. As the prevailing currents along line 90 are generally broader, and more diffuse, maximum current velocities tend to be reduced as well. The bottom topography of lines 80 and 90 are also quite different. Bottom depth along line 80 increases nearly monotonically, and rapidly, with distance offshore as it traverses the continental slope. Line 90, on the other hand, crosses over several undersea ridges and sea mounts as it traverses the Southern California Bight. The differing bathymetries of lines 80 and 90 may influence the mechanisms by which fronts form along these two lines.

While each glider transect provides only a two-dimensional slice of a complex three-dimensional flow field, the existence of a multi-year collection of

glider transects provides an excellent opportunity to examine the relationship between ocean fronts and plankton distributions. Here, I will test specific hypotheses regarding the covariability of ocean fronts and zooplankton and phytoplankton gradients within the SCCS.

Hypothesis 1: The distribution of ocean fronts is non-random, showing distinct seasonal and cross-shore patterns.

Hypothesis 2: Gradients in biotic properties co-vary with gradients in physical ocean properties.

Hypothesis 3: Ocean fronts are more likely to be zones of plankton accumulation compared with non-frontal areas.

Furthermore, if fronts are zones of changing biotic gradients and plankton accumulation, glider data can help assess which mechanisms (e.g., convergent advection, horizontal stirring, biological growth, or organismal behavioral changes) might explain the observed patterns.

Methods

Study Area and Duration

The data included in this analysis span October 2006 to July 2011, though gliders continue to be deployed at time of publication. During this period, gliders were deployed nearly continuously along lines 80 and 90 of the CalCOFI sampling area (Fig 3.1). Gliders traveling along the two lines traverse from about

20 km off the coast to a maximum 370 km (line 80) and 585 km (line 90) offshore. A total of 124 transects were completed during the study period comprising 22,942 vertical profiles.

Spray glider and instrument payload

The *Spray* glider (Sherman et al., 2001) is a buoyancy-controlled autonomous underwater vehicle capable of conducting profiles to 1000 m depth for up to 4 months at a time. The vehicle profiles in a sawtooth pattern, travelling at an average speed of 25 cm s^{-1} through the water, at an angle of 17 degrees from the horizontal. For this study, gliders descended to a maximum depth of 500 m, or to within approximately 5 m from the bottom in shallower waters. At the end of each profile, the glider surfaces, establishes a GPS fix, and uploads data through communication with the Iridium satellite system. The glider follows a pre-programmed mission along a transect until it receives instructions to change operations. In waters deeper than 500 m, the glider will complete a profile cycle every 3 hours, on average, with an average spacing between profiles of 3 km.

The *Spray's* instrument payload during this study included a Seabird 41CP Conductivity-Temperature-Depth (CTD) sensor, a mini-Seapoint chlorophyll-a fluorometer (mini-SCF), and a Sontek 750-kHz, 3-beam Acoustic Doppler Profiler (ADP). During sampling, seawater is continuously pumped through the CTD and the fluorometer to maintain a constant flow rate past the sensors. Biofouling is inhibited by pumping seawater through a biocide-treated intake tube.

The Seapoint fluorometers used in this study had a central excitation peak of 470 nm and measured fluorescence at an emission peak of 685 nm. Fluorometers were regularly calibrated between deployments using a standard set of dilutions of pure chlorophyll a (Sigma Life Sciences) dissolved in 90% acetone. The calibration procedure was consistent in that each Chl-a standard was first loaded into a 13 mm diameter borosilicate round cuvette, and then placed within a machined cuvette-holder that held the standard at a fixed distance from the optical surfaces of the fluorometer. For each calibration, a slope value (i.e., $\mu\text{g Chl-a L}^{-1} \text{ V}^{-1}$) was determined from a regression of recorded voltage with dissolved Chl-a concentrations. Regular calibration enabled inter-comparison of data from the same sensor during different deployments, and also comparability of data recorded by different sensors. The fluorometer response recorded during deployments is reported here in standardized Chl-a fluorescence units (SFU), where one SFU is defined as the measured fluorescence signal (volts) from $10 \mu\text{g L}^{-1}$ of Chl-a dissolved in 90% acetone (cf. previously reported as Dissolved Chlorophyll Fluorescence Equivalents (DCFE) in Davis et al., 2008). *In vivo* fluorescence data were converted into SFU by multiplying the recorded voltages by the mean slope value determined from pre- and post-deployment calibrations. For the fluorometers used in this study, one SFU corresponds very approximately to $2 \mu\text{g Chl-a L}^{-1}$. While SFU data cannot be directly converted into *in situ* Chl-a concentrations, SFU data do provide useful measures of standardized Chl-a fluorescence that are comparable during the study.

The Sontek *Spray* ADP is mounted on the glider so that it points directly down during glider ascent, so that each of the three beams has a slant angle of 25° from vertical. Each beam has a 3 dB beam-width of 2°. Both current velocity and acoustic backscatter (ABS) data from the ADP are recorded upon ascent in five 4-m vertical range bins so that vertical resolution of the completed profile is 4 m. The backscatter measured by the ADP is reported in acoustic counts, which is the digitized output from a log-linear amplifier. Regular calibration of each ADP instrument using a standard tungsten-carbide target suspended in a test pool revealed an average difference in ABS recorded by an individual ADP across multiple deployments of 2.5 dB, and an average difference between different ADP instruments of 3 dB. The recorded ABS is then converted into Volume Backscatter, S_v , using the sonar equation $S_v = RL - SL + 2TL - 10 \log_{10} V$, where Receiver Level (RL) is the recorded ABS in dB, Source Level (SL) in decibels is empirically determined during instrument calibration, Transmission Loss (TL) is equivalent to $20 \log_{10} R + \alpha R$, where R is the range in meters to the midpoint of the bin and α is the sound attenuation coefficient (dB m^{-1}), and V is the volume in cubic meters. Volume backscatter measurements are averaged to yield Mean Volume Backscatter (MVBS).

Previous work comparing ABS recorded by the Sontek ADP with collected net samples established that recorded ABS is proportional to the log of zooplankton biomass in the vicinity of the ADP (Powell and Ohman 2012). ZooScan image analysis of zooplankton in net samples showed ABS was most closely related to zooplankton with an equivalent circular diameter ≥ 1.6 mm,

approximately the acoustic wavelength emitted by the transducer. It is important to note, however, that the method used to calculate relative MVBS in Powell and Ohman (2012) relied on a different formulation of the sonar equation (SonTek 1997). The standard sonar equation presented here (Medwin and Clay 1998) includes a $10 \log_{10} V$ term rather than a $10 \log_{10} PL$ term (where PL is the acoustic pulse length), which permitted comparison of backscatter from different range cells. Applying this method to the data from Powell and Ohman (2012) did not alter any of the results or conclusions of that paper.

Glider data processing

Data from each glider deployment were downloaded from the glider's flash memory upon glider recovery and then imported into MATLAB for preliminary processing and quality assurance and control. Bad data, as determined by processing scripts or visual inspection, were excluded from further analysis. The data from all glider deployments were then harvested into a master MATLAB dataset and grouped by transect. Only data from complete transects, where the glider completed 90% or more of its intended trackline, were included in the analysis. Variables included in this study include temperature, salinity, density, Chl-a fluorescence (as SFU), salinity on potential isopycnals, which has the same information as spice (Flament 2002), cross-track and along-track current velocity, and MVBS. For each profile within a given transect, all data were vertically averaged into 5-m bins. Most analyses in this study examine changes in measured variables in a surface layer from 0 to 50 m.

Gradients, enhancement index and front detection.

Comparing glider data from one profile to the next is confounded by diel periodicity in biological signals (in the case of MVBS and *in vivo* fluorescence data), and by the influence of internal tides and inertial motions (in the case of hydrographic variables). For example, diel vertical migrations (DVM) by zooplankton and micronekton dramatically influence the total biomass concentrations observed in daytime surface waters (Lampert 1989). Thus, searching for biological fronts by directly comparing surface MVBS from adjacent nighttime and daytime profiles is impossible. Similarly, measured fluorescence in surface waters is strongly affected by the daytime decrease in Chl-a fluorescence due to non-photochemical quenching, and to daytime photo-protective strategies employed by phytoplankton (Cullen and Lewis 1995). Furthermore, the calculation of gradients in hydrographic variables (i.e., density, temperature, salinity, etc.), is confounded by internal tides and waves which can vertically displace physical features such as the thermocline from dive to dive. For these reasons, both physical and biological data were smoothed prior to use by averaging observations within a 24-hour period. Gradients (Fig. 2A,B) are defined as the difference between averages of properties from the 24 h periods before and after the glider reached a location. By definition here, a gradient is the offshore average minus the inshore average.

The enhancement index (Fig. 2C,D) of a given dive measures whether the waters within a 24 h block of dives just inshore of the given dive exhibit increased

(positive), decreased (negative), or neither increased or decreased (zero) enhancement of average MVBS or Chl-a fluorescence compared to the two flanking 24 h blocks. For a given dive location, the center block (“box2”), contains the 24 h period just inshore of the dive, and the two flanking blocks (“box1” and “box3”) are located inshore and offshore, respectively. The enhancement index is equal to $A \times \text{abs}(\text{Box2}-\text{Box1}) + \text{abs}(\text{Box2}-\text{Box3})$, where A equals 1 if Box2 is higher than Box1 and Box3, A equals -1 if Box2 is lower than Box1 and Box3, or A equals 0 otherwise. Fronts are identified algorithmically (Fig. 2). Dives with horizontal density gradient values greater than the 95th percentile or less than the 5th percentile are flagged as potential “positive” or “negative” density fronts, respectively. When more than one contiguous dive is flagged as a potential front, the dive with the maximum (minimum) gradient value within the contiguous run of dives is denoted as a positive (negative) density front. Other front types, identified with any of the other glider-measured or derived variables (e.g., thermal fronts, salinity fronts, MVBS fronts), are identified in an identical manner.

Results

Coincident biological and physical structures

Visual inspection of glider transects reveals that regions of increased horizontal gradients in biotic properties such as ABS and Chl-a fluorescence are often, but not always, associated with oceanic density fronts. In an example glider section (Fig. 3.3), a sharp density front is co-located with corresponding fronts in temperature, salinity, MVBS and local maxima in cross-track and along-

track current velocities in the top 50 m. There is a 9 dB drop in mean MVBS in the top 50 m across the density front which could correspond to an 8-fold change in biomass. This particular front does not manifest a corresponding front in Chl-*a* fluorescence, indicating that the relationship between physical and biological properties at fronts is variable, and that zooplankton and phytoplankton may be, at times, independently influenced by frontal conditions, or that interactions between zooplankton and phytoplankton at fronts also act to structure abundance and biomass concentrations.

Oceanic density fronts along lines 80 and 90

A total of 81 density fronts along line 80, and 73 density fronts along line 90 were identified by the front-detection criteria. Lines 80 and 90 differed somewhat in the distribution of their respective fronts in terms of location (distance offshore) and day of the year (Fig. 3.4). There were relatively few fronts in the offshore portion of transects along line 80, with most fronts found within 125 km of the shore. There were also relatively few fronts during the first 90 days of the year. A comparison of density gradients at fronts along lines 80 and 90 indicated that gradient magnitudes were significantly stronger along line 80 ($p < 0.05$, Mann-Whitney U). Tests of the effect of season upon front incidence and front strength (as measured by the magnitude of the along-track density gradient) for lines 80 and 90 (Fig. 3.5a) confirmed the seasonal patterns suggested in Figure 3.4. There were significantly fewer fronts in winter for line 80, and there were significantly more fronts in fall along line 90 ($p < 0.05$, binomial test

with Bonferroni correction). The magnitudes of density gradients at fronts did not vary significantly by season for lines 80 and 90 ($p > 0.05$, Kruskal-Wallis), although the decreased front strength observed along line 80 in winter was marginally significant ($p = 0.06$).

To test the influence of distance offshore upon front incidence and front strength, fronts along line 80 and along 90 were classified into one of three distance categories: near-shore, transitional, and offshore. The boundaries of these categories were based on dividing the full length of the nominal transect line into thirds. Thus, the length of line 80 sections is shorter than those for line 90. There were significantly more fronts inshore and significantly fewer fronts offshore for line 80 ($p < 0.05$, binomial test with Bonferroni correction; Fig. 3.5b). The magnitude of density gradients at fronts along lines 80 and 90 did not vary significantly with distance offshore ($p > 0.05$, Kruskal-Wallis).

There is also a suggestion that changes in the median distance offshore of fronts is affected by the spring transition in the CCS (Fig. 3.6). Fronts were predominantly located close to the coast during March and April along line 90 ($p < 0.05$). In contrast, median distance offshore was greater for all other bimonthly periods and greatest during January and February, a period which was marked by few fronts and decreased magnitudes of density gradients.

Covariability of density and MVBS, Chl-a gradients

Density gradients and MVBS gradients co-varied during the study period. There is a significant rank correlation between horizontal gradients in density and

horizontal gradients in MVBS (Fig. 3.7a,c) for both line 80 ($r_s = 0.42$, $p < 0.001$) and line 90 ($r_s = 0.43$, $p < 0.001$). Furthermore, the MVBS gradients at dives identified as density fronts are significantly higher compared to the MVBS gradients at dives not associated with density fronts (Fig. 3.7b,d; $p < 0.001$, Mann Whitney U). While the relationship between density and MVBS gradients is significant, it is also variable. Not all dives identified as a positive density front also exhibit a strong, positive MVBS gradient, indicating that other factors besides density gradient strength influence the distribution of zooplankton gradients.

Chlorophyll-a fluorescence gradients also show a significant, positive rank correlation with density gradients (Fig. 3.8a,c), though not as strong (line 80: $r_s = 0.31$, $p < 0.001$; line 90: $r_s = 0.36$, $p < 0.001$). Similarly, the Chl-a gradients at fronts are significantly higher than at non-fronts (Fig. 3.8 b,d; $p < 0.001$, Mann Whitney U) Interestingly, the rank correlation between MVBS gradients and Chl-a fluorescence gradients is weaker (line 80: $p < 0.001$, $r_s = 0.23$; line 90: $p < 0.001$, $r_s = 0.26$) than that of the density gradient with either the MVBS gradient or Chl-a fluorescence gradient, indicating that high horizontal gradients in chlorophyll-a are a worse predictor of zooplankton distributions than the presence of high horizontal gradients in density. This pattern may arise because zooplankton and phytoplankton distributions are independently influenced by physical ocean structures, or because grazer-herbivore interactions between zooplankton and phytoplankton do not necessarily lead to linear correlations.

Enhanced MVBS at ocean density fronts

The covariability of MVBS gradients with density gradients suggests that ocean fronts often function as borders between water parcels with differing zooplankton characteristics, indicating that denser surface waters on average either contain greater zooplankton biomass, or contain zooplankton assemblages with different backscattering characteristics. The acoustic backscatter enhancement index associated with dives identified as positive density fronts is significantly elevated compared to all other, non-front dives (Fig. 3.9a,b; line 80: $p < 0.001$; line 90: $p < 0.001$, Mann-Whitney U test), whereas negative density fronts exhibited negative acoustic backscatter enhancement (Fig. 3.9c,d; line 80: $p < 0.001$; line 90: $p < 0.001$). Similarly, the enhancement index is significantly lower inshore of dives identified as negative density fronts in which the isopycnals shoal with increasing distance offshore (line 80: $p < 0.001$; line 90: $p < 0.001$). Positive density fronts were also associated with positive Chl-a fluorescence enhancement (Fig. 3.10a,b; line 80: $p < 0.001$; line 90: $p < 0.001$), whereas negative density fronts exhibited negative Chl-a fluorescence enhancement (Figure 3.10c,d; line 80: $p < 0.001$; line 90: $p < 0.001$). Together these results indicate that fronts not only act as borders between water parcels, but also that fronts can act as zones of biological enhancement. Instances of positive, negative and zero enhancement at fronts did not show a clear pattern in seasonal or cross-shore distributions (Fig. 3.11).

Covariability of MVBS with other hydrographic variables

Other hydrographic variables in addition to density (temperature, salinity, SFU) and the respective horizontal gradients in these variables show significant relationships with mean surface MVBS and surface MVBS gradients, respectively (Table 3.1). While mean surface density and horizontal gradients in surface density remain the best predictors for mean surface MVBS and horizontal gradients in surface MVBS, respectively, temperature and temperature gradients are nearly as good predictors. Variables measuring cross-track currents (v) and shear (dv/dx), as well as along-track currents (u) and dilation or constriction in the along-track direction (du/dx) were not significantly correlated with MVBS or MVBS gradients, respectively, with the exception of a very weak correlation between cross-track and along-track current velocities with MVBS along line 80.

Glider dives identified as ocean density fronts exhibited the strongest MVBS gradients when compared to non-front dives, such that the median value of MVBS gradients at front dives was equal to the 88.1th percentile (line 80) and 91.8th percentile (line 90) of the MVBS gradients of non-front dives – a differential from the 50th percentile of 38.1 and 41.8, respectively (Table 3.2). The difference in medians between front dives and non-front dives was significant ($p < 0.001$, Mann-Whitney U). Again, other front types, particularly temperature and salinity fronts, exhibited MVBS gradients that differed significantly from non-front associated MVBS gradients, but no other front types were found to have as large a differential between MVBS gradient medians. For line 80 dives, the median MVBS gradient values at shear and dilation fronts were not significantly different

from the median MVBS gradient at non-front dives, ($p > 0.10$), while for line 90 only shear fronts were not significant ($p > 0.10$).

Correspondingly, dives identified as MVBS fronts were likely to be associated with stronger gradients in density and most other hydrographic variables when compared to non-MVBS-front dives (Table 3.3). Density remained the hydrographic variable with the greatest differential in gradients between MVBS front and non-front dives. Along lines 80 and 90, the median gradients in spice, shear and dilation were not significantly different ($p > 0.10$) for MVBS front-associated dives versus non-front dives, except for shear gradients along line 90 ($p = 0.026$). Compared with the percentile differential for gradients in density, temperature, salinity, and SFU (34.7, 29.9, 36.9, and 30.0, respectively), however, the percentile difference for shear gradients at MVBS fronts versus non-fronts was significantly smaller (10.1).

Discussion

The high spatial resolution glider data, collected over six years, made it possible to test the three hypotheses posed in the Introduction concerning the coincidence of physical and biotic gradients. My tests reveal first that open ocean density fronts in the SCCS exhibit both seasonality and, in the case of line 80, a non-random cross-shore distribution. Second, horizontal gradients in acoustic backscatter (MVBS) and Chl-*a* are typically co-located with physical fronts. Third, fronts are more likely to be zones of plankton accumulation than non-frontal areas.

Analyses of the glider data suggest that the formation of biotic fronts and the accumulation of plankton is a complex process that cannot be attributed to a single causal mechanism. Acoustic Doppler velocity data showed no consistent correlation with the presence of biotic fronts or accumulation zones, indicating that neither convergence nor horizontal shear alone (as measured by the gliders) could be the sole mechanism responsible for their formation. It also seems improbable that *in situ* growth can account solely for stronger MVBS gradients and accumulation observed at ocean fronts, since the generation time of zooplankton likely to contribute to the observed elevated MVBS is on the order of weeks to months, longer than most frontal conditions are likely to persist. However, it is conceivable that phytoplankton could accumulate within fronts in response to growth triggered by upwelled nutrients. It is also possible that alterations of zooplankton depth-seeking behaviors at fronts could lead to localized retention, but it is not possible to assess this possibility directly with the available data. It seems likely that zooplankton and phytoplankton accumulation zones form as the result of a combination of convergence, horizontal shear, altered growth rates and behaviors. Directed studies are needed to examine the relative contributions of these mechanisms to biotic front formation in the SCCS. For example, additional gliders could repeatedly sample individual fronts identified by the line-transiting gliders in order to observe time-dependent flow fields, or gliders could carry additional biologically focused sensors that measure the potential for *in situ* growth (e.g., nitrate sensors, or perhaps fast repetition rate fluorometers to ascertain the physiological state of phytoplankton).

My observations of the spatial distribution of physical fronts are consistent with findings from other studies in the SCCS. In an analysis of ship-observed dynamic height anomalies, Lynn and Simpson (1987) found that the strongest cross-shore gradients in dynamic height occur during spring and summer, while the weakest cross-shore gradients occur during the winter months. Along line 80 especially, the glider observations suggest that fronts are fewer and weaker during the winter months. Lynn and Simpson (1987) also found that variability in dynamic height is greatest in a broad transitional zone centered approximately 200 km offshore along line 80 and 300 km offshore along line 90. As the maximum gradients in dynamic height migrate offshore through the spring, summer, and fall, it would be reasonable to assume that conditions meeting the present front criteria would also match this seasonal progression and be seen in the seasonal and cross shore distributions of glider-observed density fronts. However, fronts along line 80 consistently were most common closer to shore throughout the year. Fronts along line 90 more closely matched this progression, with front occurrence increasing from a minimum during March to April. Front incidence was also maximal within the 200-400 km band along line 90, again matching dynamic height data.

Satellite altimetry data (Strub and James 2000) also corroborate the seasonal distribution of fronts detected by gliders. Strub and James (2000) found that high eddy kinetic energy (EKE) first appears in the spring near the coast; as the year progresses, the zone of highest EKE moves offshore until winter when the California Current jet collapses and generally weak EKE is present. The

seasonal progression in distance offshore of glider-detected fronts matches these observations, with the fewest fronts detected in winter months and the median distance offshore increasing from a minimum during the March-April period. The data show that the January-February months exhibited the greatest median distance offshore for fronts, but this is consistent with the idea that a combination of generally weak EKE and few fronts leads to a more random distribution of fronts spread across the entire cross-shore range.

The glider data are also partially corroborated by a study of the seasonality of satellite-detected thermal fronts in the CCS (Castelao et al. 2006), which measured the bi-monthly climatology of the magnitude of thermal gradients as well as the cross-shore probability distribution of front occurrence from 2001 to 2004. Similar to the glider results presented here, Castelao et al. (2006) found that the winter months were marked by fewer and weaker fronts that were broadly distributed cross-shore, followed by an abrupt shift to more numerous and stronger fronts that were concentrated in the near shore in the March to April period. After March and April, the zone of strong fronts and high front probability migrated farther offshore. This progression is similar to that observed by gliders along line 90, but is not clearly observable in the line 80 data. Since the glider observations do not overlap in time with the satellite observations, it is unclear whether interannual variation in seasonal patterns would explain the observed differences. However, the magnitude of temperature gradients at the satellite-detected thermal fronts closely matched those measured at glider-detected fronts, suggesting that the fronts detected in the Castelao study may represent

the same phenomena as those measured by the glider. Kahru *et al.* (2012) also found a similar seasonal pattern in satellite-detected thermal front frequency in the waters north of Point Conception, with the fewest fronts occurring in winter followed by steadily increasing frontal frequencies throughout the spring and summer.

The heterogeneous distribution of food resources throughout the ocean has important consequences for herbivorous and carnivorous animals. Mullin and Brooks (1976) observed that most marine animals would likely starve if food were uniformly distributed throughout the ocean. For both mobile planktivorous predators, and for zooplankton that might alter their vertical migration behavior to improve their retention in fronts, the observed enhancement of potential food resources at fronts could represent an important foraging opportunity. Thus, the results presented here demonstrating that both Chl-*a* fluorescence gradients and MVBS gradients covary with hydrographic gradients during an extended sampling period and over a wide geographic area are important for several reasons. First, both satellite-based observational studies and modeling studies have demonstrated that open ocean fronts are a common feature in the ocean, especially in Eastern Boundary Upwelling Ecosystems such as the CCS (Belkin *et al.* 2009). Seasonal changes in the distribution of fronts (and therefore potentially the seasonal changes in food availability) may influence the timing of reproduction, feeding and migration strategies for many species.

Second, the demonstrated covariability of physical and biological gradients complements observations that mobile predators like tuna target

thermal fronts (Fiedler and Bernard 1987). Given that there is increased likelihood of potential prey at these locations, the ability of a predator to swim up gradients would be an adaptive trait. Foraging strategies of highly mobile predators are not well understood., and it is unclear whether predators follow physical (e.g., temperature) gradients or gradients of prey concentration. The present results at least suggest that following physical gradients alone could be a successful strategy.

Third, given the glider data presented here, we can estimate a mobile predator's success rate in locating waters with better foraging potential if they were to travel up horizontal density gradients. As Figure 3.12 demonstrates, mobile predators traveling up a strong density gradient, such as would be found in a frontal zone, will encounter waters with higher mean acoustic backscatter (implying higher zooplankton densities) approximately 85% of the time, while a mobile predator traveling down this density gradient would find richer waters only 15% of the time. These foraging success rates are independent of whether the predator is moving inshore or offshore. Thus, there would seem to be a strong selective pressure for mobile predators to preferentially travel up density gradients.

Additionally, strictly physical accumulation mechanisms that entrain and concentrate plankton within frontal zones could have other important ecological effects such as stimulating rates of zooplankton grazing on phytoplankton, zooplankton mate encounter, reproductive success and fecundity, and somatic

growth. Population dynamics may be significantly altered at fronts compared to non-frontal zones.

A recent analysis of satellite data found a long-term increase in the frequency of satellite-detected Chl-a and SST fronts within a 110,000 km² study area in the SCCS (Kahru et al. 2012). The frequency of SST fronts increased almost 35% between 1981 and 2011, while the frequency of Chl-a fronts increased over 50% between 1997 and 2011. Kahru *et al.* (2012) attributed the increased frequency of fronts to the increased incidence of filaments and eddies driven by an increase in upwelling-favorable winds and coastal upwelling during the period (Garcia-Reyes and Largier 2010). Since ocean models of a warming SCCS project an intensification of mean currents and increased mesoscale eddy variance (Di Lorenzo et al. 2005), it seems likely that the frequency of fronts, and their importance to regional ecology, will continue to increase in the future.

Acknowledgements

I gratefully acknowledge Russ Davis, Dan Rudnick, Robert Todd, Jeff Sherman for the provision of *Spray* Glider data, and for their advice on glider instrumentation and technical issues. I am also indebted to Mark Ohman, Russ Davis, Peter Franks and Mike Landry who all provided important feedback during the preparation of this manuscript. Funding for this work was provided by NSF via the California Current Ecosystem LTER site, and by the Gordon and Betty Moore Foundation, in awards to M.D. Ohman. Glider observations were supported by the NOAA Ocean Climate Observation Program through the

Consortium on the Ocean's Role in Climate, and by the US Integrated Ocean Observation System through the Southern California Coastal Ocean Observing System (SCCOOSs).

Chapter 3, in part, is currently submitted for publication in *Deep Sea Research II*, 2013, Powell, J.R., Elsevier Press, 2013. The dissertation author was the primary investigator and author of this paper.

References

- Ainley, D. G., K. D. Dugger, R. G. Ford, S. D. Pierce, D. C. Reese, R. D. Brodeur, C. T. Tynan, and J. A. Barth. 2009. Association of predators and prey at frontal features in the California Current: competition, facilitation, and co-occurrence. *Marine Ecology Progress Series* **389**:271-294.
- Belkin, I. M., P. C. Cornillon, and K. Sherman. 2009. Fronts in large marine ecosystems. *Progress in Oceanography* **81**:223-236.
- Bost, C. A., C. Cotte, F. Bailleul, Y. Cherel, J. B. Charrassin, C. Guinet, D. G. Ainley, and H. Weimerskirch. 2009. The importance of oceanographic fronts to marine birds and mammals of the southern oceans. *Journal of Marine Systems* **78**:363-376.
- Boucher, J., F. Ibanez, and L. Prieur. 1987. Daily and seasonal-variations in the spatial-distribution of zooplankton populations in relation to the physical structure in the Ligurian Sea Front. *Journal of Marine Research* **45**:133-173.
- Bower, A. S. 1991. A simple kinematic mechanism for mixing fluid parcels across a meandering jet. *Journal of Physical Oceanography* **21**:173-180.
- Capet, X., J. C. McWilliams, M. J. Molemaker, and A. F. Shchepetkin. 2008. Mesoscale to submesoscale transition in the California current system. Part II: Frontal processes. *Journal of Physical Oceanography* **38**:44-64.
- Castelao, R. M., T. P. Mavor, J. A. Barth, and L. C. Breaker. 2006. Sea surface temperature fronts in the California Current System from geostationary

satellite observations. *Journal of Geophysical Research: Oceans* **111**: C09026, doi:10.1029/2006JC003541.

- Claustre, H., P. Kerherve, J. C. Marty, L. Prieur, C. Videau, and J. H. Hecq. 1994. Phytoplankton dynamics associated with a geostrophic front: ecological and biogeochemical implications. *Journal of Marine Research* **52**:711-742.
- Cullen, J. J. and M. R. Lewis. 1995. Biological processes and optical measurements near the sea surface: some issues relevant to remote sensing. *Journal of Geophysical Research: Oceans* **100**:13255-13266.
- D'Asaro, E., C. Lee, L. Rainville, R. Harcourt, and L. Thomas. 2011. Enhanced Turbulence and Energy Dissipation at Ocean Fronts. *Science* **332**:318-322.
- Davis, R. E., M. D. Ohman, D. L. Rudnick, J. T. Sherman, and B. Hodges. 2008. Glider surveillance of physics and biology in the southern California Current System. *Limnology and Oceanography* **53**:2151-2168.
- Di Lorenzo, E., A. J. Miller, N. Schneider, and J. C. McWilliams. 2005. The warming of the California current system: Dynamics and ecosystem implications. *Journal of Physical Oceanography* **35**:336-362.
- Fiedler, P. C. and H. J. Bernard. 1987. Tuna aggregation and feeding near fronts observed in satellite imagery. *Continental Shelf Research* **7**:871-881.
- Flament, P. 2002. A state variable for characterizing water masses and their diffusive stability: spiciness. *Progress in Oceanography* **54**:493-501.
- Franks, P. J. S. 1992. Sink or Swim - Accumulation of Biomass at Fronts. *Marine Ecology Progress Series* **82**:1-12.
- Franks, P. J. S. and L. J. Walstad. 1997. Phytoplankton patches at fronts: A model of formation and response to wind events. *Journal of Marine Research* **55**:1-29.
- Garcia-Reyes, M. and J. Largier. 2010. Observations of increased wind-driven coastal upwelling off central California. *Journal of Geophysical Research: Oceans* **115**.
- Haury, L. R., E. L. Venrick, C. L. Fey, J. A. McGowan, and P. P. Niiler. 1993. The Ensenada Front: July 1995. *California Cooperative Oceanic Fisheries Investigations Reports* **34**:69-88.
- Johnston, T. M. S., D. L. Rudnick, and E. Pallas-Sanz. 2011. Elevated mixing at a front. *Journal of Geophysical Research: Oceans* **116**.

- Kahru, M., E. Di Lorenzo, M. Manzano-Sarabia, and B. G. Mitchell. 2012. Spatial and temporal statistics of sea surface temperature and chlorophyll fronts in the California Current. *Journal of Plankton Research* **34**:749-760.
- Kai, E. T., V. Rossi, J. Sudre, H. Weimerskirch, C. Lopez, E. Hernandez-Garcia, F. Marsac, and V. Garcon. 2009. Top marine predators track Lagrangian coherent structures. *Proceedings of the National Academy of Sciences of the United States of America* **106**:8245-8250.
- Lampert, W. 1989. The Adaptive Significance of Diel Vertical Migration of Zooplankton. *Functional Ecology* **3**:21-27.
- Landry, M. R., M. D. Ohman, R. Goericke, M. R. Stukel, K. A. Barbeau, R. Bundy, and M. Kahru. 2012. Pelagic community responses to a deep-water front in the California Current Ecosystem: overview of the A-Front Study. *Journal of Plankton Research*. **34**: 739-748
- Lefevre, J. 1986. Aspects of the Biology of Frontal Systems. *Advances in Marine Biology* **23**:163-299.
- Legeckis, R. 1978. Survey of worldwide sea-surface temperature fronts detected by environmental satellites. *Journal of Geophysical Research-Oceans and Atmospheres* **83**:4501-4522.
- Lynn, R. J. and J. J. Simpson. 1987. The California Current System - the Seasonal Variability of Its Physical Characteristics. *Journal of Geophysical Research: Oceans* **92**:12947-12966.
- Mackas, D. L., L. Washburn, and S. L. Smith. 1991. Zooplankton Community Pattern Associated with a California Current Cold Filament. *Journal of Geophysical Research-Oceans* **96**:14781-14797.
- Marchesiello, P., J. C. McWilliams, and A. Shchepetkin. 2003. Equilibrium structure and dynamics of the California Current System. *Journal of Physical Oceanography* **33**:753-783.
- Medwin, H. and C. S. Clay. 1998. *Fundamentals of acoustical oceanography*. Academic Press, Boston.
- Ohman, M. D., J. R. Powell, M. Picheral, and D. W. Jensen. 2012. Mesozooplankton and particulate matter responses to a deep-water frontal system in the southern California Current System. *Journal of Plankton Research* **34**:815-827.
- Pingree, R. D., P. R. Pugh, P. M. Holligan, and G. R. Forster. 1975. Summer phytoplankton blooms and red tides along tidal fronts in approaches to English channel. *Nature* **258**:672-677.

- Podesta, G. P., J. A. Browder, and J. J. Hoey. 1993. exploring the association between swordfish catch rates and thermal fronts on United States longline grounds in the western North Atlantic. *Continental Shelf Research* **13**:253-277.
- Powell, J. R. and M. D. Ohman. 2012. Use of glider-class acoustic Doppler profilers for estimating zooplankton biomass. *Journal of Plankton Research* **34**:563-568.
- Samo, T. J., B. E. Pedler, G. I. Ball, A. L. Pasulka, A. G. Taylor, L. I. Aluwihare, F. Azam, R. Goericke, and M. R. Landry. 2012. Microbial distribution and activity across a water mass frontal zone in the California Current Ecosystem. *Journal of Plankton Research* **34**:802-814.
- Smith, S. L. and P. V. Z. Lane. 1991. The jet off Point Arena, California: its role in aspects of secondary production in the copepod *Eucalanus californicus johnson*. *Journal of Geophysical Research: Oceans* **96**:14849-14858.
- SonTek. 1997. SonTek Doppler current meters: using signal strength data to monitor suspended sediment concentration. *Application Note*:1-7.
- Sournia, A. 1994. Pelagic Biogeography and Fronts. *Progress in Oceanography* **34**:109-120.
- Strub, P. T. and C. James. 2000. Altimeter-derived variability of surface velocities in the California Current System: 2. Seasonal circulation and eddy statistics. *Deep-Sea Research II* **47**:831-870.
- Taylor, A. G., R. Goericke, M. R. Landry, K. E. Selph, D. A. Wick, and M. J. Roadman. 2012. Sharp gradients in phytoplankton community structure across a frontal zone in the California Current Ecosystem. *Journal of Plankton Research* **34**:778-789.
- Tynan, C. T., D. G. Ainley, J. A. Barth, T. J. Cowles, S. D. Pierce, and L. B. Spear. 2005. Cetacean distributions relative to ocean processes in the northern California Current System. *Deep-Sea Research Part II* **52**:145-167.

Table 3.1. Spearman's rank correlation (r_s) of hydrographic and biotic variables and their respective gradients with MVBS and MVBS gradients. Asterisks indicate correlations that are not significant ($p > 0.05$).

| Variable Type | Line 80 | | Line 90 | |
|-------------------------|------------|----------------|------------|----------------|
| | Mean r_s | Gradient r_s | Mean r_s | Gradient r_s |
| Density | 0.73 | 0.42 | 0.60 | 0.43 |
| Temperature | -0.69 | -0.31 | -0.53 | -0.33 |
| Salinity | 0.45 | 0.28 | 0.42 | 0.22 |
| SFU | 0.51 | 0.23 | 0.48 | 0.26 |
| Spice | -0.48 | -0.06 | -0.30 | -0.16 |
| Cross-track current (v) | -0.09 | -0.00* | -0.11* | 0.00* |
| Along-track current (u) | -0.26 | 0.00* | 0.01* | 0.01* |

Table 3.2. Comparison of median MVBS gradients at hydrographic or biotic fronts versus non-fronts.

| Front Type | Line 80 | | | Line 90 | | |
|-------------------------|-------------------------------|---------|-------------------------|-------------------------------|---------|-------------------------|
| | Median MVBS gradients Differ? | p-value | Percentile Differential | Median MVBS gradients Differ? | p-value | Percentile Differential |
| Density | Yes | <0.001 | 38.1 | Yes | <0.001 | 41.8 |
| Temperature | Yes | <0.001 | 28.5 | Yes | <0.001 | 29.5 |
| Salinity | Yes | <0.001 | 38.1 | Yes | <0.001 | 32.5 |
| SFU | Yes | <0.001 | 30.7 | Yes | <0.001 | 28.4 |
| Spice | Yes | 0.040 | 16.7 | No | 0.030 | 7.4 |
| $\partial v/\partial x$ | No | 0.188 | 4.2 | No | 0.517 | 7.6 |
| $\partial u/\partial x$ | No | 0.107 | 1.0 | Yes | <0.001 | 11.8 |

Table 3.3. Comparison of median hydrographic or biotic gradients at MVBS fronts versus non-fronts.

| Variable Type | Line 80 | | | Line 90 | | |
|-------------------------|---|---------|-------------------------|---|---------|-------------------------|
| | Median gradients differ at MVBS fronts? | p-value | Percentile Differential | Median gradients differ at MVBS fronts? | p-value | Percentile Differential |
| Density | Yes | <0.001 | 39.7 | Yes | <0.001 | 34.7 |
| Temperature | Yes | <0.001 | 36.9 | Yes | <0.001 | 29.9 |
| Salinity | Yes | <0.001 | 31.3 | Yes | <0.001 | 36.9 |
| SFU | Yes | <0.001 | 26.2 | Yes | <0.001 | 30.0 |
| Spice | No | 0.711 | 5.2 | No | 0.142 | 7.9 |
| $\partial v/\partial x$ | No | 0.121 | 8.3 | Yes | 0.026 | 10.1 |
| $\partial u/\partial x$ | No | 0.790 | 0.9 | No | 0.678 | 3.0 |

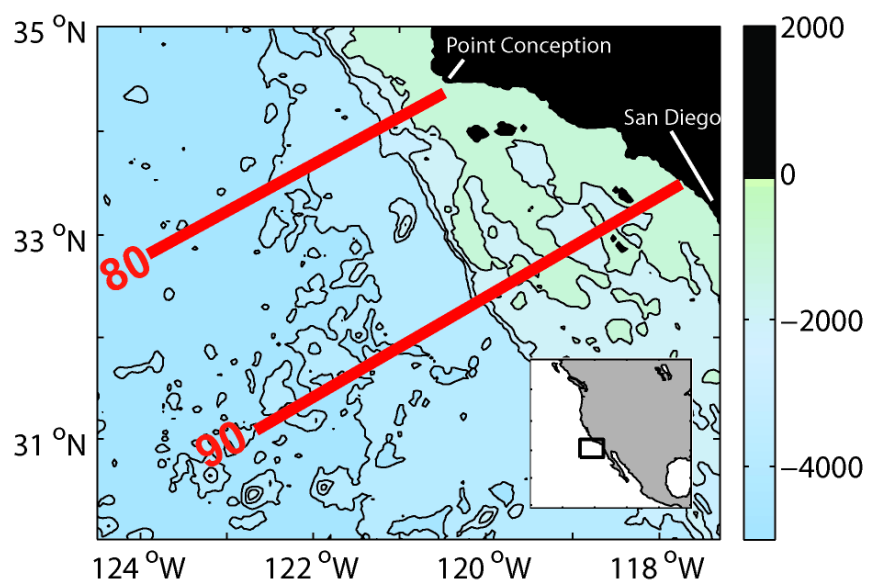


Figure 3.1. CCE-LTER Spray glider transect lines 80 and 90.

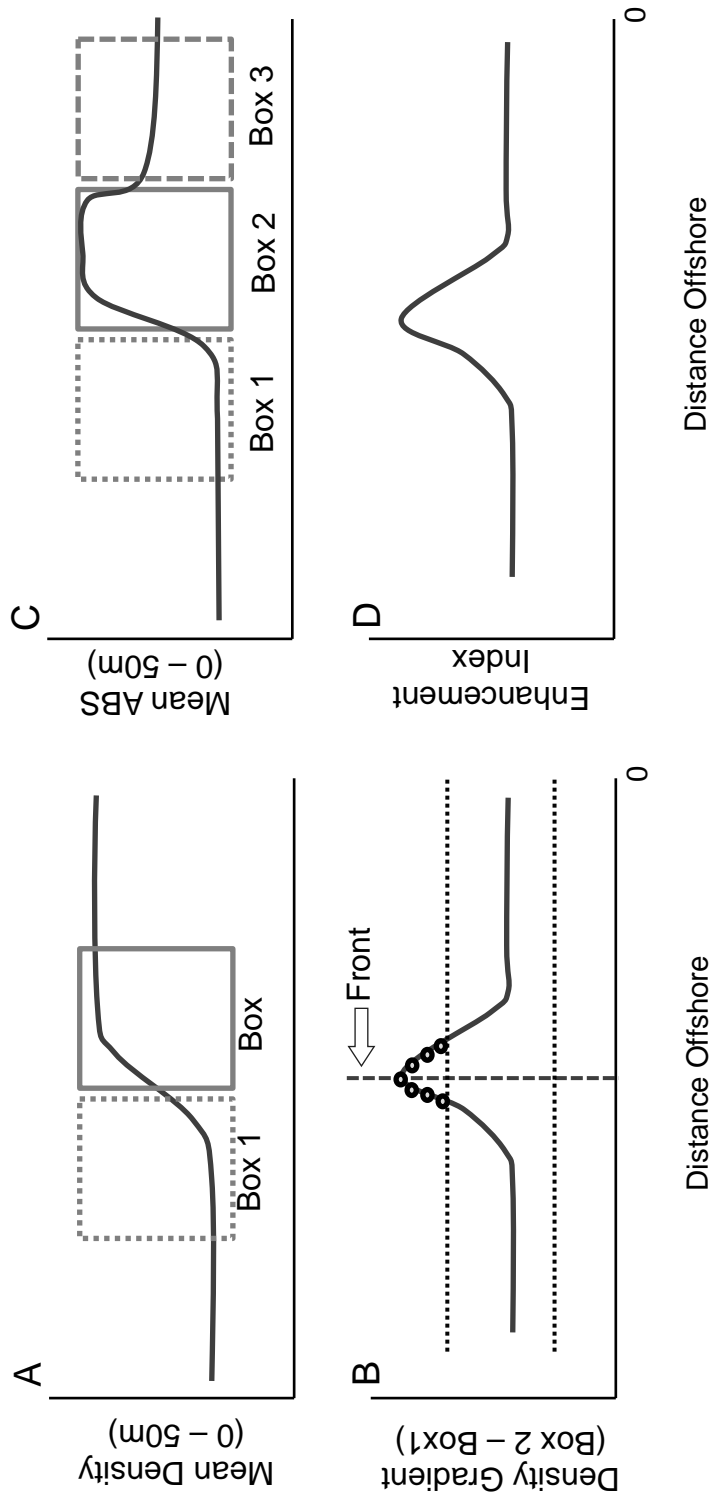


Figure 3.2. Schematic diagrams depicting the definition of gradients, fronts and enhancement indices. Gradients are calculated by subtracting the mean of mean surface density values (A and B) recorded during a 24h block of dives located offshore (Box 1) of a given dive from the 24h average inshore of a dive (Box 2). Fronts (vertical dashed line) are picked from contiguous run of dives (black circles, panel B) having gradients higher than the 95th or lower than the 5th percentile (dotted lines) of density gradients. The enhancement index (C and D) is equal to $A \times \text{MVBS}(\text{Box}2 - \text{Box}1) + \text{MVBS}(\text{Box}2 - \text{Box}3)$, where A equals 1 if Box2 is higher than Box1 and Box3, A equals -1 if Box2 is lower than Box1 and Box3, or A equals 0 otherwise.

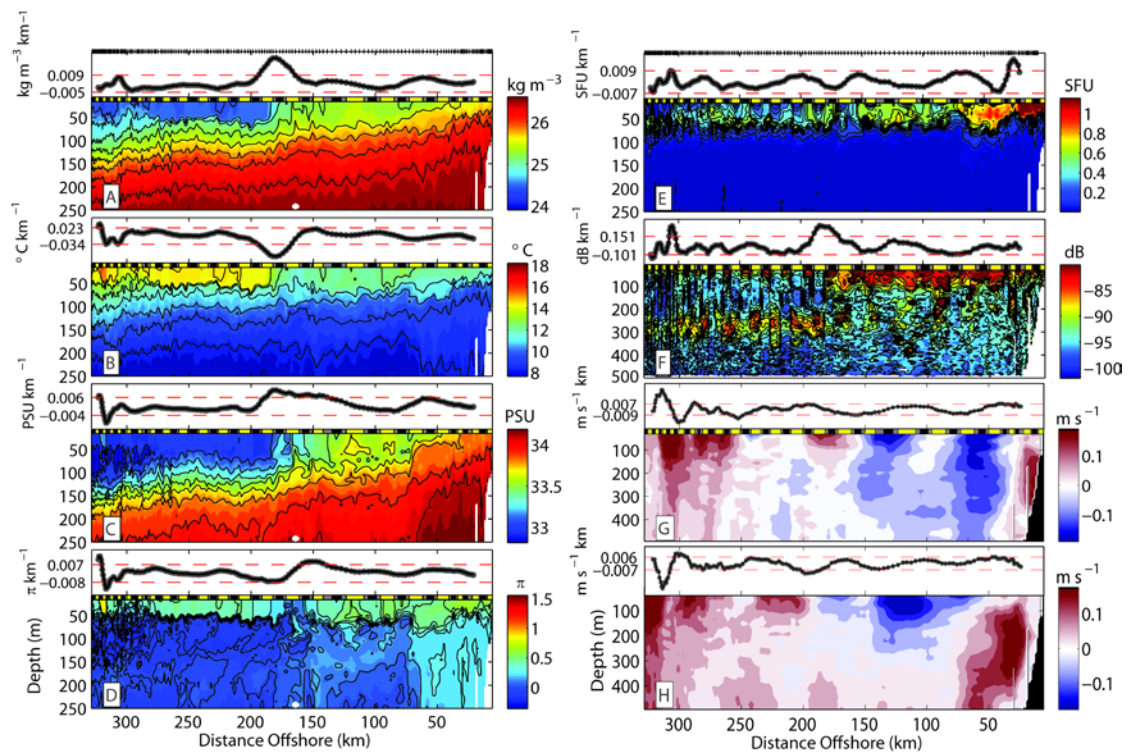


Figure 3.3. Glider sections along line 80 showing (A) density, (B) temperature, (C) salinity, (D) spiciness, (E) Chl-a (SFU), (F) acoustic backscatter (MVBS), (G) cross-track current velocity, and (H) along-track current velocity. Each panel shows a vertical section of a variable (in color), overlain by the near-surface (0 – 50 m) horizontal gradient of that variable (dark line). Tick marks at the top of panels A and E show the location of glider dives along the transect. Black and yellow bars at the top of each section plot indicate night and day periods, respectively. Dotted red lines in each gradient plot indicate the value of the 5th and 95th percentiles of the gradient calculated for the entire dataset.

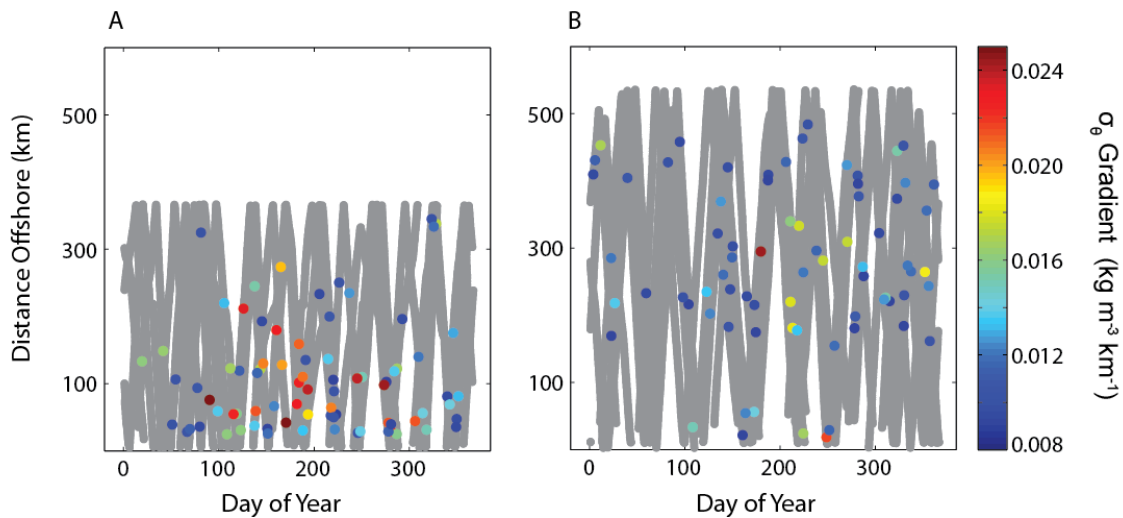


Figure 3.4. Seasonal and cross-shore distribution of density fronts along (A) line 80, and (B) line 90. Grey dots show the distribution of all dives from October 2006 through November 2011. Colored dots show dives that were identified as density fronts. Color scale depicts the strength of the horizontal density gradient.

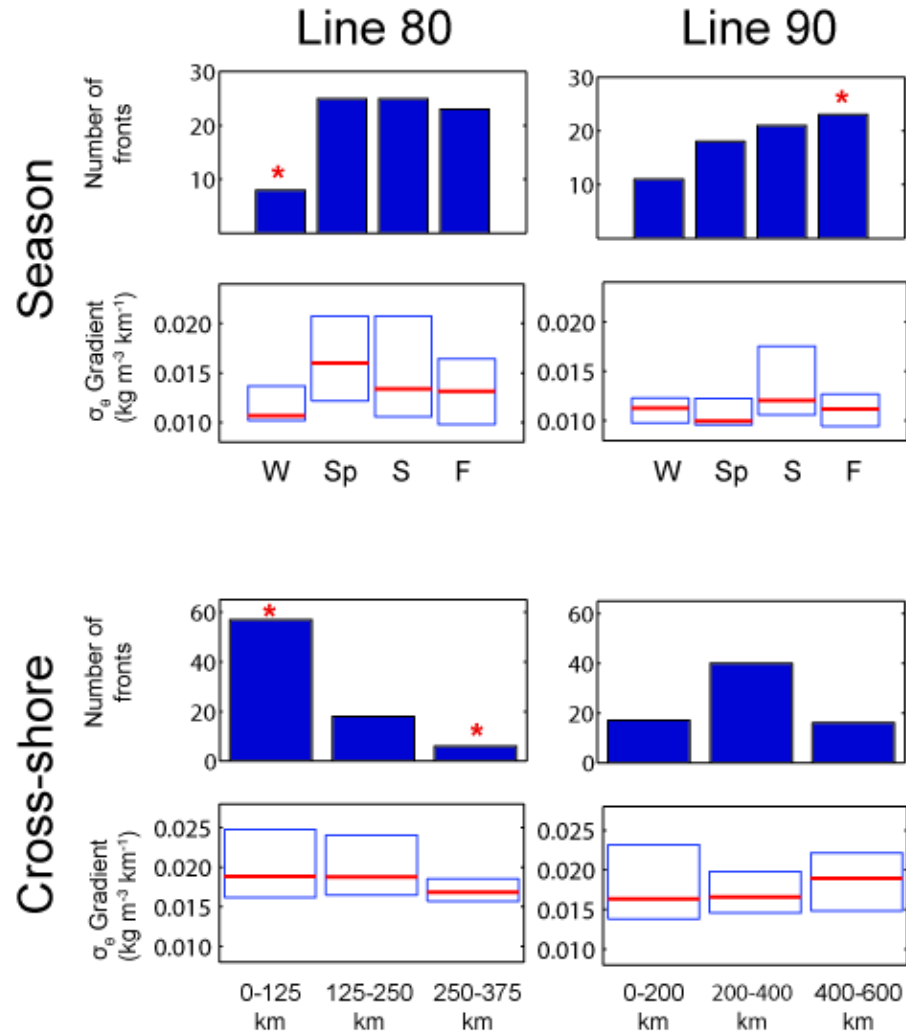


Figure 3.5. Incidence and gradient strength of density fronts along line 80 and line 90 by season and distance offshore. The upper and lower bounds of boxplots mark the 75th and 25th percentile values of the density gradients, respectively, the red line marks the median gradient value, and the p-value refers to significance of median difference. Red asterisks in bar charts indicate significantly increased or decreased front incidence ($p < 0.05$, binomial test with Bonferroni correction).

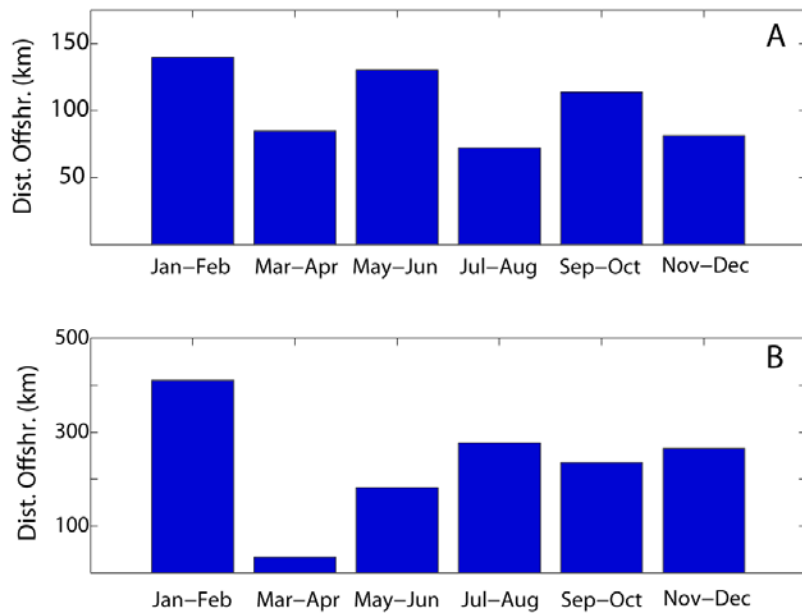


Figure 3.6. Median distance offshore of density fronts along (A) Line 80 and (B) Line 90 during bi-monthly periods throughout the year.

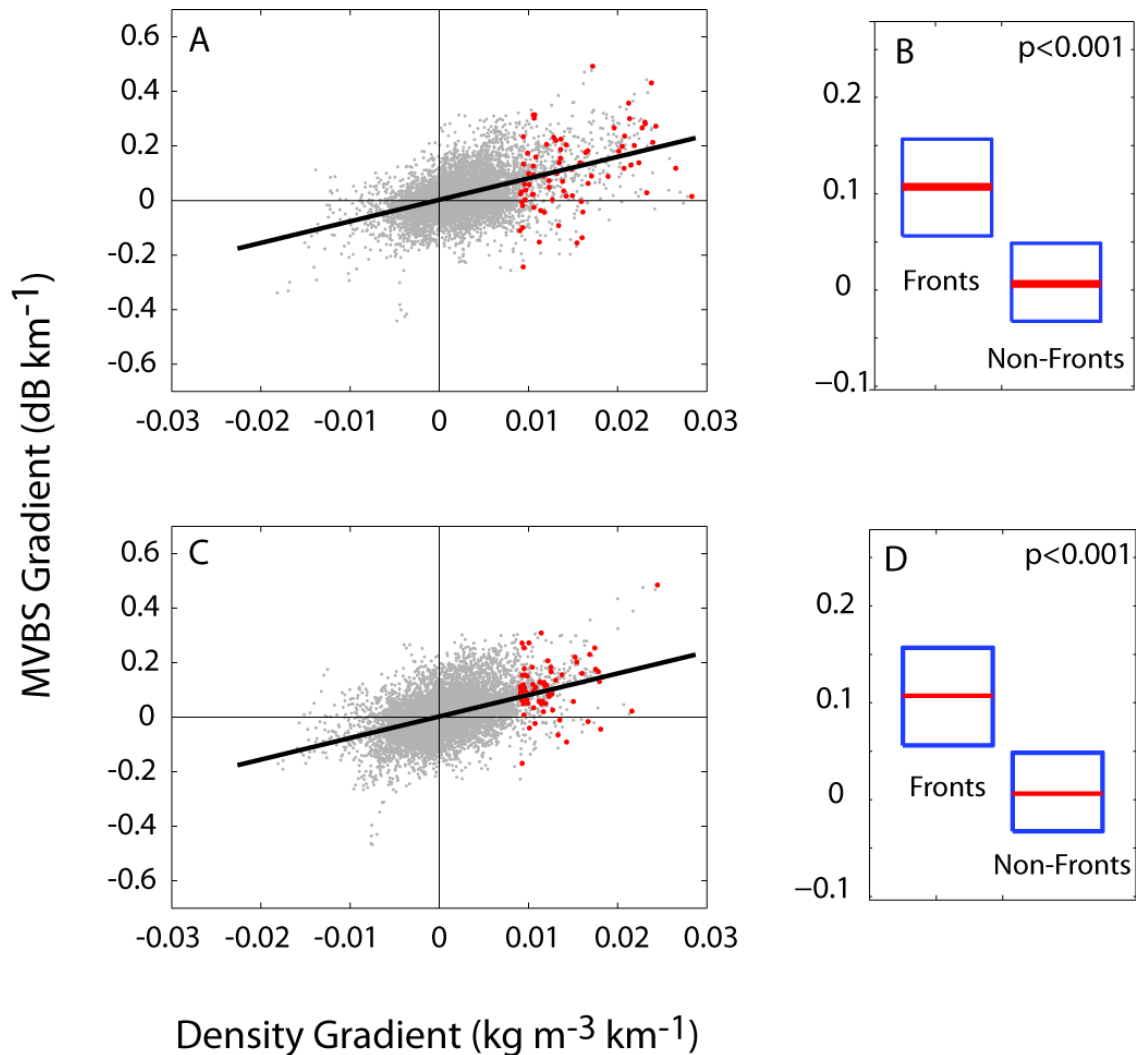


Figure 3.7. Covariability of horizontal gradients in Acoustic Backscatter (MVBS) and seawater density for (A and B) line 80 and (C and D) line 90 at fronts and non-frontal regions. Grey points in the scatterplots indicate all dives and red points are dives identified as density fronts. For boxplots, the upper and lower bounds mark the 75th and 25th percentile values of the MVBS gradients, respectively, the red line marks the median gradient value, and the p-value refers to significance of median difference.

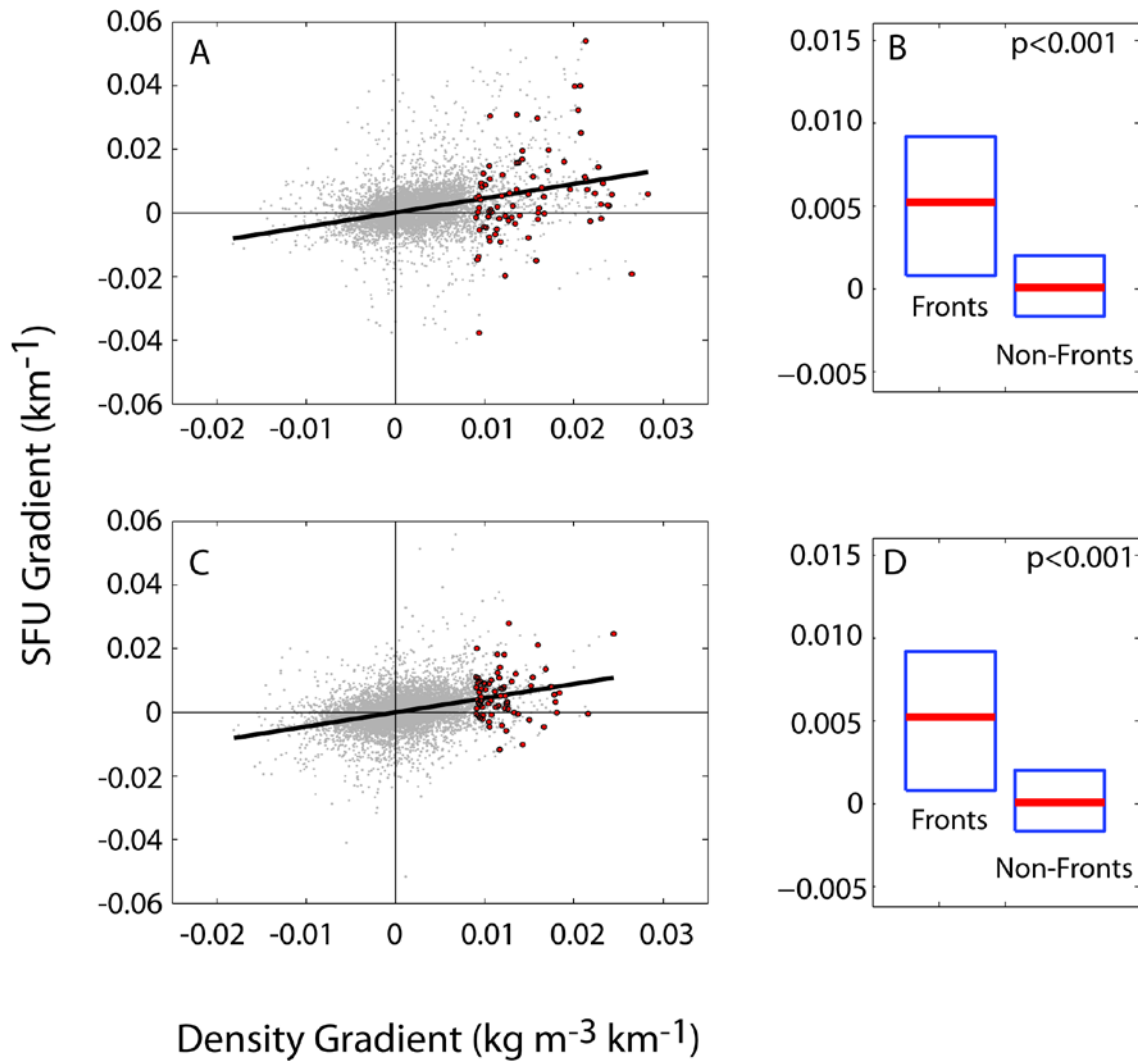


Figure 3.8. Covariability of horizontal gradients in Standard Fluorescence Units (SFU) and seawater density for (A and B) line 80 and (C and D) line 90 at fronts and non-frontal regions. Grey points in the scatterplots indicate all dives and red points are dives identified as density fronts. For boxplots, the upper and lower bounds mark the 75th and 25th percentile values of the SFU gradients, respectively, the red line marks the median gradient value, and the p-value refers to significance of median difference.

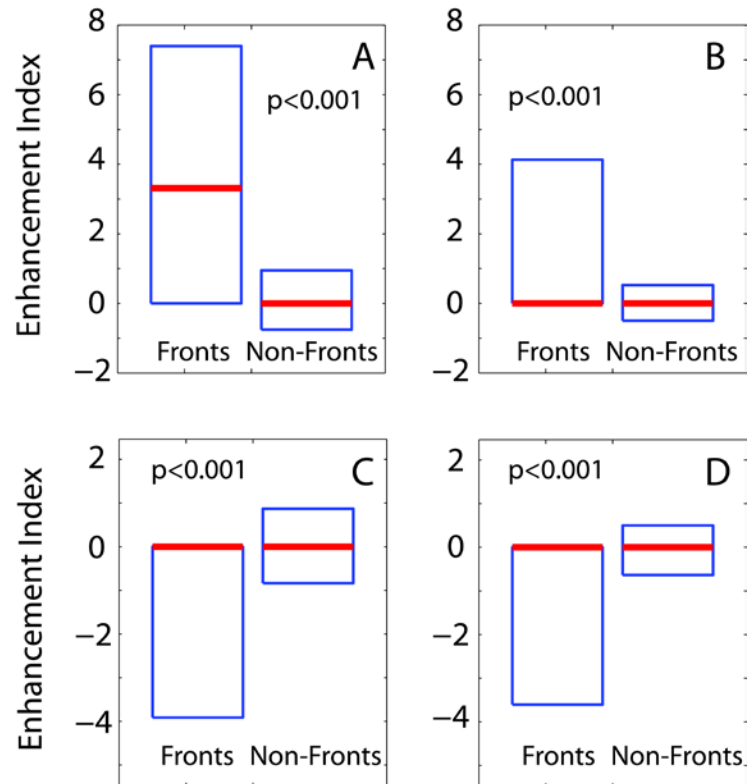


Figure 3.9. (A and C) Line 80 and (B and D) Line 90 MVBS Enhancement Index values in relation to fronts. A and B compare the enhancement index at fronts vs. non-fronts in regions of positive density fronts (i.e., where inshore density > offshore density). C and D compare the enhancement index in regions of negative density fronts (i.e., where offshore density < inshore density). Upper and lower bounds of each boxplot mark the 75th and 25th percentile values of the ABS gradients, respectively, red line marks the median gradient, and the p-value refers to significance of median difference.

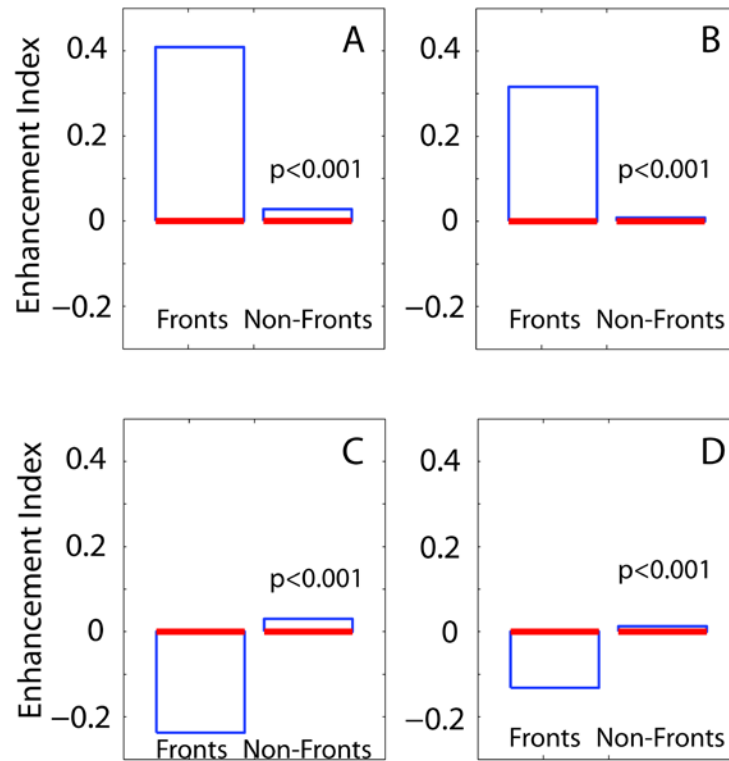


Figure 3.10. (A and C) Line 80 and (B and D) Line 90 Chl-a Fluorescence enhancement index in relation to fronts. A and B compare the enhancement index at fronts vs. non-fronts in regions of positive density fronts (i.e., where inshore density > offshore density). C and D compare the enhancement index in regions of negative density fronts (i.e., where offshore density < inshore density). Upper and lower bounds of each boxplot mark the 75th and 25th percentile values of the ABS gradients, respectively, red line marks the median gradient, and the p-value refers to significance of median difference.

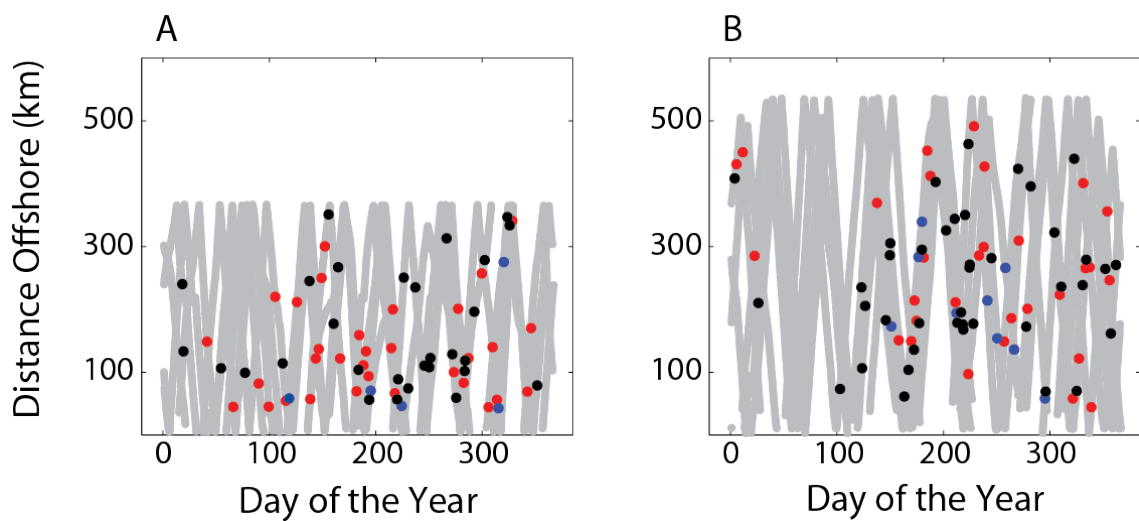


Figure 3.11. MVBS Enhancement Index at density fronts for A) line 80, and B) line 90. Red, blue and black dots indicate positive, negative and zero enhancement, respectively, at glider dives associated with density fronts. Grey dots indicate non-front dives.

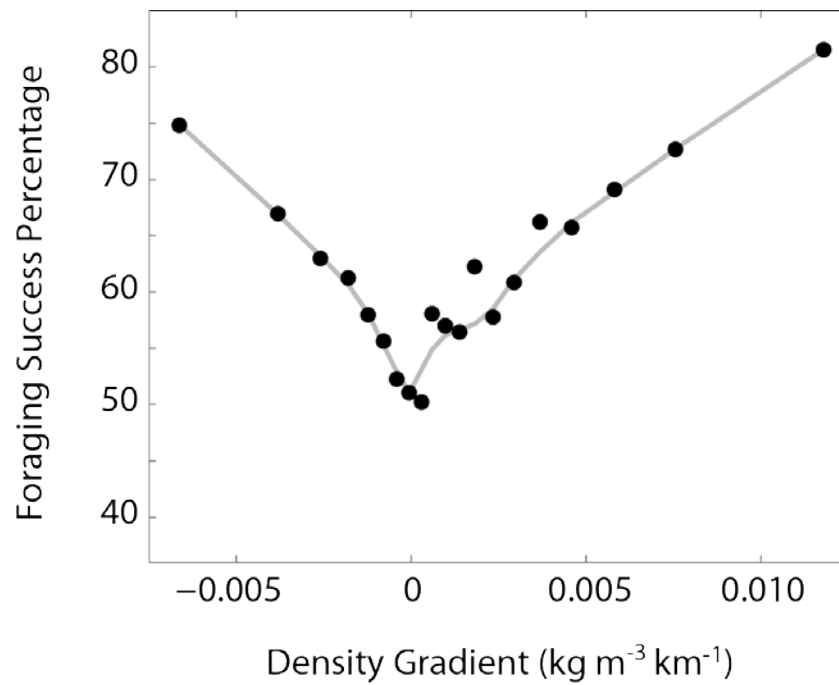


Figure 3.12. Percent chance for a mobile predator of locating waters with higher mean acoustic backscatter (MVBS) by migrating up a local density gradient. Positive density gradients indicate that the waters inshore of the location are denser than offshore while negative density gradients are opposite. The grey curve is generated with Loess smoothing.

CHAPTER 4:

Changes in zooplankton behavior and size distributions across glider-detected fronts in the Southern California Current System

Abstract

We report cross-frontal changes in the characteristics of plankton proxy variables as observed by autonomous ocean gliders operating within the Southern California Current System (SCCS). *Spray* gliders were deployed nearly continuously between 2006 and 2011 along two transect lines within the SCCS, during which time they conducted 22,942 profiles and identified 154 ocean fronts. A comparison of conditions across all of the identified fronts showed that waters inshore of the fronts were consistently colder, saltier and denser than waters offshore of the fronts. The average Chl-a fluorescence decreased and the depths of maximum Chl-a fluorescence and the euphotic zone increased offshore of fronts. Average Mean Volume Backscatter (MVBS) from a 3-beam 750 kHz acoustic doppler profiler was lower offshore of fronts, on average. The amplitude of diel vertical migration (DVM) increased offshore and covaried with optical transparency of the water column. Average interbeam variability in acoustic backscatter also changed across fronts within 3 depth strata (0-150 m, 150-400 m, and 400-500 m), revealing an intensification of vertical stratification of distinct scattering assemblages offshore of fronts. A Monte Carlo simulation was used to model the expected size spectra of faunal assemblages given glider

observations. Compared to offshore assemblages, inshore assemblages were best described with flatter size spectra, suggesting that larger-bodied zooplankters and micronekton contributed a greater portion to the overall biomass. Depth-stratified zooplankton samples collected by Mowness nets and analyzed digitally by ZooScan corroborated the pattern of increased zooplankton body sizes inshore of fronts.

Introduction

Ocean fronts can separate waters with very different temperature, salinity and nutrient profiles. Consequently, the floral and faunal assemblages on either side of a front can diverge. On one side of a front, for example, zooplankton may encounter relatively warm, clear and oligotrophic waters, while on the other, cold, turbid, and food-rich waters. Fronts, therefore, have long been thought to play an important role in spatially structuring biomass and species distributions (Lefevre, 1986; Sournia, 1994). Much of the research into the ecology of fronts, however, has focused on fronts that are either relatively persistent in time and space, such as occur at large-scale ocean convergences (Polovina et al., 2001), or else recur predictably due to their association with continental shelf breaks (Munk et al., 2003), tides (Pingree et al., 1975), nearshore upwelling (Smith et al., 1986), or estuarine mixing (Eggleston et al., 1998). Here we assess the roles of deep-water (sub)mesoscale fronts in structuring marine assemblages and habitats in an eastern boundary current system.

Oceanic fronts, particularly within boundary current systems, are dynamic features formed by quasi-geostrophic turbulence at the mesoscale (Spall, 1995), and by ageostrophic secondary circulation at the submesoscale (Capet et al., 2008). Such fronts span length scales of 1 to 500 km and persist from days to weeks. Mesoscale horizontal stirring can create a mosaic of potential habitats (Martin, 2003). Each of the many whorls and filaments visible in a satellite ocean color image may have experienced its own hydrographic evolution over a period of days to weeks, or longer, allowing the emergence of a dominant phytoplankton assemblage selected by the specific conditions of that water parcel (d'Ovidio et al., 2010). How zooplankton and nekton assemblages are affected by these shifting habitats is an open research area.

The California Current System (CCS) is an eastern boundary current flowing along the west coast of North America from Vancouver to Baja California (Hickey, 1979). Within the CCS there are three major interacting currents which transport four distinct water masses: the equatorward California Current transports cold, low-salinity, high nutrient, subarctic water from the north, and forms the eastern boundary to the warm, high-salinity, low nutrient waters of the Central North Pacific gyre. The Inshore Counter Current (ICC) transports water poleward in the nearshore region. The subsurface (200-500 m), poleward California Undercurrent (CUC) transports relatively warm, high-salinity, high nutrient waters from more southern sources (Gay and Chereskin, 2009; Simpson, 1984; Todd et al., 2011). The CCS is also notable for its complex and

vigorous mesoscale flows, which are primarily forced by seasonal upwelling-favorable winds along the coast (Marchesiello et al., 2003).

The CCS is therefore a mosaic of different water masses, horizontally stirred by eddies and jets, brought in close proximity to each other, and separated by ocean fronts. Within each filament or water parcel can exist a distinct phytoplankton assemblage. Satellite studies have been particularly useful in revealing the correspondence between physical features and phytoplankton within the CCS. Autocorrelation and analysis of coherence spectra of satellite SST and ocean color imagery reveal that, over a time scale of weeks, phytoplankton are passive tracers of the flows in which they are embedded (Denman and Abbott, 1994).

Ship-based studies of ocean fronts in the CCS have demonstrated that zooplankton biomass and abundance can change rapidly at ocean fronts. For example, Mackas et al. (1991) found a 3-4 fold increase in zooplankton biomass across a cold-water filament extending offshore from Point Arena, California. These authors also documented a clear shift from a more doliolid-dominated assemblage on the warm side of the filament to a crustacean-dominated assemblage within the filament and extending to its cold side. In a study of the Ensenada Front within the southern CCS (SCCS), Haury et al. (1993) noted a 3-fold change in primary productivity and 3-4 fold change in zooplankton displacement volume over a distance of less than 15 km across the front. In a study of a different front (the A-front) in the same area, abundances of calanoid copepods were elevated within the front, and a herbivorous, particle-

grazing zooplankton assemblage on the cool side of the front shifted to a more carnivorous-dominated assemblage on the warm side (Ohman et al., 2012).

Fronts are also ecologically important because of their potential as regions of altered zooplankton reproduction and growth rates. Increased food availability at fronts due to convergent flows or local production can promote increased egg production and spawning. Smith and Lane (1991) found that *Eucalanus californicus* within the Point Arena cold filament were able to maintain increased egg production without drawing down their lipid reserves, due to the increased food availability within the filament. In the A-Front study, Ohman *et al.* (2012) also noted an increased abundance of copepod nauplii within the front, suggesting that secondary production was increased there. Balancing this potential for increased secondary production is the potential for increased predation rates. Fronts have long been known to attract highly-mobile planktivorous predators, including fish (Humston et al., 2000), seabirds (Ainley et al., 2009), baleen whales (Munger et al., 2009), as well as turtles (Polovina et al., 2004). Increased abundances of carnivorous zooplankton such as narcomedusae can also be found at fronts (McClatchie et al., 2012).

Many of the ecosystem changes observed across fronts are not due to the presence of the front *per se*, but because the waters on either side of the front provide contrasting environments where different assemblages come to dominate. Ship-based studies within the SCCS have identified cross-shore trends in phytoplankton and zooplankton assemblages in relation to cross-shore hydrographic trends. An analysis of recurrent assemblages of phytoplankton

within the SCCS found two major assemblages: an inshore group dominated by diatoms that varied strongly by season, and a less variable offshore group dominated by coccolithophorids and dinoflagellates (Venrick, 2009). Offshore assemblages were associated with the formation of a deep chlorophyll maximum (usually near the base of the euphotic zone and slightly above the nitracline). The transition from waters with low surface chlorophyll (i.e., an offshore-type assemblage) to high-surface chlorophyll often occurred abruptly across the inshore edge of the low-salinity core of the California Current (about 100-150 km offshore).

Zooplankton within the SCCS also show some general cross-shore trends in zooplankton biomass. Ohman and Wilkinson (1989) found that the ash-free dry weight of zooplankton decreased offshore along cross-shore transects in the CalCOFI survey region. Other studies have found a long-term local maximum in zooplankton displacement volume located approximately 100 km offshore, that is maintained either due to advection of zooplankton-enriched waters from the north (Chelton et al., 1982), or possibly due to increased secondary production fostered by strong wind-stress curl driven upwelling offshore (Chelton, 1982; Rykaczewski and Checkley, 2008). Offshore of the local maxima, however, the long-term average of zooplankton displacement volumes decreases monotonically.

Our understanding of the ecological changes across ocean fronts come mostly from limited duration ship-based studies of individual fronts, rather than an extended program of study spanning a variety of frontal conditions over a multi-

year period. To effectively quantify the ecological changes observed across fronts within a region, it is necessary to sample a representative distribution of such features, not just anecdotal examples. The advent of autonomous ocean gliders has opened new opportunities for continuous *in situ* measurements across (sub)mesoscale features in the California Current System (Davis et al., 2008). Within the SCCS, an analysis of data collected over a six-year period Powell (in review) using six years of observations from *Spray* ocean gliders concluded that horizontal gradients in physical properties (e.g., temperature, salinity and density) co-varied with horizontal gradients in Chl-*a* fluorescence and acoustic backscatter at 750 kHz. Frontal regions were more likely to be zones of elevated acoustic backscatter (inferred to be zooplankton) compared to non-frontal regions. Powell (in review) also estimated that large mobile, planktivorous predators were likely to encounter more favorable foraging conditions up to 77% of the time when travelling up a density gradient.

In the present analysis, we examine cross-frontal changes within the SCCS in the vertical distribution of phytoplankton Chl-*a* and the acoustic characteristics, body size, taxonomic composition and diel vertical migration behavior of faunal assemblages. We test three hypotheses related to glider-detected fronts in the SCCS:

Hypothesis 1: The depth of the chlorophyll maximum and the depth of the euphotic zone increase when crossing from the denser to less dense side of fronts.

Hypothesis 2: The amplitude of Diel Vertical Migration behavior increases when crossing from the denser to less dense side of fronts.

Hypothesis 3: The size structure of zooplankton and micronekton assemblages changes across fronts.

Methods

Study area and duration

Spray ocean gliders were deployed nearly continuously along lines 80 and 90 of the California Current Ecosystem Long-Term Ecological Research (CCE-LTER) and CalCOFI sampling area (Fig. 4.1) between October 2006 and July 2011 (and continue to operate to present). The gliders traveled along the two lines from about 20 km off the coast to a maximum 370 km (line 80) and 585 km (line 90) offshore. A total of 124 transects were completed during the study period comprising 22,942 vertical profiles.

Spray glider and instrument payload

The *Spray* glider (Sherman et al., 2001) is an autonomous underwater vehicle capable of conducting profiles to 1000 m depth for up to 4 months at a time. The *Spray* glider profiles in a sawtooth pattern, travelling through the water at an angle of 17° from the horizontal and at an average speed of 25 cm s⁻¹. For this study, gliders descended to a maximum depth of 500 m, or to within approximately 5 m from the bottom in shallower waters. Upon completion of each profile, the glider surfaces, establishes a GPS fix, and uploads data via the

Iridium satellite system. The glider follows a pre-programmed mission along a transect until it receives instructions to change operations. In waters deeper than 500 m, the glider completes a profile cycle every 3 hours, on average, with an average spacing between profiles of 3 km.

The *Spray's* instrument payload during this study included a pumped Seabird 41CP Conductivity-Temperature-Depth (CTD) sensor, a Sontek 750-kHz, 3-beam Acoustic Doppler Profiler (ADP), and a mini-Seapoint chlorophyll a fluorometer (mini-SCF). The fluorometers used in this study had a central excitation peak of 470 nm and measured fluorescence at an emission peak of 685 nm. Seawater is pumped through the CTD and the fluorometer to maintain a constant flow rate past the sensors. A biocide inhibits Biofouling when the pump is not operating. Sensors are powered and data recorded only during ascent.

Fluorometers were calibrated before and after each glider deployment using a standard set of dilutions of pure chlorophyll a (Sigma Life Sciences) dissolved in 90% acetone. Each Chl-a standard was placed within a machined cuvette-holder that held the standard solution in a 13-mm diameter borosilicate cuvette at a fixed distance from the optical surfaces of the fluorometer. For each calibration, a slope ($\mu\text{g Chl-a L}^{-1} \text{ V}^{-1}$) was determined from a regression of recorded voltage with dissolved Chl-a concentrations. Regular calibration permitted sensor drift and biofouling to be tested, enabled inter-comparison of data from the same sensor during different deployments, and also comparability of data recorded by different sensors. Biofouling was never detected, and sensor drift was negligible and corrected for by our calibration procedure. We report the

observed fluorometer response in standardized Chl-a fluorescence units (SFU), where one SFU is defined as the measured fluorescence signal (in volts) from 10 $\mu\text{g L}^{-1}$ of Chl-a dissolved in 90% acetone at a fixed path length (SFUs were previously reported as Dissolved Chlorophyll Fluorescence Equivalents (DCFU) in Davis et al., 2008). In vivo fluorescence data were converted into SFU by multiplying the recorded voltages by the mean slope value determined from pre- and post-deployment calibrations. For the fluorometers used in this study, one SFU corresponds very approximately to 2 $\mu\text{g Chl-a L}^{-1}$.

The Sontek ADP mounted on *Spray* points directly down during glider ascent, so that each of the three beams has a slant angle of 25° from vertical. Each beam has a 3 dB beam-width of 2°. Both current velocity and acoustic backscatter (ABS) data from the ADP are recorded upon ascent in five 4-m vertical range bins so that vertical resolution of the completed profile is 4 m. The acoustic backscatter measured by the ADP is reported in acoustic counts, which is the digitized output from a log-linear amplifier. Regular calibration of each ADP instrument before and after each glider mission using a standard tungsten-carbide target suspended in a test pool revealed an average difference in ABS recorded by an individual ADP across multiple deployments of 2.5 dB, and an average difference between different ADP instruments of 3 dB.

ABS recorded during glider deployments is converted into Volume Backscatter, S_v , using the sonar equation $S_v = RL - SL + 2TL - 10 \text{Log}_{10} V$, where Receiver Level (RL) is the recorded ABS in dB, Source Level (SL) in decibels is empirically determined during instrument calibration, Transmission

Loss (TL) is equivalent to $20 \text{ Log}_{10} R + \alpha R$, where R is the range in meters to the midpoint of the bin and α is the sound attenuation coefficient (dB m^{-1}), and V is the volume in cubic meters. Volume backscatter measurements are averaged to yield Mean Volume Backscatter (MVBS).

Previous work comparing ABS recorded by the Sontek ADP with collected net samples established that recorded ABS is proportional to the log of zooplankton biomass in the vicinity of the ADP (Powell and Ohman, 2012). ZooScan image analysis of zooplankton in net samples showed ABS was most closely related to zooplankton with an equivalent circular diameter ≥ 1.6 mm, approximately the acoustic wavelength emitted by the transducer. In Powell and Ohman (2012), the method used to calculate relative MVBS relied on a different formulation of the sonar equation (SonTek, 1997). The standard sonar equation presented here (Medwin and Clay, 1998) includes a $10 \text{ Log}_{10} V$ term rather than a $10 \text{ Log}_{10} PL$ term (where PL is the acoustic pulse length), which permitted comparison of backscatter from different range cells. Applying this method to the data from Powell and Ohman (2012) did not alter any of the results or conclusions of that paper.

Glider data processing

Data from each glider deployment were checked for quality and imported into MATLAB for subsequent processing. Bad data, as determined by quality control processing scripts or visual inspection, were excluded from further analysis. The data from all glider deployments were then harvested into a master

MATLAB dataset and grouped by transect. Only data from complete transects, where the glider completed 90% or more of its intended trackline, were included in the analysis. Variables included in this study include temperature, salinity, potential density, Chl-a fluorescence (as SFU), salinity on potential isopycnals, which has the same information as spice (Flament, 2002), and MVBS measured within each of the three acoustic beams. For each profile within a given transect, all data were vertically averaged into 5-m bins.

Front definition and canonical front construction

Directly comparing glider data from one profile to the next is difficult due to diel periodicity in biological signals (in both MVBS and *in vivo* fluorescence data), and by the influence of internal tides and inertial motions (in the case of hydrographic variables). Comparing MVBS data, in particular, is complicated by diel vertical migrations (DVM) by zooplankton (Ohman et al., 1998) and micronekton (Pearcy et al., 1977). Also, measured fluorescence in surface waters is strongly affected by the daytime decrease in Chl-a fluorescence due to non-photochemical quenching, and to daytime photo-protective strategies employed by phytoplankton (Cullen and Lewis, 1995). For these reasons, both physical and biological data were smoothed prior to use by averaging observations within a 24-hour period. Gradients are defined as the difference between averages of properties from the 24 h periods before and after the glider reached a location. By definition here, a gradient is the offshore average minus the inshore average.

Fronts within any particular transect were identified algorithmically. Dives with horizontal density gradient values greater than the 95th percentile (of all line 80 or line 90 values within the dataset) or less than the 5th percentile (of all line 80 or line 90 values within the dataset) are flagged as potential “positive” or “negative” density fronts, respectively. When more than one contiguous dive is flagged as a potential front, the dive with the maximum (minimum) gradient value within the contiguous run of dives is denoted as a positive (negative) density front. Only positive density fronts (i.e., those where surface density is higher on the inshore side of the front) are considered in this analysis.

Averaged, or ‘canonical’ front sections were created by first aligning all glider sections containing individual fronts relative to the front location ($x=0$). Then all data located inshore and offshore of those frontal locations were binned by distance from the front in 10-km increments. Vertical binning remained at 5 m. The average value of data within each bin was then computed to produce canonical sections of hydrographic and biological variables.

Interbeam differencing and smoothing algorithms

The *Spray* ADP has three acoustic beams. Starting with raw, unbinned volume backscatter (S_v) data, the maximum interbeam difference in volume backscatter (maxDSV) is defined as the maximum difference in recorded S_v between any two of the beams within ADP range cell 3 (16-20 m). The maxDSV from cell 3 for each profile was then binned into 5-m vertical bins and averaged. A smoothed binned maxDSV section was generated by filtering the binned raw

maxDSV data using a two-pass Gaussian filter with a kernel window five rows by N columns, where N equals the number of dives occurring within a 24 h window centered on the dive of interest.

Mocness sample processing and ZooScan analysis

Vertically stratified net samples of zooplankton were collected by Mocness (Wiebe et al., 1985) tows during the P0605, P0704 and P0810 process cruises of the CCE-LTER program (<http://cce.lternet.edu/data/cruises/>). For each cruise, Mocness tows were categorized by their location with respect to the major frontal feature along line 80 (identified contemporaneously either by *Spray* glider (P0704 and P0810) or by ship-based Moving Vessel Profiler (P0605)). Tows were categorized as either inshore or offshore of the front (Fig. 4.1).

For each Mocness tow, nine nets were opened sequentially to collect zooplankton in 50-m vertical strata from 450 m to the surface. All plankton net samples were preserved in 1.8% formaldehyde buffered with sodium tetraborate. The plankton within each net sample were then processed ashore using ZooScan (Gorsky et al., 2010). Prior to digital imaging, the sample was first passed sequentially through 1000- μm and 202- μm mesh filters. The zooplankton retained on each filter were then resuspended in a measured volume of filtered seawater, and aliquots were removed from each of the size-fractionated samples for ZooScan imaging. Resuspension volumes and aliquot volumes were chosen so that an average of approximately 1500-2000 animals from the 202- μm size fraction and 400-700 animals from 1000- μm size fraction were imaged per scan.

Two scans of each size fraction were performed. Because large-bodied zooplankters were thought to be underrepresented in the above scans, a secondary set of scans of a 5000- μm mesh-filtered fraction was subsequently performed. All animals retained on the 5000- μm mesh were imaged. To avoid double counting the larger zooplankters that might have been imaged in the original set of scans, a sample-specific zooplankter size threshold was identified using the zooplankters' Equivalent Spherical Diameters (ESD) as measured by the ZooProcess software. The size threshold was defined as the ESD value where the numerical abundance of zooplankters measured in the original scans dipped below the numerical abundance of zooplankters measured in the secondary scans. All data from zooplankters above this size limit present in the original scans were discarded, and the remaining data from the original and secondary scans were merged.

Each zooplankter within the merged dataset is associated with a suite of feature measurements (e.g., ESD, area, ferret length, etc.) as measured by the ZooProcess software (see Gorsky et al., 2010). The images containing individual zooplankters, also termed Regions of Interest (ROI), were then categorized into one of 20 zooplankton taxonomic categories using the Random Forest algorithm. All machine-classified images were checked manually and the classifications corrected as necessary. For presentation, categories were aggregated here into: calanoid copepods excluding eucalanids, euphausiids, chaetognaths, eucalanid copepods (which were an optically distinctive group), and all other taxa combined. Two specific feature measurements (feret diameter and area

excluded) were used to calculate carbon biomass of each imaged zooplankter, using taxon-specific relationships (Lavaniegos and Ohman, 2007). Finally, sample-specific C biomass concentrations and abundances for the different taxonomic categories were calculated using sampling depth, volume filtered by the net, and fraction of sample scanned.

Estimating depth of Chl-a max and the euphotic zone.

The depth of the *Chl-a* fluorescence maximum along the length of a transect was estimated using nighttime glider profiles. Daytime profiles were not used for this purpose due to daytime quenching of fluorescence near the sea surface. Daytime depths of the *Chl-a* fluorescence maximum were estimated by fitting a cubic spline to the flanking nighttime data.

Euphotic zone depths were estimated by finding the depth at which the interpolated light level was 1% of the surface. The percent light level at the bottom of each depth bin was determined iteratively, where light level, I_{k+1} , at bin $k+1$ was calculated as:

$$I_{k+1} = I_k \times e^{-KZ_w} \quad [1]$$

where I_k is the light level at the bottom of the depth bin immediately above bin $k+1$, Z_w is the thickness of the depth bin (5 m), K is the diffuse attenuation coefficient for type I oceanic waters (Morel, 1988), defined as $K=0.121 \times C^{0.428}$, and C is the mean chlorophyll concentration (mg m^{-3}) of the bin $k+1$ and is equal to $C= \text{SFU} \times 2$.

DVM calculations

For each glider dive, the depth of the layer of maximum acoustic backscatter was estimated by calculating the median depth of bins containing MVBS values above the 85th percentile for that dive. The amplitude of DVM for a given dive was then calculated by subtracting the median daytime scattering layer depth from the median nighttime scattering layer depth within a window including all dives plus or minus 12 hr from the given dive. The gradient in DVM amplitude at a given dive location was the mean DVM amplitude occurring in a 24-hr window inshore of the dive minus the mean DVM amplitude in a 24-hr window offshore of the dive.

Acoustic modeling and Monte Carlo simulations

Single-beam, single-frequency echosounders are often considered to be of limited utility when characterizing a population of acoustic scatterers (Lavery et al., 2007). However, with enough data, the variability of acoustic backscatter can be used to model potential size distributions within target assemblages. We model the most likely size spectra of zooplankton assemblages within an area given a large number of glider observations. First, the expected mean volume backscatter (MVBS) and expected maximum interbeam difference in volume backscatter (maxDSV) were estimated for simulated zooplankton assemblages using a Monte Carlo approach for a range of possible zooplankton size spectra. For each given zooplankton size spectrum, n (where $n=ad^{-b}$, d is the zooplankton's ESD in cm, and the intercept, a , and slope, b , are specified

parameters), 1000 simulated sampling volumes containing synthetic assemblages of zooplankton were created by assigning a numerical density of zooplankters within each of 1000 logarithmically-spaced size bins ranging from 0.01 cm to 10 cm ESD. For each simulated sampling volume, numerical density of zooplankters within each size bin was generated by sampling from a Poisson distribution (where the lambda parameter is the expected numerical density of zooplankton for a given size spectrum). The expected volume backscatter, S_v , of the simulated assemblage was then calculated by summing the acoustic backscatter (conventionally identified as lower case "sv") of each individual zooplankter within the sampling volume: $S_v = 10 \log \sum sv$ (Medwin and Clay, 1998). Acoustic backscatter, sv, from individual zooplankters was estimated using a bent cylinder acoustic model (Greene et al., 1998) where the length parameter, L, was calculated for the zooplankter given the ESD and an aspect ratio of 3:1. The average expected MVBS and expected maxDSV for assemblages created from a given size spectrum were then calculated by averaging across all 1000 simulated sampling volumes the simulated MVBS values and the absolute value of differences between simulated values, respectively. Expected MVBS and expected maxDSV across a range of size spectrums were thus estimated by varying the slope and intercept values of the size spectrum.

General functions relating MVBS [eq. 1] and maxDSV [eq. 2] to spectral slope and intercept values were then generated by fitting a surface to the output data from the Monte Carlo simulations.

$$MVBS = 10.19 a - 4.911 b - 27.4 \quad [1]$$

$$maxDSV = -0.556a - 1.875b + 0.159a^2 - 0.578ab - 3.304 \quad [2]$$

Inverse modeling of zooplankton size spectra

The expected intercept [eq. 3] and expected slope [eq. 4] were solved using a system of equations with [eq. 1] and [eq. 2]:

$$Intercept = \left(\frac{MVBS}{10.19} \right) + 0.78DSV + 1.08 \quad [3]$$

$$slope = \frac{DSV + 3.304 + 0.556\alpha - 0.159\alpha^2}{-0.578\alpha - 1.875} \quad [4]$$

where, $\alpha = (MVBS/10.19) - 2.855$

Results

Zooplankton habitat changes across fronts

When transiting any particular front along both glider lines 80 and 90, surface waters (0-50 m) are consistently colder and saltier inshore of fronts compared with offshore (Fig. 4.2). The hydrographic conditions of fronts and their flanking regions vary on a case by case basis. Fronts occurring during summer and fall, for instance, often occur in warmer waters than those of spring and summer. Thus, waters inshore of a front in summer can be warmer than offshore waters during the winter. Nonetheless, when all fronts are averaged together to create a canonical front, the density and salinity structures in regions flanking a front are markedly different in the upper 100 m (Fig. 4.3).

Cross-frontal changes in acoustic backscatter (MVBS) and Chl-*a* fluorescence (Fig 4.4) are more variable than those for density or salinity. In some cases, MVBS or fluorescence increases offshore of fronts. However, on average, MVBS and Chl-*a* fluorescence are lower offshore of fronts. Both MVBS and fluorescence are lower offshore of the reconstructed canonical front (Fig. 4.5). Inshore of the line 80 and line 90 canonical fronts, MVBS is not only greater overall, but the mean vertical gradient in MVBS from the surface to 100 m is increased as well. Similarly, there are changes in mean Chl-*a* fluorescence and in vertical distributions of Chl-*a* fluorescence across the line 80 and line 90 canonical fronts. Offshore regions for both lines 80 and 90 exhibit a subsurface maximum in Chl-*a*, whereas inshore of canonical fronts only line 90 shows a consistent subsurface maximum.

*Chl-*a* fluorescence maximum and the euphotic zone depth*

The depth of the Chl-*a* fluorescence maximum generally increases with distance offshore, although the depth of Chl-*a* fluorescence maximum can increase and decrease multiple times along a given transect (e.g., Fig. 4.6). However, the trend when crossing density fronts is clear: on average, the depth of the Chl-*a* maximum increases when moving offshore across fronts (line 80: $p < 0.001$; line 90: $p < 0.001$; Fig. 4.7a,b), and the change in depth is greater at fronts compared with non-fronts (line 80: $p < 0.001$; line 90: $p < 0.001$; Fig. 4.7c,d). The median cross-front change in depth for line 80 and line 90 is 9.2 m and 7.9 m, respectively. The modeled depth of the euphotic zone (i.e., the depth at which

modeled light levels are 1% those of the surface) is correlated with the depth of maximum Chl-a fluorescence ($r^2=0.61$; Fig 4.8), suggesting that, on average, water clarity is greater offshore of fronts compared to inshore.

DVM amplitude changes across fronts

The amplitude of diel vertical migration (DVM), i.e., the difference in depth between daytime and nighttime layers of maximum acoustic backscatter, is often greater offshore of fronts compared to inshore (Fig. 4.9). The change in DVM amplitude (Fig. 4.10) is significantly greater across fronts compared to non-fronts for both line 80 ($p=0.030$) and line 90 ($p=0.001$). In some cases, migrating animals located offshore of a front descend 200-300 m deeper during the day compared with animals located immediately inshore of a front. Across the entire dataset, DVM amplitude is non-linearly related to the modeled depth of the euphotic zone (Fig. 4.11). When the euphotic zone is shallower than 50 m, the median DVM amplitude is less than 25 m. However, when euphotic zone depths are deeper than 50 m, the median DVM increases greatly to over 200 m in some cases.

Horizontal gradients in maxDSV

Changes in interbeam differences in acoustic backscatter (i.e., maxDSV) at fronts were analyzed to gain insight into front-associated changes in the scattering characteristics of faunal assemblages. Fronts were sometimes associated with altered horizontal gradients in maxDSV, but only within specific

depth strata (Fig. 4.12b). Along line 80, the magnitude of horizontal gradients in maxDSV were significantly greater at fronts compared to non-fronts in the 400-500 m depth stratum ($p < 0.001$; Fig. 4.13c), suggesting that maxDSV increases when moving offshore across fronts within this layer. There were no significant cross-frontal differences observed in the 0-150 m or 150-400 m depth strata along line 80 ($p > 0.05$; Fig. 4.13a,b). In contrast, along line 90, the magnitude of horizontal gradients in maxDSV was significantly greater at fronts compared to non-fronts in the 0-150 m and the 150-400 m depth strata ($p = 0.033$ and 0.035 , respectively; Fig. 4.13d,e), but not within the 400-500 m stratum ($p > 0.05$; Fig. 4.13f).

Cross-frontal water column scattering characteristics

Both MVBS and maxDSV are a function of the scattering characteristics of the resident assemblage. Offshore of fronts, there were strata within the water column with similar MVBS values (suggesting potentially similar biomass concentrations) but with dissimilar maxDSV values. For example, although MVBS is similarly low between 100-200 m and 400-500 m strata in Figure 4.12a, these layers comprise very different scattering populations, as shown by the maxDSV values in Figure 4.12b. For waters located within a 24-hr window offshore of fronts, the observed MVBS of these two depth strata overlap considerably, while the observed maxDSV values are more separated for both lines 80 and 90 (Fig. 4.14). Offshore of fronts, the maxDSV values of 400-500 m strata are significantly greater than those of the 100-200 m strata for line 80 and

line 90 (Mann-Whitney U: $p < 0.001$), with a median maxDSV difference between the two strata of 1.29 dB and 1.40 dB for lines 80 and 90, respectively. Inshore, the maxDSV values of the 400-500 m strata are still significantly greater than those of the 100-200 m strata (Mann-Whitney U: $p < 0.001$). The median maxDSV differences between the two strata are 1.03 dB and 1.29 dB for lines 80 and 90, respectively.

Modeled changes in zooplankton size structure

Glider-observed scattering characteristics (i.e., MVBS and maxDSV) change significantly across fronts for both the daytime and nighttime layers of maximum acoustic backscatter. For both line 80 and line 90, waters inshore of fronts exhibited higher average MVBS and lower average maxDSV for both daytime and nighttime scattering layers (Table 4.1).

To examine this relationship further, we conducted a Monte Carlo simulation of expected MVBS and maxDSV (Figs. 4.15a and 4.15b, respectively) given a range of zooplankton size spectra, $n=ad^b$, where a is the spectral intercept, b is the spectral slope, and d is the ESD in centimeters of a given zooplankter. The Monte Carlo results reproduced expected trends in MVBS and maxDSV given changing spectral parameters. For example, MVBS increases with increasing spectral intercept values (Fig. 4.15a), and slightly decreases with less negative slope values (due to the increasing likelihood that a significant portion of biomass contained in large but rare zooplankters will be located outside the sampling volume). Model results also reproduce expected trends in

maxDSV, where maxDSV increases with less negative slope values (Fig. 4.15b) due to greater stochasticity of occurrence of large zooplankters within the sampling volume, and decreases with increasing intercept values (because with greater overall MVBS, the interbeam difference in acoustic backscatter is likely to be proportionally smaller). Using these model output data, we generated inverse functions (from equations 4.1, 4.2) that calculated expected spectral slope and intercept values given the glider-observed MVBS and maxDSV data (Fig. 4.15c and 4.15d, respectively).

The expected spectral slopes and spectral intercepts are different inshore and offshore of fronts for daytime and nighttime scattering layers. During both day and night, the expected spectral slopes and intercepts are greater inshore of fronts compared to offshore of fronts (Fig 4.16). Therefore, it is expected also that zooplankton size distributions differ across our California Current fronts, with larger-bodied zooplankton contributing more biomass proportionally in inshore assemblages compared with offshore assemblages.

Even larger changes in scattering characteristics were seen in the vertical dimension. We modeled zooplankton size spectra for 100-200 m and 400-500 m layers using MVBS and maxDSV data. The estimated slopes of the 400-500 m layer were less negative than those of the 100-200 m layer (Fig. 4.17), suggesting that larger-bodied scatterers in the deeper layer comprised a greater portion of the biomass than in the shallow layer. The modeled size spectra for the 100-200 m and 400-500 m layers (Fig. 4.18) reveal that these two layers differed from daytime and nighttime scattering layers on either side of the front.

Net samples: zooplankton assemblages and DVM

To corroborate acoustically inferred cross-frontal changes in DVM behavior and zooplankton assemblages, we examined plankton net samples collected inshore and offshore of major frontal features. The weighted mean depths (WMD) of zooplankton carbon biomass in daytime offshore Moccness tows were deeper than those of daytime inshore tows (Fig. 4.19; median WMDs were 278 m and 227 m for offshore (N=13) and inshore (N=10), respectively; $P < 0.001$). Nighttime WMDs did not differ significantly between inshore and offshore samples (median WMDs were 86 m and 113 m for offshore (N=6) and inshore (N=10), respectively; Mann-Whitney U: $P > 0.05$). The median of offshore DVM amplitudes (i.e., all possible pairwise differences between daytime and nighttime WMDs) was greater than the median of inshore DVM amplitudes (182 m versus 98 m for offshore and inshore, respectively; Mann-Whitney U: $P < 0.001$).

The taxonomic composition of zooplankton assemblages also differed between inshore and offshore samples (Figs. 4.20, 4.21). Here we emphasize the nighttime abundances because they are less susceptible to bias due to net avoidances than the daytime abundances. In nighttime zooplankton samples, calanoid copepods (excluding eucalanids) contributed the most biomass on a percentage basis (with median 48.7% and 71.0% for inshore and offshore samples, respectively). However, when considering only zooplankters with an ESD greater than 1.6 mm (i.e., those likely to contribute more to observed

acoustic backscatter at 750 kHz), calanoid copepods remained the dominant taxonomic group offshore (median = 75% of biomass), but they contributed significantly less ($P=0.031$; Mann-Whitney U) biomass inshore (median = 21.3%) compared with the dominant inshore taxonomic group, euphausiids (median = 36.5%).

The size distribution of zooplankton also differed inshore compared with offshore (Figs 4.22, 4.23). Specifically, inshore, zooplankters with ESDs greater than 3.8 mm contributed a greater percentage of biomass compared with offshore zooplankters (25.8% versus 5.8%, respectively). Inshore, zooplankters with ESDs greater than 8.5 mm contributed a greater percentage of biomass compared with offshore zooplankters (9.5% versus 2.7%, respectively). The percentage of biomass contributed by each size class varied substantially from sample to sample (Fig. 4. 23). However, when all net samples were considered, the percent of biomass found inshore in the two largest size classes was significantly greater than that of biomass found offshore in those same size classes ($P<0.001$ for both cases; Mann-Whitney U test).

Discussion

Six years of autonomous glider measurements along lines 80 and 90 reveal that there are consistent ecological changes that occur across frontal boundaries in the Southern California Current System (SCCS). Our analysis supported three hypotheses: 1) The depths of the Chl-a fluorescence maximum and the euphotic zone were consistently deeper offshore of fronts compared to

onshore of fronts, and horizontal gradients in these two properties were greater across fronts than across non-frontal regions; 2) DVM amplitude increased on the lighter (offshore) side of fronts; and, 3) the size structure of zooplankton assemblages changed across fronts.

The depth of subsurface chlorophyll maxima in the SCCS is determined by available light and nutrient levels (Cullen and Eppley, 1981; Aksnes et al., 2007). Most likely, the observed deeper fluorescence maxima and euphotic zones offshore of fronts reflect changing nutrient levels. By definition, the fronts described in this study are areas with shoaling isopycnals, and therefore are areas that might bring deep nutrients closer to the surface on the inshore side of fronts.

Floristically, Hayward and Venrick (1998) found that the inshore edge of the low-salinity core of the CC often marked a sharp boundary between an offshore and inshore phytoplankton community. The offshore community is dominated by dinoflagellates and coccolithophorids while the inshore community is diatom-dominated (Venrick, 2002, 2009). Venrick also found that standing stocks in inshore communities were much more variable than offshore communities. Inshore community standing stocks were also seasonal, with a springtime maximum, while the offshore community showed little seasonality. Shoaling nitraclines, as would be found at the inshore edge of the California Current jet, have been shown to be positively correlated with increasing biomass of large ($>8 \mu\text{m}$) phytoplankton (Mullin, 1998).

The increase in Diel Vertical Migration (DVM) amplitude seen offshore of fronts is probably associated with changing phytoplankton biomass and associated optical changes. Many studies have shown that DVM is primarily an adaptive response to predation pressure (Lampert, 1989; Ohman, 1990; De Robertis et al., 2000). Consequently, animal responses are strongly affected by ambient light levels and associated risk due to sight-hunting predators. For example, animals will begin their surfaceward migration midday in response to a solar eclipse (Backus et al., 1965). In the present study, prey items are more likely to be vulnerable during the day to visually-hunting predators offshore of fronts where euphotic depths are deeper and waters clearer. However, we also found that the relationship between DVM amplitude and modeled water clarity is non-linear. Glider-observed DVM amplitudes did not increase appreciably until the estimated depth of the euphotic zone surpassed 40-50 m. This result suggests that there may be a threshold light level for the response or that factors in addition to ambient light levels are influencing DVM behavior.

Our evidence also suggests that the observed cross-frontal changes in DVM amplitude may be attributable to differing zooplankton and micronekton species assemblages, and not merely to behavioral changes of the same organisms across these fronts. While it is not possible to identify assemblage composition by acoustic backscatter alone, several lines of evidence support the hypothesis that the composition of the acoustic scattering assemblage changed across these fronts. Cross-frontal changes in the maximum interbeam difference in acoustic backscatter (maxDSV) within specific depth strata suggest that either

the fine-scale aggregation of the assemblage of scattering animals changes across fronts, or that the size distribution of the animals changes. We also found that the mean volume backscatter (MVBS) decreased and maxDSV increased offshore of fronts for both the daytime and nighttime layers of maximum backscatter, which suggests a shift in the size spectrum of scattering animals. The size spectrum results from our inverse model (Fig. 4.16) suggest two important changes in the scattering assemblage of the day and night layers across fronts. First, the integrated areas under the modeled size spectra are higher inshore compared to offshore for both the day and night scattering layers, indicating that biomass is generally higher inshore of our fronts. Second, the less negative spectral slopes (i.e., flatter slopes) of inshore assemblages compared with offshore assemblages indicates that, within inshore assemblages, larger-bodied animals contribute proportionally more biomass to the total biomass compared to the proportion of larger-bodied zooplankton within offshore assemblages.

Results from Mocness net tows, although sampled at different times and locations from the gliders (though within the same general region), support these interpretations. Integrated zooplankton biomass in the net samples was larger inshore than offshore, and larger-bodied zooplankters within the inshore assemblage, especially within the two largest size classes (greater than 3.8 mm, and greater than 8.5 mm), contributed more to the total biomass compared to the offshore assemblage. Furthermore, the composition of assemblages of higher taxonomic groups shifted from a more copepod-dominated assemblage offshore

to a more euphausiid-dominated assemblage inshore. The modeled size spectra of animal scatterers in the deepest strata (400-500 m) offshore of the fronts studied here appears to be an exception to the trend of more negative (steeper) spectral slopes and decreasing intercepts when moving offshore. A coherent, apparently non-migratory layer characterized by less negative spectral slopes at 400-500 m underlies the daytime migratory, high-backscatter layer at 250-350 m. Comparing the scattering characteristics of the migratory layer with the non-migratory layer, it seems likely that the shallower, migratory layer is composed of more numerous, but smaller-bodied scatterers that are more evenly distributed at the fine scale. In contrast, the deeper, non-migratory layer is composed of fewer, but larger scatterers which, due to their low abundance, are more variably sampled by the acoustic beams of the ADP.

Although it is possible that the deep layer of large scatterers might be zooplankton taxa such as pteropods known to scatter sound much more efficiently than other zooplankters of equivalent biomass and dimensions (Stanton et al., 1998), the pervasiveness of the deep layer over many glider deployments implies a taxonomic group less subject to the intermittent occurrences which typify pteropods. Mesopelagic micronekton (primarily myctophids and the gonostomatids *Cyclothone* spp.) are a likely candidate group to comprise the layer. Mesopelagic micronekton are abundant in the deep sea (Pearcy et al., 1977), and many non-migratory species remain at depths between 400 to 1000 m during the night and day in this region (Davison, 2011). Even amongst some of the more abundant migratory species (e.g., *Stenobrachius*

leucopsarus), a significant fraction does not participate daily in DVM (Pearcy et al., 1977). Mesopelagic fish are also likely to be strong acoustic scatterers since many species either contain swimbladders throughout their lives, or at least during their juvenile forms (Davison, 2011). Other studies have also found that deep layers of non-migratory fish underlie daytime layers of migratory zooplankton in the Mediterranean (Andersen et al., 2004). While mesopelagic fishes may occasionally contribute to the somewhat shallower, migratory layer measured acoustically as well, the relatively small acoustic volume ensonified by the glider ADP, the consistency of occurrence of the mid-water layer, and the agreement of the patterns from our MOCNESS zooplankton analyses with acoustic backscatter results (both the present study and those in Powell and Ohman 2012), suggest that these midwater migrators are principally mesozooplankton scatterers.

The cross-frontal changes in size spectra that we observed are in contrast with some zooplankton biomass spectrum theory that holds that oligotrophic waters should exhibit less negative (flatter) spectral slopes due to greater biomass recycling and increased average trophic levels (TL) of the animal assemblages (Zhou, 2006). Although our results are reported as number spectra, while many others report results as biomass spectra (Platt and Denman, 1977; Zhou and Huntley, 1997), the trends in each case should be analogous: total biomass is proportional to the area under the curve, and the slope of the curve determines how the biomass is distributed amongst different size classes. Zhou (2006) found less negative slopes (i.e., flatter curves) in oligotrophic waters

compared with more negative slopes (i.e., steeper curves) in more eutrophic waters, by measuring particle size distributions at a range of locations with an optical plankton counter (OPC). This pattern held when comparing offshore CC waters with inshore waters, in contrast to what we observed in our modeled spectra. However, Zhou's estimates for spectral slope within the inshore waters of the CC excluded OPC counts from a larger size range which he termed a "euphausiid anomaly." When specific size ranges are not excluded, other OPC-based studies have found that slopes are flatter inshore of fronts (Baird et al., 2008; Basedow et al., 2010). Another reason why OPC-based studies may find steeper slopes in mesotrophic and eutrophic waters may be because the OPC cannot distinguish mesozooplankton from the numerous and comparatively small but abundant detritus particles in the SCCS. A comparison of *in situ* OPC-measured size distributions with laboratory OPC measurements of preserved plankters collected by net found that fragile particles (assumed to be detritus) were on average much smaller and 4 times as abundant as the zooplankton, with higher detritus:zooplankton ratios occurring in high-chlorophyll waters (Gonzalez-Quiros and Checkley, 2006). Other studies within the SCCS have also shown a positive relationship between increased upwelling (as would be more likely to be found inshore compared with offshore) and flatter size spectra of net-collected zooplankton (Rykaczewski and Checkley, 2008).

Taken together, the cross-frontal changes in phytoplankton Chl-a, DVM behavior, acoustic backscattering characteristics, zooplankton samples, and modeled size-spectra indicate that fronts in the Southern California Current

System often act as boundaries between waters with very different ecosystem characteristics. Offshore of these fronts, zooplankton inhabit waters that are optically clearer and characterized by deeper chlorophyll maxima compared with inshore waters, and where zooplankton in the offshore waters display increased DVM amplitudes. Our new approach to modeling zooplankton size spectra allowed us to infer from glider acoustic backscatter data that offshore environments are dominated by smaller bodied zooplankters compared with inshore environments. These gradient regions not only restructure the plankton assemblages, but also markedly alter the prey field for diverse pelagic predators.

Acknowledgements

We gratefully acknowledge Russ Davis, Dan Rudnick, Robert Todd, Jeff Sherman for the provision of *Spray* Glider data, and for their advice on glider instrumentation and technical issues. We are also indebted to Russ Davis, Peter Franks and Mike Landry who all provided important feedback during the preparation of this manuscript. Funding for this work was provided by NSF via the California Current Ecosystem LTER site, and by the Gordon and Betty Moore Foundation, in awards to M.D. Ohman. Glider observations were supported by the NOAA Ocean Climate Observation Program through the Consortium on the Ocean's Role in Climate, and by the US Integrated Ocean Observation System through the Southern California Coastal Ocean Observing System (SCCOOSs).

Chapter 4, in part, is being prepared for submission to *Limnology and Oceanography*, 2013, Powell, J.R., and Ohman, M.D., Association for the

Sciences of Limnology and Oceanography, Inc., 2013. The dissertation author was the primary investigator and author of this paper.

References

- Ainley, D.G., Dugger, K.D., Ford, R.G., Pierce, S.D., Reese, D.C., Brodeur, R.D., Tynan, C.T., Barth, J.A., 2009. Association of predators and prey at frontal features in the California Current: competition, facilitation, and co-occurrence. *Marine Ecology Progress Series* **389**: 271-294.
- Aksnes, D.L., Ohman, M.D., Riviere, P., 2007. Optical effect on the nitracline in a coastal upwelling area. *Limnology and Oceanography* **52**: 1179-1187.
- Andersen, V., Devey, C., Gubanova, A., Picheral, M., Melnikov, V., Tsarin, S., Prieur, L., 2004. Vertical distributions of zooplankton across the Almeria-Oran frontal zone (Mediterranean Sea). *Journal of Plankton Research* **26**: 275-293.
- Backus, R.H., Clark, R.C., Wing, A.S., 1965. Behaviour of certain marine organisms during solar eclipse of July 20, 1963. *Nature* **205**: 989-991.
- Baird, M.E., Timko, P.G., Middleton, J.H., Mullaney, T.J., Cox, D.R., Suthers, I.M., 2008. Biological properties across the Tasman Front off southeast Australia. *Deep-Sea Research I* **55**: 1438-1455.
- Basedow, S.L., Tande, K.S., Zhou, M., 2010. Biovolume spectrum theories applied: spatial patterns of trophic levels within a mesozooplankton community at the polar front. *Journal of Plankton Research* **32**: 1105-1119.
- Capet, X., McWilliams, J.C., Molemaker, M.J., Shchepetkin, A.F., 2008. Mesoscale to submesoscale transition in the California current system. Part II: Frontal processes. *Journal of Physical Oceanography* **38**: 44-64.
- Chelton, D.B., 1982. Large-scale response of the California Current to forcing by the wind stress curl. *California Cooperative Oceanic Fisheries Investigations Report* **23**: 130-148.

- Chelton, D.B., Bernal, P.A., McGowan, J.A., 1982. Large-scale interannual physical and biological interaction in the California Current. *Journal of Marine Research* **40**: 1095-1125.
- Cullen, J.J., Eppley, R.W., 1981. Chlorophyll maximum layers of the Southern California Bight and possible mechanisms of their formation and maintenance. *Oceanologica Acta* **4**: 23-32.
- Cullen, J.J., Lewis, M.R., 1995. Biological processes and optical measurements near the sea surface: some issues relevant to remote sensing. *Journal of Geophysical Research: Oceans* **100**: 13255-13266.
- Davis, R.E., Ohman, M.D., Rudnick, D.L., Sherman, J.T., Hodges, B., 2008. Glider surveillance of physics and biology in the southern California Current System. *Limnology and Oceanography* **53**: 2151-2168.
- Davison, P., 2011. The specific gravity of mesopelagic fish from the northeastern Pacific Ocean and its implications for acoustic backscatter. *ICES Journal of Marine Science* **68**: 2064-2074.
- De Robertis, A., Jaffe, J.S., Ohman, M.D., 2000. Size-dependent visual predation risk and the timing of vertical migration in zooplankton. *Limnology and Oceanography* **45**: 1838-1844.
- Denman, K.L., Abbott, M.R., 1994. Time scales of pattern evolution from cross-spectrum analysis of Advanced Very High-Resolution Radiometer and Coastal Zone Color Scanner Imagery. *Journal of Geophysical Research-Oceans* **99**: 7433-7442.
- Eggleston, D.B., Armstrong, D.A., Elis, W.E., Patton, W.S., 1998. Estuarine fronts as conduits for larval transport: hydrodynamics and spatial distribution of Dungeness crab postlarvae. *Marine Ecology Progress Series* **164**: 73-82.
- Flament, P., 2002. A state variable for characterizing water masses and their diffusive stability: spiciness. *Progress in Oceanography* **54**: 493-501.
- Gay, P.S., Chereskin, T.K., 2009. Mean structure and seasonal variability of the poleward undercurrent off southern California. *Journal of Geophysical Research-Oceans* **114**:

- Gonzalez-Quiros, R., Checkley, D.M., 2006. Occurrence of fragile particles inferred from optical plankton counters used in situ and to analyze net samples collected simultaneously. *Journal of Geophysical Research-Oceans* **111**:
- Gorsky, G., Ohman, M.D., Picheral, M., Gasparini, S., Stemmann, L., Romagnan, J.B., Cawood, A., Pesant, S., Garcia-Comas, C., Prejger, F., 2010. Digital zooplankton image analysis using the ZooScan integrated system. *Journal of Plankton Research* **32**: 285-303.
- Greene, C.H., Wiebe, P.H., Pershing, A.J., Gal, G., Popp, J.M., Copley, N.J., Austin, T.C., Bradley, A.M., Goldsborough, R.G., Dawson, J., Hendershott, R., Kaartvedt, S., 1998. Assessing the distribution and abundance of zooplankton: a comparison of acoustic and net-sampling methods with D-BAD MOCNESS. *Deep-Sea Research II* **45**: 1219-1237.
- Haury, L.R., Venrick, E.L., Fey, C.L., McGowan, J.A., Niiler, P.P., 1993. The Ensenada Front: July 1995. *California Cooperative Oceanic Fisheries Investigations Reports* **34**: 69-88.
- Hickey, B.M., 1979. The California current system—hypotheses and facts. *Progress in Oceanography* **8**: 191-279.
- Humston, R., Ault, J.S., Lutcavage, M., Olson, D.B., 2000. Schooling and migration of large pelagic fishes relative to environmental cues. *Fisheries Oceanography* **9**: 136-146.
- Lampert, W., 1989. The Adaptive Significance of Diel Vertical Migration of Zooplankton. *Functional Ecology* **3**: 21-27.
- Lavaniegos, B.E., Ohman, M.D., 2007. Coherence of long-term variations of zooplankton in two sectors of the California Current System. *Progress in Oceanography* **75**: 42-69.
- Lavery, A.C., Wiebe, P.H., Stanton, T.K., Lawson, G.L., Benfield, M.C., Copley, N., 2007. Determining dominant scatterers of sound in mixed zooplankton populations. *Journal of the Acoustical Society of America* **122**: 3304-3326.
- Lefevre, J., 1986. Aspects of the Biology of Frontal Systems. *Adv. Mar. Biol.* **23**: 163-299.

- Mackas, D.L., Washburn, L., Smith, S.L., 1991. Zooplankton Community Pattern Associated with a California Current Cold Filament. *Journal of Geophysical Research-Oceans* **96**: 14781-14797.
- Marchesiello, P., McWilliams, J.C., Shchepetkin, A., 2003. Equilibrium structure and dynamics of the California Current System. *Journal of Physical Oceanography* **33**: 753-783.
- Martin, A.P., 2003. Phytoplankton patchiness: the role of lateral stirring and mixing. *Progress in Oceanography* **57**: 125-174.
- McClatchie, S., Cowen, R., Nieto, K., Greer, A., Luo, J.Y., Guigand, C., Demer, D., Griffith, D., Rudnick, D., 2012. Resolution of fine biological structure including small narcomedusae across a front in the Southern California Bight. *Journal of Geophysical Research-Oceans* **117**: C04020, doi:10.1029/2011JC007565
- Medwin, H., Clay, C.S., 1998. *Fundamentals of acoustical oceanography*. Academic Press, Boston.
- Morel, A., 1988. Optical modeling of the upper ocean in relation to its biogenous matter content (case-I waters). *Journal of Geophysical Research-Oceans* **93**: 10749-10768.
- Mullin, M.M., 1998. Biomasses of large-celled phytoplankton and their relation to the nitricline and grazing in the California current system off southern California, 1994-1996. *California Cooperative Oceanic Fisheries Investigations Reports* **39**: 117-123.
- Munger, L.M., Camacho, D., Havron, A., Campbell, G., Calambokidis, J., Douglas, A., Hildebrand, J., 2009. Baleen whale distribution relative to surface temperature and zooplankton abundance off Southern California, 2004-2008. *California Cooperative Oceanic Fisheries Investigations Reports* **50**: 155-168.
- Munk, P., Hansen, B.W., Nielsen, T.G., Thomsen, H.A., 2003. Changes in plankton and fish larvae communities across hydrographic fronts off West Greenland. *Journal of Plankton Research* **25**: 815-830.
- Ohman, M.D., 1990. The Demographic Benefits of Diel Vertical Migration by Zooplankton. *Ecological Monographs* **60**: 257-281.

- Ohman, M.D., Drits, A.V., Clarke, M.E., Plourde, S., 1998. Differential dormancy of co-occurring copepods. *Deep-Sea Research Part I* **45**: 1709-1740.
- Ohman, M.D., Powell, J.R., Picheral, M., Jensen, D.W., 2012. Mesozooplankton and particulate matter responses to a deep-water frontal system in the southern California Current System. *Journal of Plankton Research* **34**: 815-827.
- Pearcy, W.G., Krygier, E.E., Mesecar, R., Ramsey, F., 1977. Vertical distribution and migration of oceanic micronekton off Oregon. *Deep-Sea Research* **24**: 223-245.
- Pingree, R.D., Pugh, P.R., Holligan, P.M., Forster, G.R., 1975. Summer phytoplankton blooms and red tides along tidal fronts in approaches to english channel. *Nature* **258**: 672-677.
- Platt, T., Denman, K., 1977. Organization in pelagic ecosystem. *Helgolander Wissenschaftliche Meeresuntersuchungen* **30**: 575-581.
- Polovina, J.J., Balazs, G.H., Howell, E.A., Parker, D.M., Seki, M.P., Dutton, P.H., 2004. Forage and migration habitat of loggerhead (*Caretta caretta*) and olive ridley (*Lepidochelys olivacea*) sea turtles in the central North Pacific Ocean. *Fisheries Oceanography*. **13**: 36-51.
- Polovina, J.J., Howell, E., Kobayashi, D.R., Seki, M.P., 2001. The transition zone chlorophyll front, a dynamic global feature defining migration and forage habitat for marine resources. *Progress in Oceanography* **49**: 469-483.
- Powell, J.R., Ohman, M.D., 2012. Use of glider-class acoustic Doppler profilers for estimating zooplankton biomass. *Journal of Plankton Research* **34**: 563-568.
- Rykaczewski, R.R., Checkley, D.M., 2008. Influence of ocean winds on the pelagic ecosystem in upwelling regions. *Proceedings of the National Academy of Sciences of the United States of America* **105**: 1965-1970.
- Simpson, J.J., 1984. El Nino-induced onshore transport in the California Current during 1982-3. *Geophysical Research Letters* **11**: 233-236236.
- Smith, S.L., Jones, B.H., Atkinson, L.P., Brink, K.H., 1986. Zooplankton in the upwelling fronts off Pt. Conception, California. *Elsevier Oceanography Series* **42**: 195-213.

- SonTek, 1997. SonTek Doppler current meters: using signal strength data to monitor suspended sediment concentration. Application Note, 1-7.
- Sournia, A., 1994. Pelagic Biogeography and Fronts. *Progress in Oceanography* **34**: 109-120.
- Spall, M.A., 1995. Frontogenesis, Subduction, and Cross-Front Exchange at Upper Ocean Fronts. *Journal of Geophysical Research-Oceans* **100**: 2543-2557.
- Stanton, T.K., Chu, D.Z., Wiebe, P.H., 1998. Sound scattering by several zooplankton groups. II. Scattering models. *Journal of the Acoustical Society of America* **103**: 236-253.
- Todd, R.E., Rudnick, D.L., Mazloff, M.R., Davis, R.E., Cornuelle, B.D., 2011. Poleward flows in the southern California Current System: Glider observations and numerical simulation. *Journal of Geophysical Research-Oceans* **116**: C02026, doi:10.1029/2010JC006536
- Venrick, E.L., 2002. Floral patterns in the California Current System off southern California: 1990-1996. *Journal of Marine Research* **60**: 171-189.
- Venrick, E.L., 2009. Floral patterns in the California Current: The coastal-offshore boundary zone. *Journal of Marine Research* **67**: 89-111.
- Wiebe, P.H., Morton, A.W., Bradley, A.M., Backus, R.H., Craddock, J.E., Barber, V., Cowles, T.J., Flierl, G.R., 1985. New Developments in the MOCNESS, an Apparatus for Sampling Zooplankton and Micronekton. *Marine Biology* **87**: 313-323.
- Zhou, M., 2006. What determines the slope of a plankton biomass spectrum? *Journal of Plankton Research* **28**: 437-448.
- Zhou, M., Huntley, M.E., 1997. Population dynamics theory of plankton based on biomass spectra. *Marine Ecology Progress Series* **159**: 61-73.

Table 4.1: Comparison of inshore and offshore (relative to frontal location) scattering characteristics of daytime and nighttime layers of maximum backscatter.

| | Line 80 | | | Line 90 | | |
|------------------------------|---------|----------|---------|---------|----------|---------|
| | Inshore | Offshore | p-value | Inshore | Offshore | p-value |
| Daytime MVBS (dB) | -69.1 | -75.1 | <0.001 | -71.7 | -77.5 | <0.001 |
| Daytime maxDSV (dB) | 2.31 | 2.55 | 0.018 | 2.46 | 2.79 | 0.007 |
| Nighttime MVBS (dB) | -65.5 | -68.2 | <0.001 | -67.4 | -70.5 | <0.001 |
| Nighttime maxDSV (dB) | 2.3 | 2.4 | 0.073 | 2.4 | 2.5 | 0.019 |

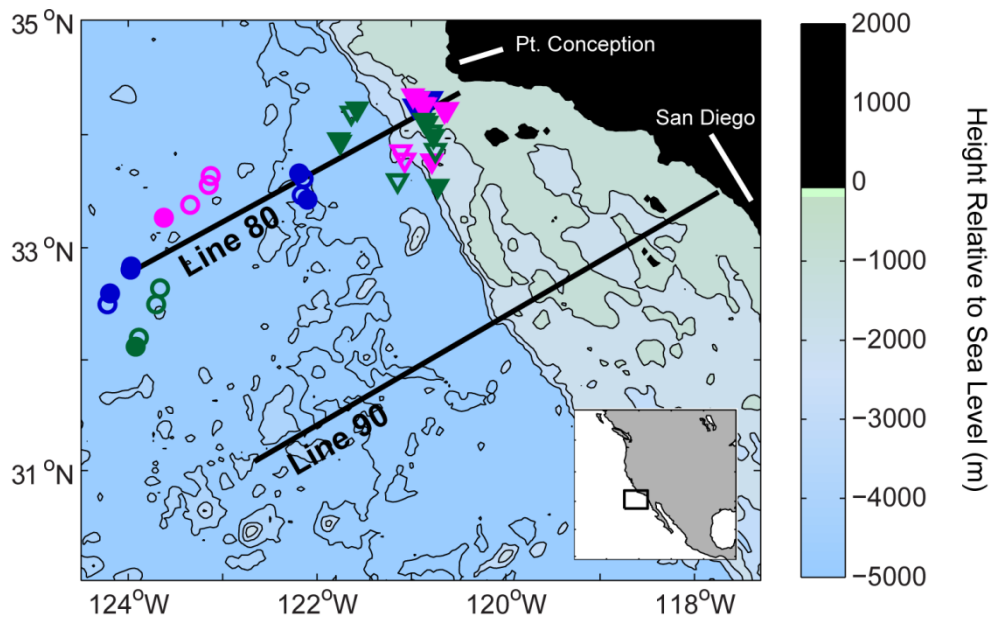


Figure 4.1. CCE-LTER *Spray* glider transect lines 80 and 90, off the Southern California coast superimposed on bathymetry. Inset shows location off North America. Symbols depict location of Moccness tows conducted during three cruises: P0605 (blue), P0704 (green), and P0810 (pink). Circles and triangles indicate tows occurring offshore and inshore, respectively, of a contemporaneous major frontal feature along line 80. Open (closed) symbols indicate daytime (nighttime) tows.

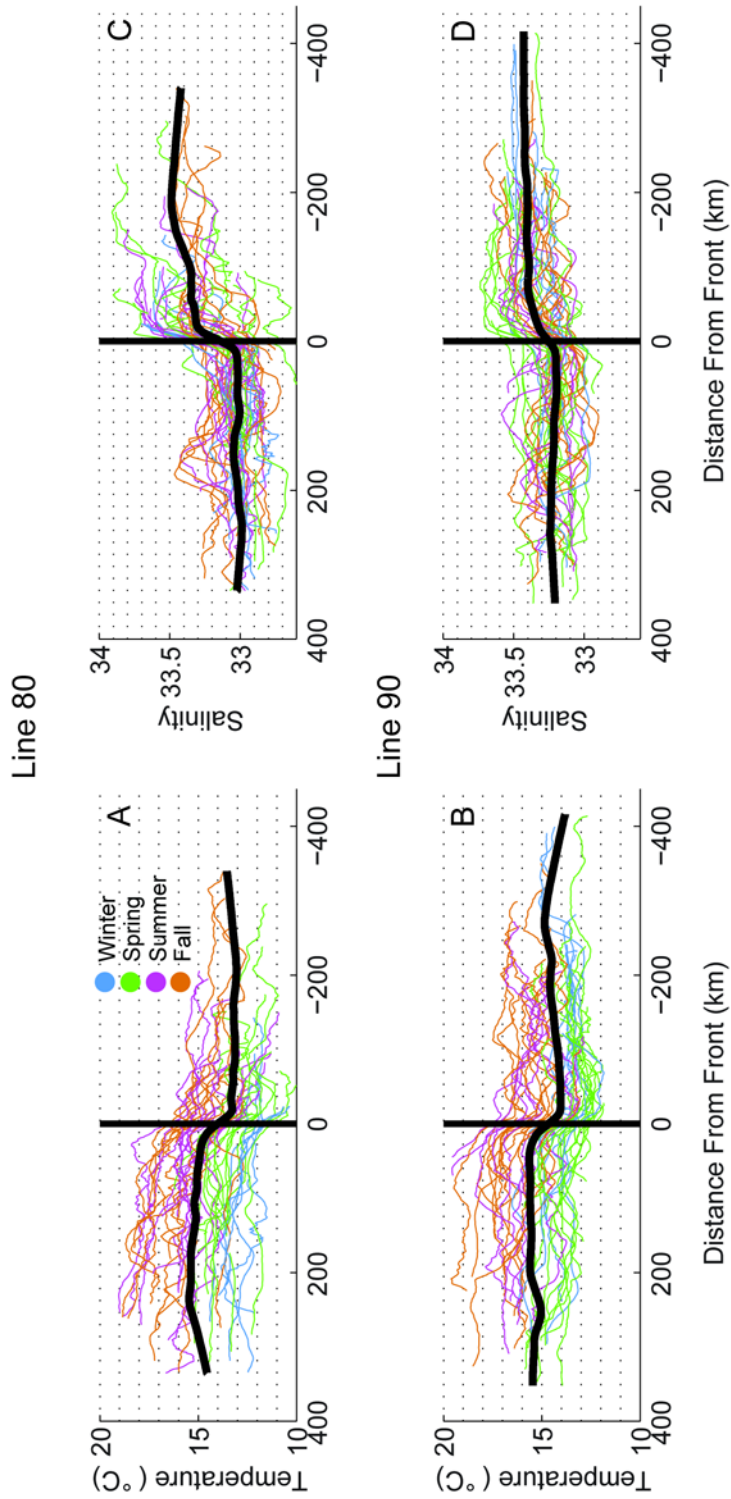


Figure 4.2. Mean surface layer (0-50 m) temperatures (A,B) and Salinities (C,D) across fronts along Line 80 (A,C) and Line 90 (B,D). Fronts along each glider transect are aligned to 0 km. Negative distances represent distance inshore from the front, positive distances offshore from the front. Color refers to season in which the transect occurred.

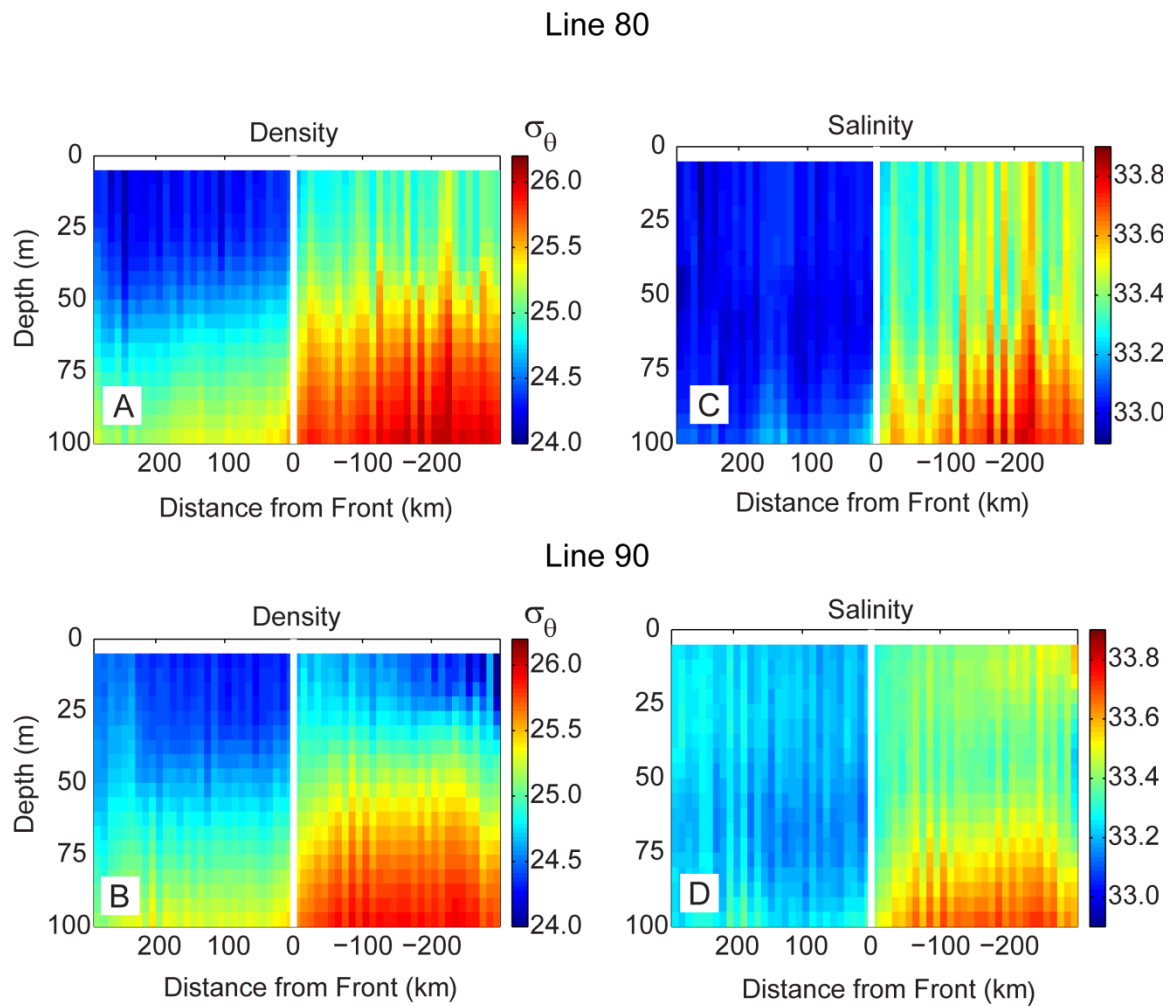


Figure 4.3. (A,B) Mean density, σ_θ , and (C,D) salinity structure inshore and offshore of canonical fronts for (A,C) Line 80 and (B,D) Line 90.

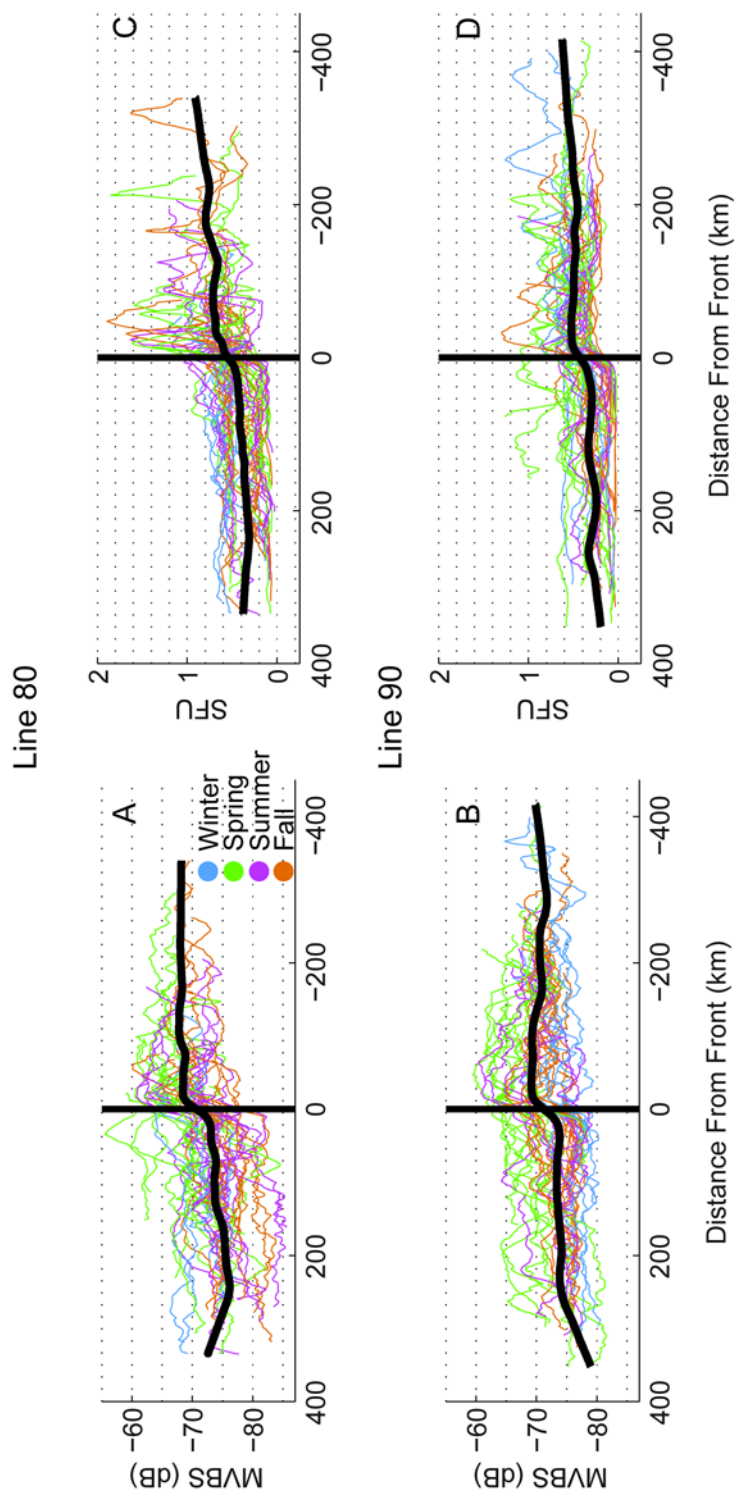


Figure 4.4. Mean surface layer (0-50 m) mean volume backscatter (A,B) and Chl-a fluorescence (C,D) across fronts along Line 80 (A, C) and Line 90 (B, D). Fronts along each glider transect are aligned to 0 km. Negative distances represent distance inshore from the front, positive distances offshore from the front. Color refers to season in which the transect occurred.

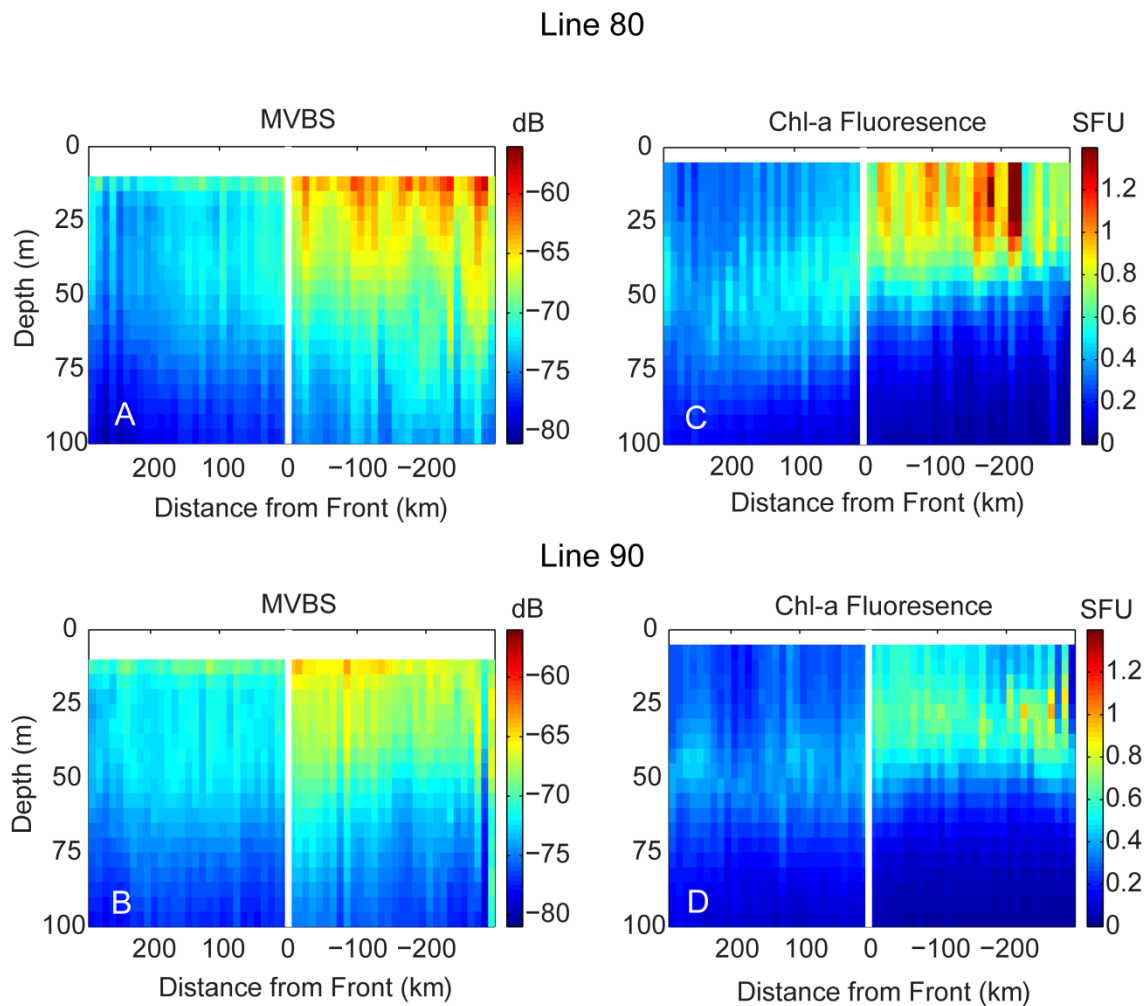


Figure 4.5. (A,B) Mean volume backscatter (MVBS) and (C,D) Chl-a fluorescence structure inshore and offshore of canonical fronts for (A,C) Line 80 and (B,D) Line 90.

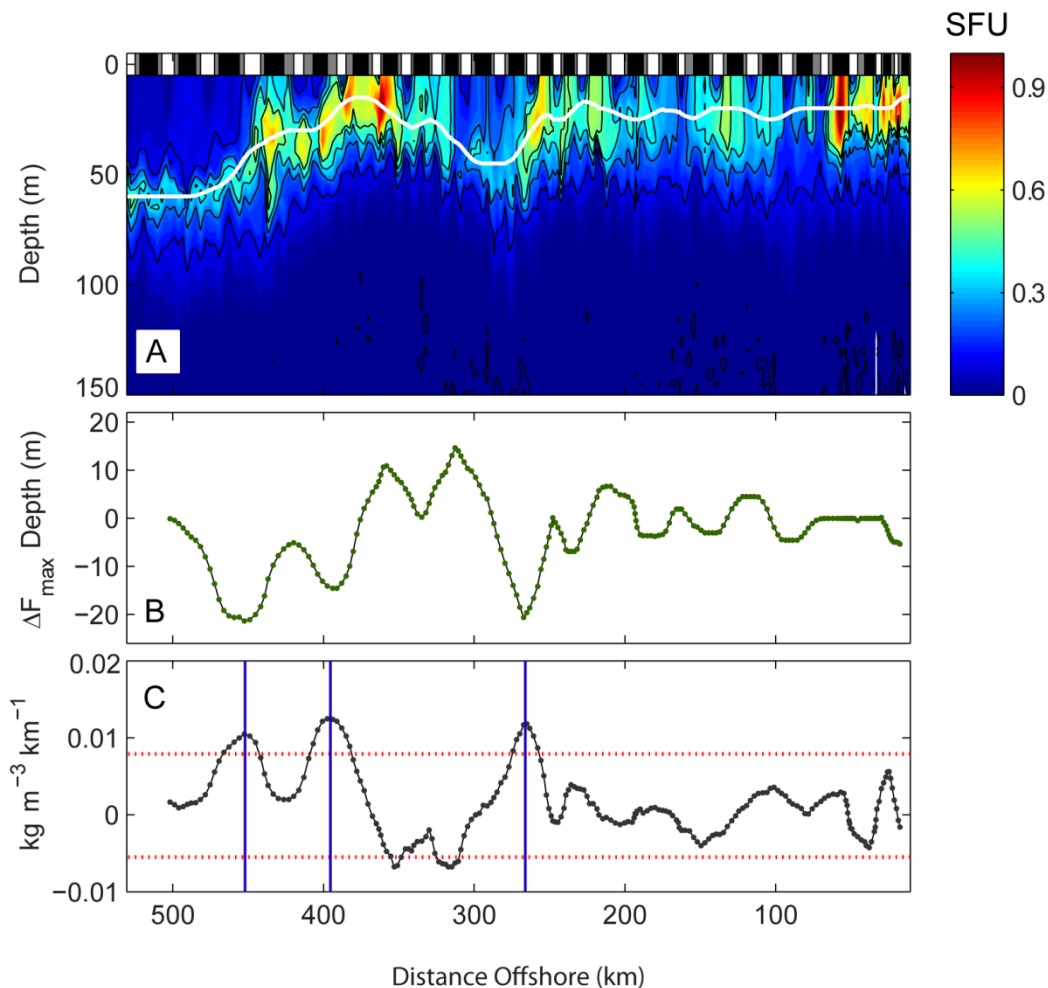


Figure 4.6. Changes in the depth of Chl-*a* fluorescence maximum across ocean fronts in the Southern California Current System. (A) Vertical section of fluorescence structure along line 90 (depth of the Chl-*a* maximum is denoted by the solid white line). (B) Average change in depth of the Chl-*a* maximum as recorded by a glider, between a 24 hr period inshore of given dive minus the average depth offshore of that dive. (C) Horizontal gradient in surface layer (0-50 m) density recorded by the glider. Dotted red lines are the threshold above or below which a front is defined. Vertical lines indicate the presence of a positive front where the average surface layer density is greater inshore than offshore.

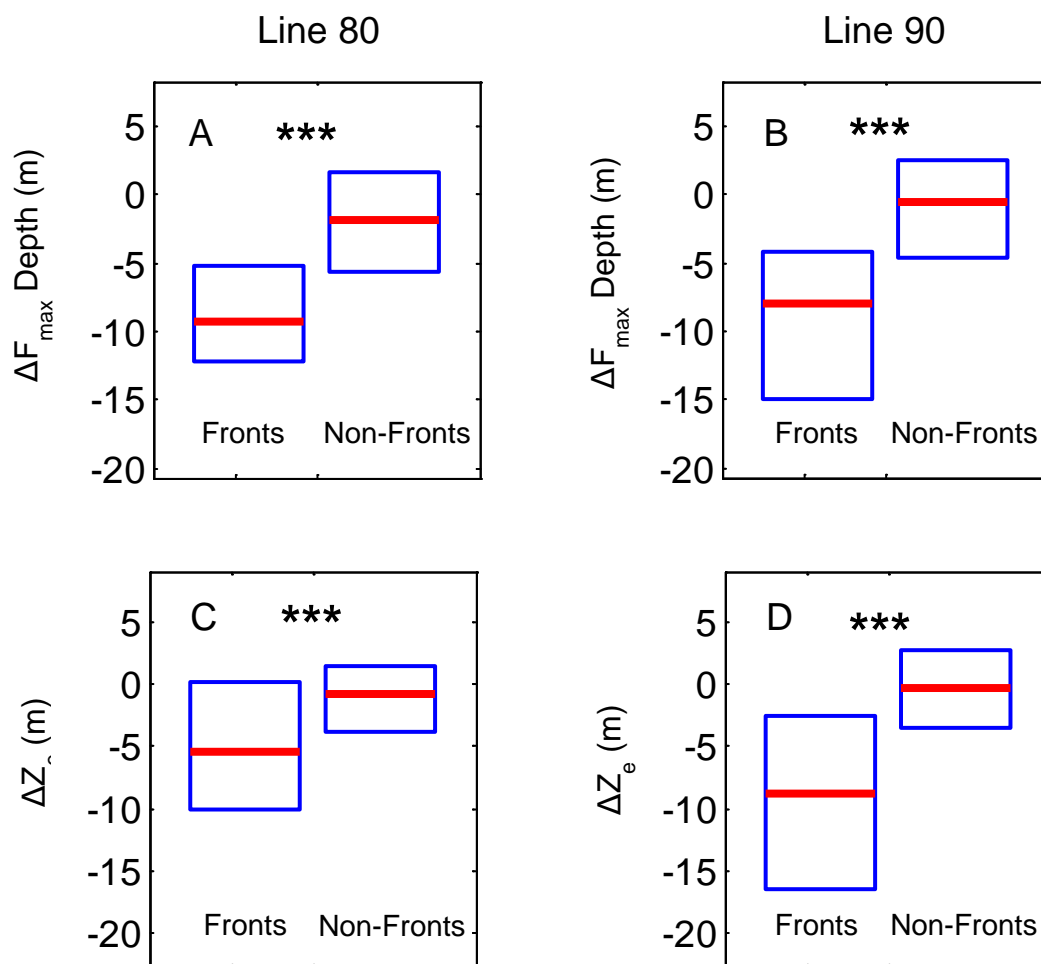


Figure 4.7. Average inshore to offshore change in the depth of the (A,B) Chl-a fluorescence maximum and (C,D) euphotic zone across fronts compared to non-frontal regions for (A,C) line 80 and (B,D) line 90. The upper and lower boundaries of each box represent the 75th and 25th percentiles of values, respectively, and the red line represents the median of recorded values. Triple asterisks indicate $P < 0.001$ (Mann Whitney U).

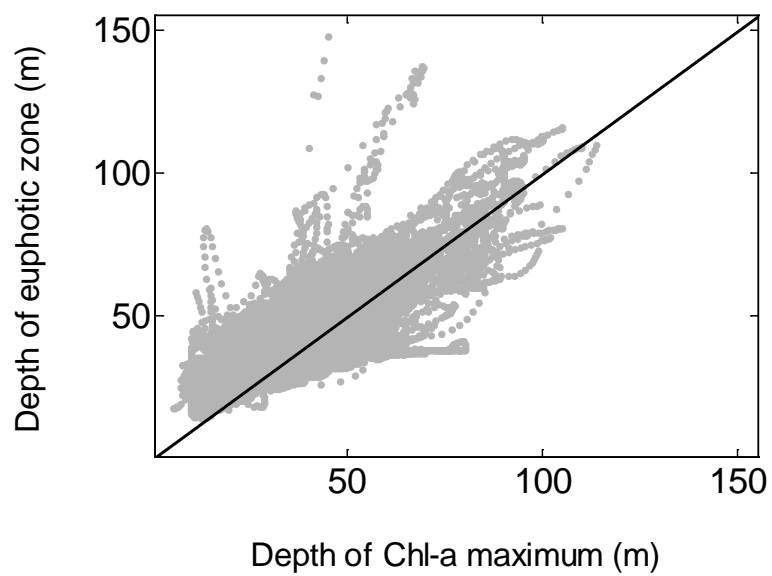


Figure 4.8. Depth of the Chl-a maximum versus the modeled depth of the euphotic zone. The black line shows a 1:1 relationship.

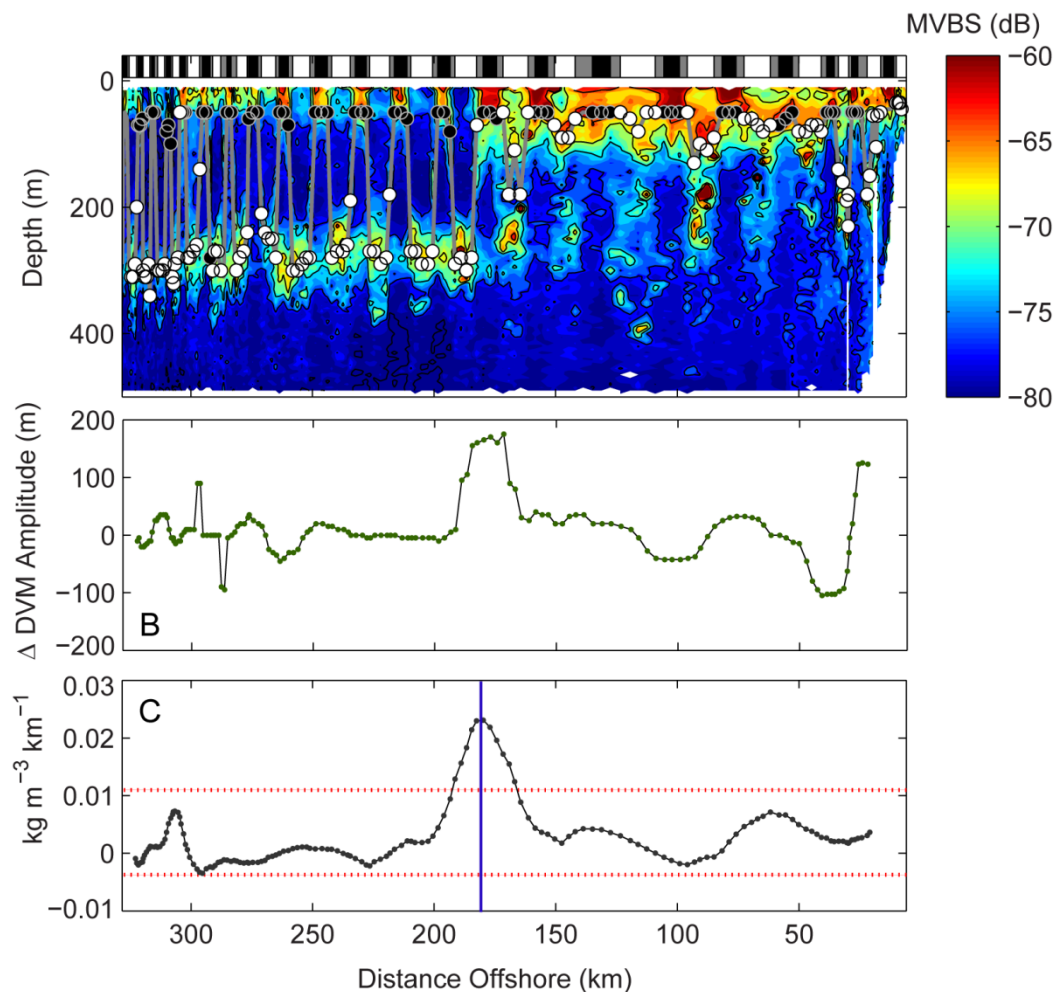


Figure 4.9. Changes in DVM amplitude across ocean fronts. (A) Vertical section of MVBS along line 80. Black (night), white (day), and gray (dawn,dusk) symbols estimate the position the layer of maximum backscatter as the median depth of samples with MVBS values above the 85th percentile for a given dive. (B) Average change in DVM amplitude as between the two 24 hr periods inshore and offshore of given dive. (C) Horizontal gradient in surface layer (0-50 m) density recorded by the glider. Dotted red lines are the threshold above or below which a front is defined. Vertical lines indicate the presence of a positive front where the average surface layer density is greater inshore than offshore.

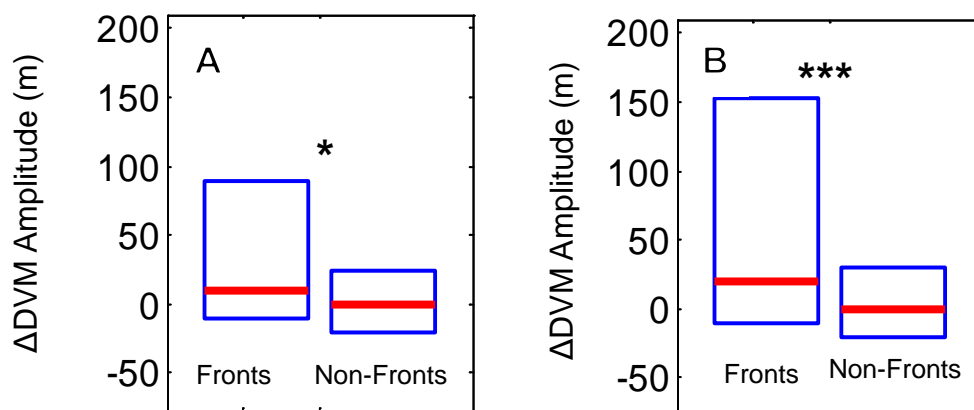


Figure 4.10. Average inshore to offshore change in DVM amplitude across fronts compared to non-frontal regions for (A) line 80 and (B) line 90. The upper and lower boundaries of each box represent the 75th and 25th percentiles of values, respectively, and the red line represents the median of recorded values. Single asterisks indicate $P < 0.05$, double asterisks indicate $P < 0.01$ (Mann-Whitney U).

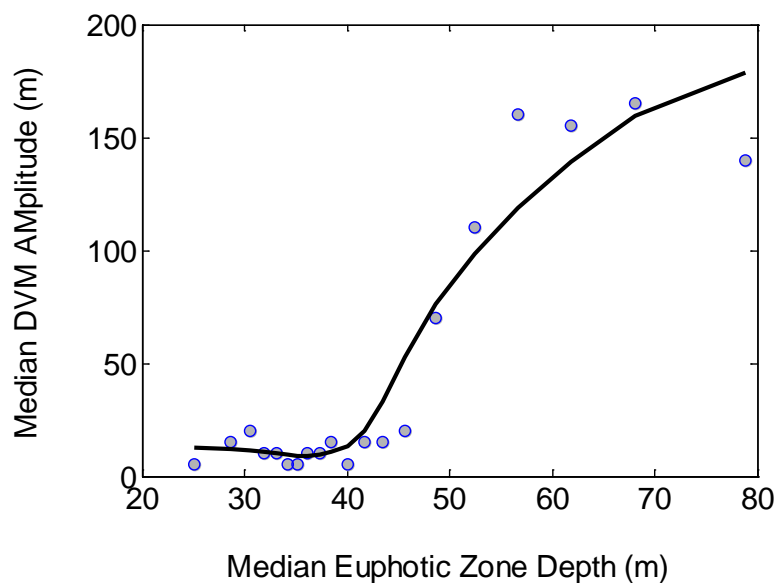


Figure 4.11. Relationship between median DVM amplitude and the median depth of the euphotic zone. The modeled depth of the euphotic zone (i.e., the 1% light level) of all dives was binned into twenty 5 percentile-wide bins (e.g., 0-5th percentile, 5th-10th percentile, etc.). Gray dots indicate the euphotic zone depth and median DVM amplitude of the dives within each of those twenty bins. The black line is a loess fit.

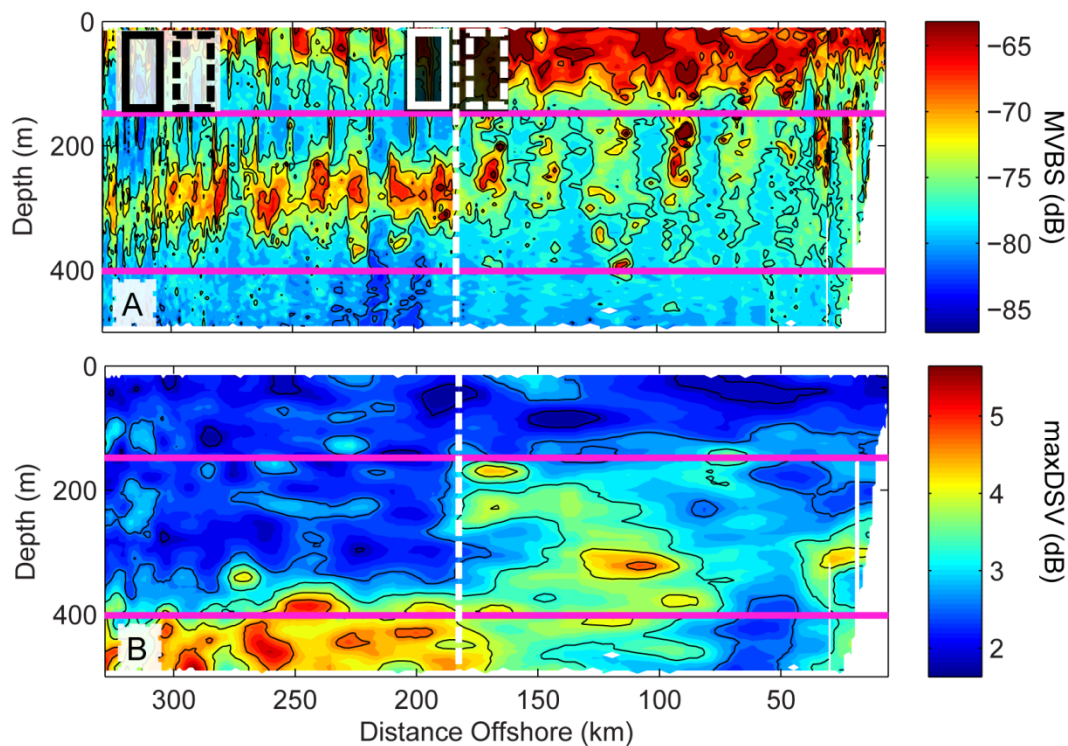


Figure 4.12. Vertical sections of (A) MVBS and (B) maxDSV values along a line 80 transect. The position of an ocean front is indicated by the dotted white line. Magenta lines separate three depth strata (0-150 m, 150-400 m, and 400-500 m) which are analyzed further in figure 13. Boxes indicate the extent of data used to calculate average maxDSV inshore of each dive (dashed line box) and offshore (solid line box), and used to calculate horizontal changes in maxDSV across frontal regions (white boxes) and non-frontal regions (black boxes).

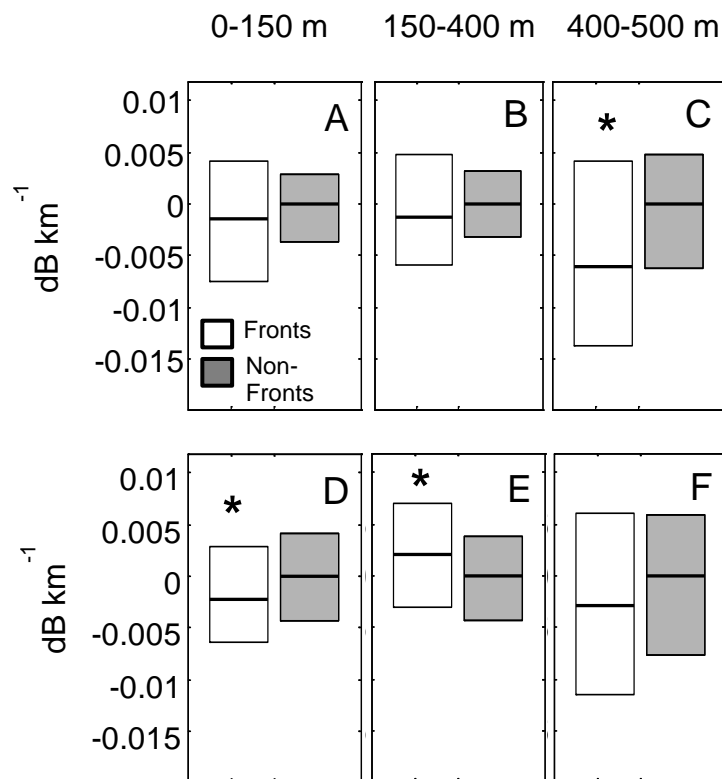


Figure 4.13. Horizontal gradients in maxDSV across frontal regions (white boxes) versus non-frontal regions (shaded boxes) for (A-C) line 80 and (D-F) line 90, for three depth strata (indicated above the panels). The upper and lower boundaries of each box show the 75th and 25th percentiles of recorded values, respectively. Asterisks indicate significant ($p < 0.05$) differences in the horizontal gradient at frontal regions compared to non-frontal regions.

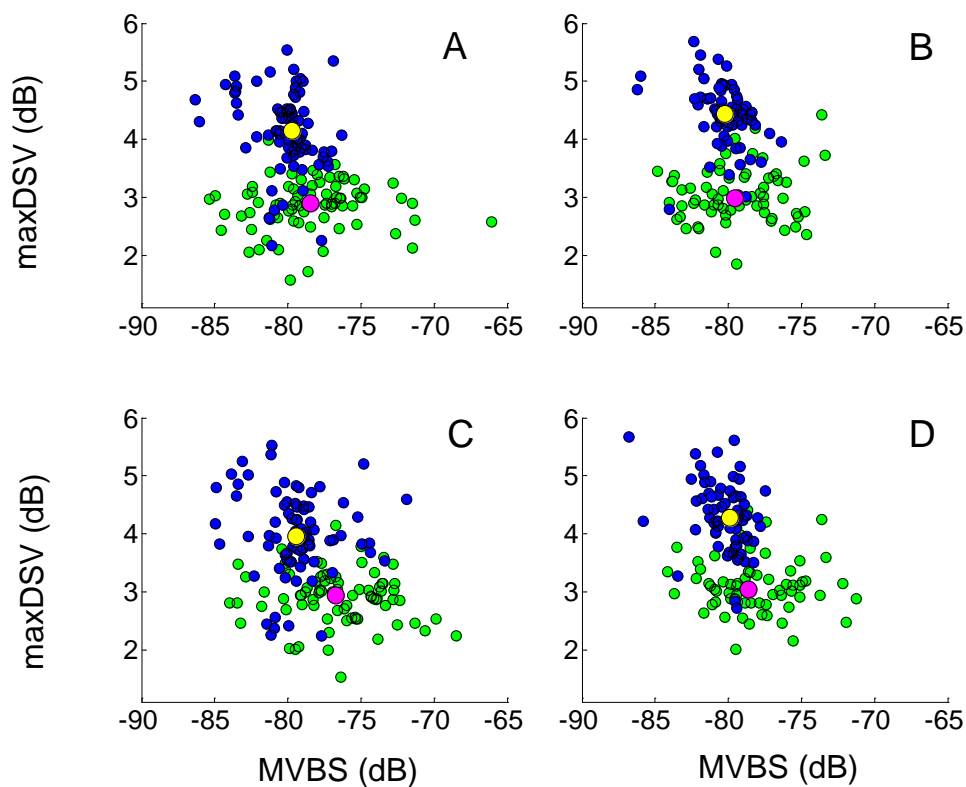


Figure 4.14. Acoustic backscattering characteristics of different depth strata (A,C) offshore, and (B,D) inshore of (A,B) line 80 fronts ($n=81$), and (C,D) line 90 fronts ($n=73$). Blue (400-500 m) and green (100-200 m) dots show the median MVBS and maxDSV within a specific depth stratum spanning a 24 hr travel window from the front. Yellow symbols show the median position of the blue dots and the magenta symbols show the median position of the green dots.

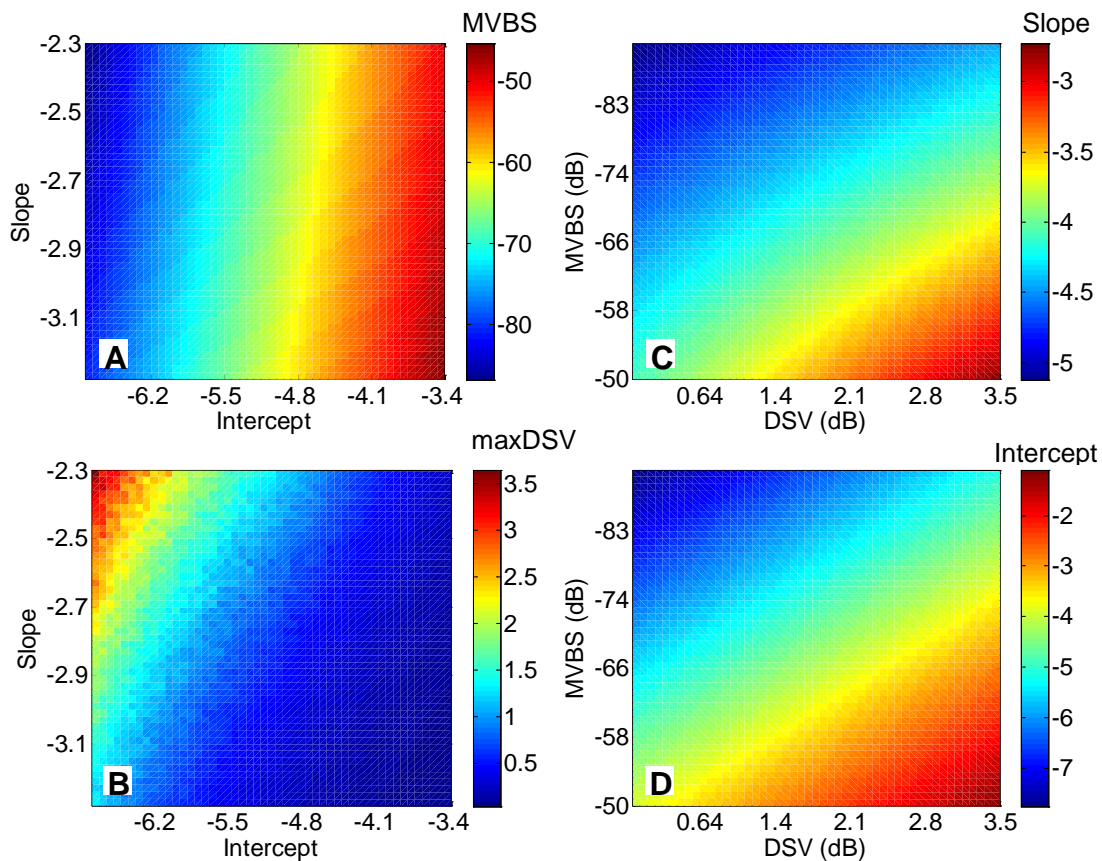


Figure 4.15. Acoustic modeling of zooplankton assemblages. Acoustic model output from a Monte Carlo simulation of (A) expected MVBS, and (B) expected maxDSV of an ensonified volume containing simulated zooplankton assemblages. Slope and intercept refer to the input parameters of the size spectrum ($n = 10adb$, where d is the body length of a given zooplankter, and a and b are the intercept and slope, respectively of the spectrum) used to create the simulated assemblages. Inverse functions showing the expected (C) slope and (D) intercept values of a zooplankton size spectrum given glider-observed MVBS and maxDSV.

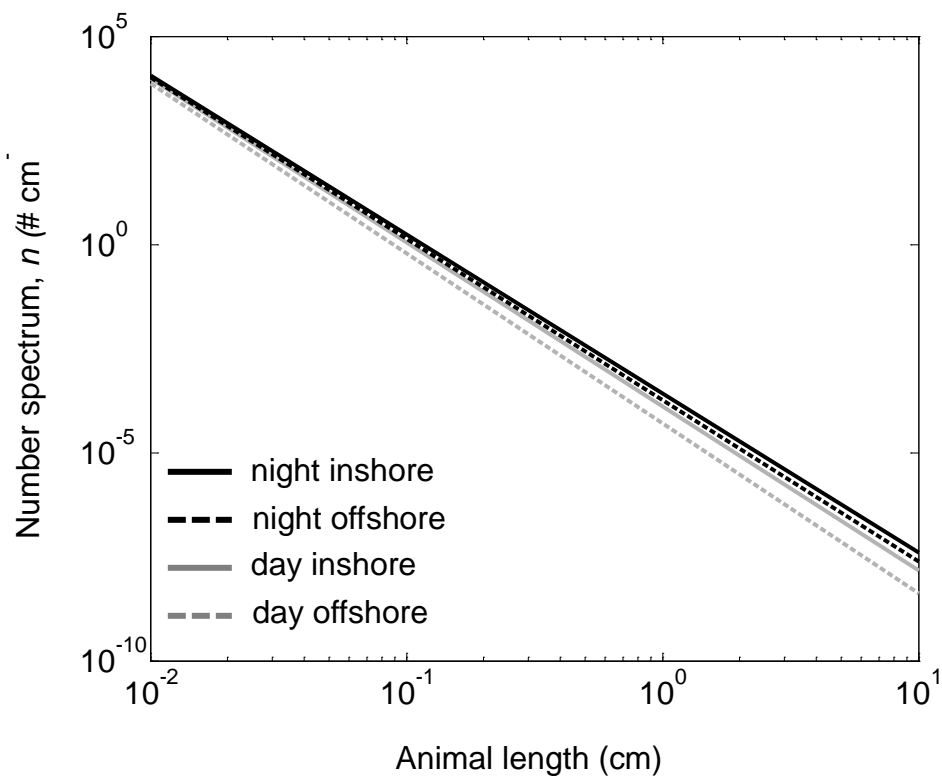


Figure 4.16. Expected size spectra of daytime and nighttime scattering layers. Size spectra of ensonified zooplankton assemblages were estimated with an inverse model using observed MVBS and maxDSV data from within a 24 hr glider travel window inshore and offshore of fronts along lines 80 and 90.

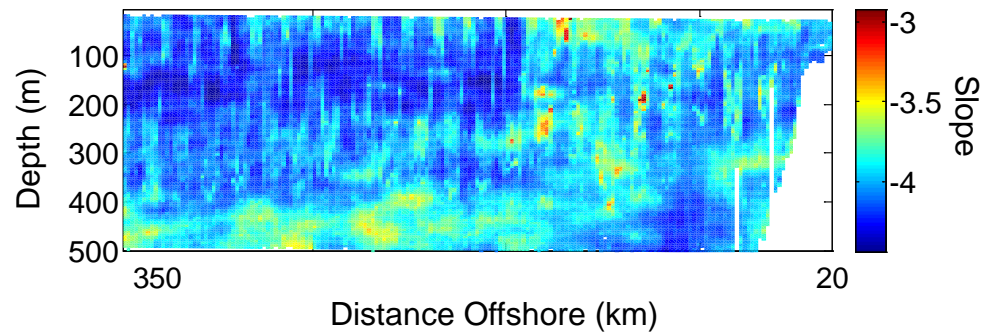


Figure 4.17. Inverse model output showing variation in expected slopes of size spectra of assemblages ensonified by the glider ADP along a line 80 transect.

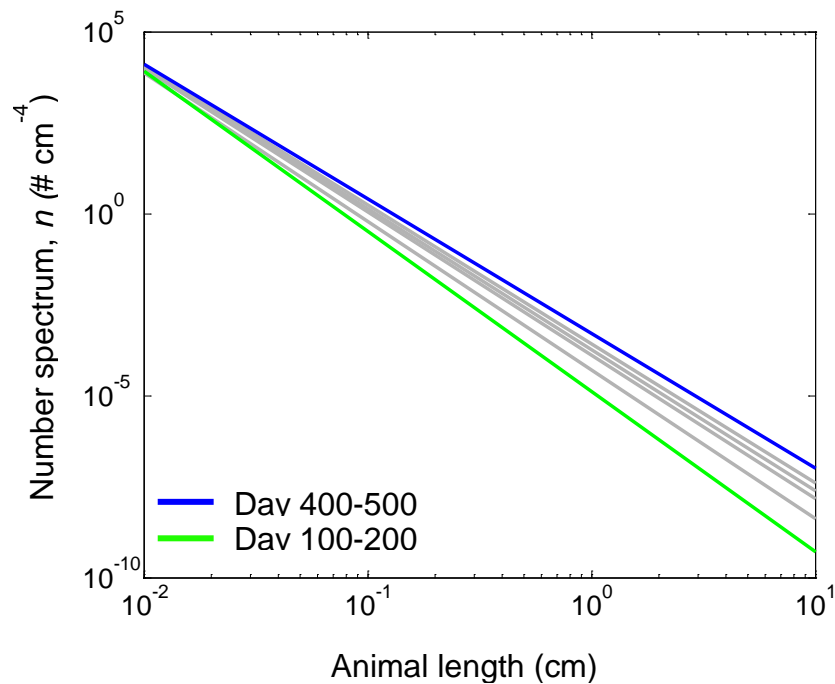


Figure 4.18. Expected size spectra of vertically stratified scattering layers. The blue and green lines show the size spectra of ensonified zooplankton assemblages of the 400-500 m and 100-200 m scattering layers, respectively, located within a 24 hr window of glider travel from fronts along lines 80 and 90. For comparison, the gray lines show the expected size spectra from figure 16.

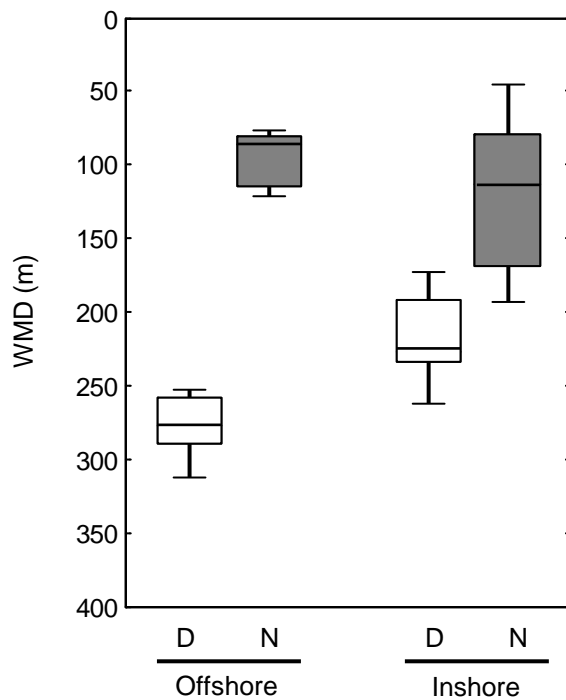
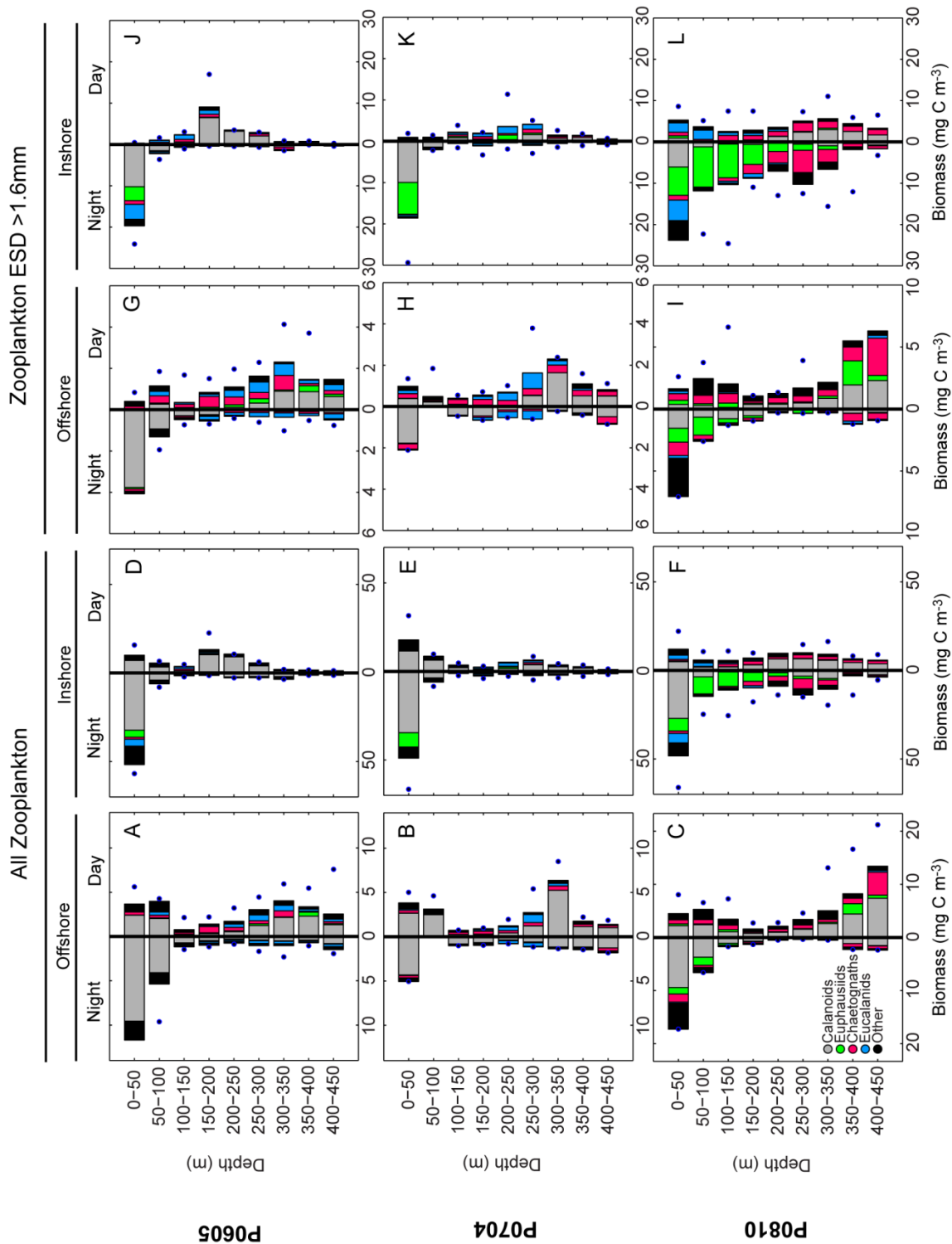


Figure 4.19. Day (D) and Night (N) weighted mean depths (WMD) of zooplankton in the offshore and inshore regions. Box plots show WMD of zooplankton collected by Mocness offshore by day (N=10, open) and night (N=6, filled) and zooplankton collected inshore during day (N=13) and night (N=10).

Figure 4.20. Vertical distributions of carbon biomass of major zooplankton taxa in the inshore and offshore regions on three cruises: P0605, P0704, P0810. The depth distributions of (A-F) all zooplankters, and (G-L) zooplankters with an ESD greater than 1.6 mm are shown for (A-C,G-I) offshore and (D-F,J-L) inshore Mocness tows. Each bar shows the median carbon biomass concentration of all Mocness nets collected from the indicated depth stratum. Divisions within each bar indicate the mean percentage of biomass that was contributed by each major taxonomic group (calanoid copepods excluding eucalanids, euphausiids, eucalanid copepods, chaetognaths, and all others). Blue dots accompanying each bar indicate the maximum biomass value recorded at that depth. Note that horizontal scales differ.



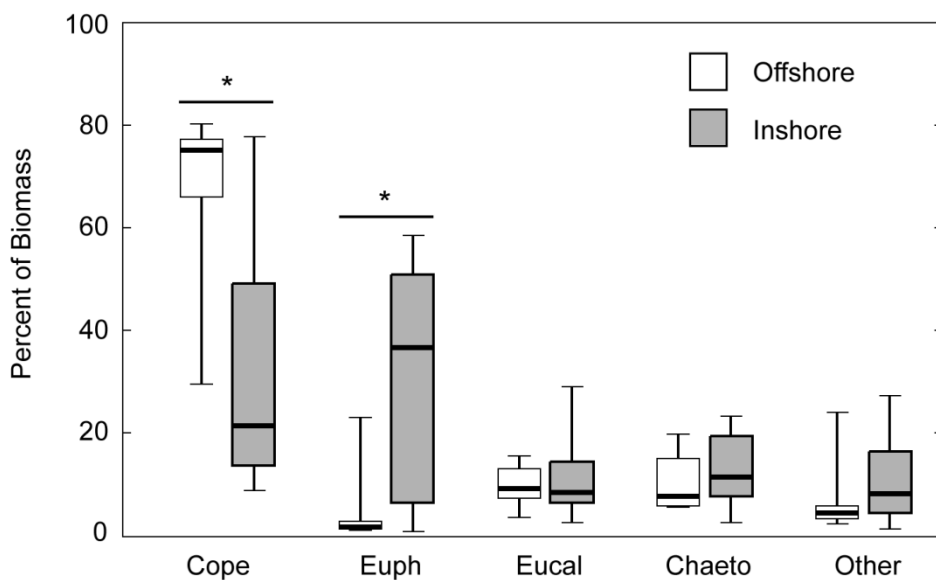


Figure 4.21. Comparison of inshore and offshore carbon biomass contributions of different taxonomic groups for the three cruises combined (P0605, P0704, P0810). Boxplots shows the percent of biomass contributed to total biomass by a taxon (calanoid copepods excluding eucalanids, euphausiids, eucalanid copepods, chaetognaths, and all others) for inshore tows (N=10) and offshore tows (N=6). Each box spans the 25th to 75th percentile range of biomass, upper and lower whiskers show the minimum and maximum, and the black line within each box shows the median value. Asterisks indicate significant differences (P<0.05; Mann-Whitney U test) between inshore and offshore percent biomass contributions for that taxonomic group. Absence of asterisks indicates P>0.05.

Figure 4.22. Vertical distributions of carbon biomass different zooplankton size categories in the inshore and offshore regions on three cruises: P0605, P0704, P0810.. The depth distributions of (A-F) all zooplankters, and (G-L) zooplankters with an ESD greater than 1.6 mm are shown for (A-C,G-I) offshore and (D-F,J-L) inshore Mocness tows. Each bar shows the median carbon biomass concentration of all Mocness nets collected from the indicated depth stratum. Divisions within each bar indicate the mean percentage of biomass that was contributed by each size category. Blue dots accompanying each bar indicate the maximum biomass value recorded at that depth. Note that horizontal scales differ.

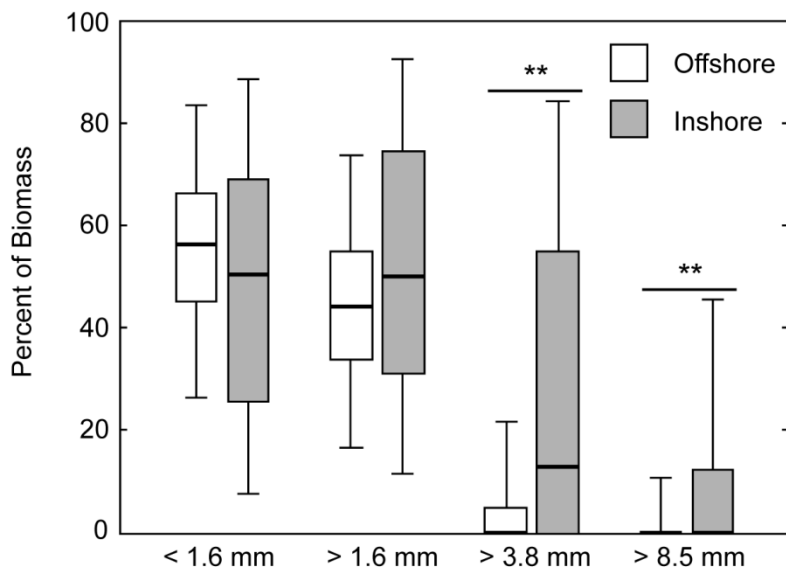


Figure 4.23. Comparison of inshore and offshore carbon biomass contributions of different size classes for three cruises combined (P0605, P0704, P0810). Boxplots shows the percent of biomass contributed to total biomass by a size class for inshore net samples (N=89) and offshore net samples (N=45). Each box spans the 25th to 75th percentile range of biomass contributions, upper and lower whiskers show the 95th and 5th percentile, and the black line within each box shows the median value. Double asterisks indicate significant differences (P<0.001; Mann-Whitney U test) between inshore and offshore percent biomass contributions for that size class. Absence of asterisks indicates P>0.05.

Chapter 5.

Summary and conclusions

Life in a turbulent ocean... as observed by Spray gliders

In this dissertation I have sought to describe some of the general characteristics and biological consequences of fronts within the Southern California Current System (SCCS) using data collected by *Spray* ocean gliders. Unlike previous studies which focused on individual fronts, I compared the conditions found at 154 fronts occurring over a 6 year period with the conditions found in areas located away from fronts, in order to describe the role fronts play in the regional ecosystem. I describe the spatial and seasonal distribution of fronts during the six-year period, as well as how fronts structure habitat types, biomass distributions, and zooplankton vertical migration behavior (DVM) within the region. I also examine cross-frontal changes in zooplankton assemblages, or at least those changes detectable by *Spray's* instruments. In this concluding chapter, I will review these main results, and also suggest future research directions which will expand our understanding of the ecological importance fronts in the SCCS.

This dissertation represents the first multi-year, *in situ* study of fronts within a broader region like the SCCS. This dissertation would not exist if it were not for autonomous ocean gliders like *Spray*. Autonomous technologies in general, and gliders in particular, are enabling a new approach to biological oceanography and pelagic ecology. In the final parts of this concluding

chapter, I examine where gliders could and should take our discipline. Gliders will enable a much tighter coupling between empirical observations and real-time ecosystem modeling, and I believe this will lead to a new era of discovery in the ocean sciences.

Estimating zooplankton biomass with the Spray ADP

The results presented in this dissertation relied extensively on data collected by *Spray* gliders whose instrument packages were pre-determined prior to my research. As such, my results pertaining to zooplankton distributions used acoustic backscatter (ABS) from Sontek acoustic doppler profilers (ADP) instead of a purpose-built scientific echosounder optimized for the study of zooplankton distributions. In Chapter 2, I demonstrate that the ABS measured by Sontek ADPs is proportional to the biomass of zooplankton ensonified within the beam, and that zooplankton with equivalent spherical diameters (ESD) greater than 1.6 mm account for most of the observed ABS. Copepods contribute proportionally more to observed ABS at the low end of ABS observations, whereas euphausiids and other larger-bodied zooplankton contribute more when observed ABS is high.

Although the Sontek ADP is adequate for estimating bulk biomass distributions, more advanced acoustic instrumentation would augment future studies. One possibility would be to alter the Sontek ADP firmware. The Sontek ADP records ABS within 4 m range bins, but the firmware could be modified to record ABS within much narrower range bins (< 10 cm). With

narrower range bins and shorter pulse lengths, the inverse methods I explored in Chapter 4 (which infer zooplankton size spectra from ABS data) would have been more robust to noise due to a greater number of possible interbeam comparisons. Another possibility would be to augment the glider with a purpose-built scientific echosounder to further improve our ability to estimate zooplankton biomass and detect changes in assemblages. Indeed, the integration of multi-frequency echosounders into gliders and AUVs now seems possible (Lemon et al. 2012).

Front distribution and seasonality in the SCCS, and their role in structuring plankton distributions

Several satellite-based studies (Castelao et al. 2006, Belkin et al. 2009, Kahru et al. 2012) have demonstrated that fronts are a common feature in the SCCS. The *in situ* glider-based observations of front seasonality and spatial distribution presented in Chapter 3 corroborate these studies. Perhaps more importantly, the glider observations elucidate the role that fronts play in structuring zooplankton biomass distributions (as inferred from ABS data) and phytoplankton distributions (as inferred from chlorophyll-*a* (Chl-*a*) fluorescence). I found that horizontal gradients in ABS and Chl-*a* covaried with horizontal gradients in physical variables such as density, salinity and temperature, and that physical fronts (marked by the strongest gradients in density) were often colocated with biological fronts (marked by the strongest gradients in ABS or Chl-*a*). Previous ship-based studies have shown that

physical ocean fronts were also biological ocean fronts, but I showed that this was a general characteristic of fronts and not just a statistical fluke or artifact due to confirmation bias.

I also found that fronts were typically zones of plankton biomass accumulation, as opposed to merely zones of altered biomass gradients. Using these data, I estimated that large mobile predators would find better foraging grounds up to 77% of the time simply by traveling up horizontal density gradients. These results illustrate the true value of extended observations of dynamic, ephemeral structures like fronts enabled by gliders.

While the glider data were useful for describing the average characteristics of fronts and their relationship to inferred biomass gradients and accumulation zones, the data were less useful in determining the physical mechanisms through which these gradients and accumulation zones were generated. There was no consistent correlation between horizontal gradients in acoustic backscatter and horizontal gradients in either along-track or cross track flow. One might expect that advection would play an important role in creating and maintaining the enhanced zooplankton biomass gradients and accumulation patterns seen at fronts. However, zooplankton distributions at any given time point are the result of an integration of many processes (e.g., advection, reproduction, growth, predation, and vertical migration) occurring over a period of weeks to months. It is perhaps not surprising that resolving the pattern-generating mechanisms would be difficult with glider passes that sampled the same location every 2-3 weeks.

One future approach to resolving mechanisms may be to deploy two gliders concurrently along each glider line. The first glider would transit back and forth along the line as usual, but the second glider would focus on frontal features found by the first. The second glider could cross the front many times, building up a time-varying picture of the front and capture the evolution of velocity fields and biomass distributions over a period of weeks.

It would also be interesting to extend the results of Chapter 3 by combining both glider and satellite data in order to place the glider-observed fronts in a broader context. The glider provides only a snapshot of conditions along a 2-D section as it crosses a front. There are many things we cannot deduce from a snapshot. For example, is a particular glider-observed front a mesoscale or submesoscale feature? Did the glider cross the front orthogonally? Do satellite altimetry data predict enhanced geostrophic flow? Did the glider cross the front at a cyclonic or anti-cyclonic bend? How long has the front persisted? Answers to these questions could help define which frontal conditions are most associated with increased biomass accumulation and to what degree advection influences biomass distributions.

Another area of future research is determining the degree to which *in situ* growth contributes to observed plankton distributions seen at fronts, and under what conditions physically caused accumulation predominates. Currently, the *Spray* glider can only measure proxies for the standing stocks of phytoplankton and zooplankton; it cannot measure rates such as primary and secondary productivity. Measuring rates is critical to understanding how fronts

impact the ecology of a wider region. Adding a nitrate sensor (to estimate the potential for increased primary productivity), and a multi-spectral, variable fluorescence fluorometer (to identify dominant phytoplankton taxa, and estimate photosynthetic potential and phytoplankton health) would improve our ability to model the primary productivity of a water parcel. Integrating a plankton imaging camera in the glider would improve our ability to estimate secondary production by identifying dominant plankton taxa and measuring abundances of eggs and nauplii within a water parcel.

It may also be possible to apply more sophisticated methods of analysis to elucidate mechanisms than were done in this dissertation. The results presented in Chapter 3 relied mostly on simple correlations, linear regression, and non-parametric methods to compare median values. These methods were appropriate for quantifying general characteristics of fronts, but they are less useful for unraveling mechanisms. More flexible methods such as general additive models (GAMS) (Hastie and Tibshirani 1987) may provide more insight into how biomass distributions are generated in the SCCS. Recently, state space reconstruction (SSR) methods (Deyle et al. 2013) have proven useful in estimating a variable (e.g., accumulated biomass) that is part of a dynamical system controlled by interacting, non-linear processes (e.g., advection, primary production, growth, predation). One powerful advantage of SSR methods is their robust ability to estimate a variable such as biomass accumulation even when data for some of the other explanatory variables are missing.

Fronts as boundaries between planktonic ecosystems.

In Chapter 3, I found that the time-evolution and spatial context of a front makes each front unique. For example, not all fronts were associated with strong gradients in biomass distribution. Nonetheless, in Chapter 4, average cross-frontal changes in temperature, salinity, and the depth of the euphotic zone suggest that planktonic habitats are consistently different when crossing a front from inshore to offshore in the SCCS. Inshore waters were consistently colder, saltier, and more turbid compared with offshore waters that were warmer, fresher, and clearer. These physical changes were accompanied by changes in some characteristics of the in situ plankton assemblages. Offshore of fronts I found increased depths of the chlorophyll maximum (DCM) and increased amplitude of diel vertical migration (DVM). Others have noted similar cross-frontal changes in the vertical distribution of chlorophyll fluorescence and the depth of the euphotic zone (Andersen et al. 2004), but the present study was able to measure the average depth change of the DCM across fronts during an extended study period of six years. Likewise, others have noted changes in diel vertical migration (DVM) behavior across individual fronts (Moser and Smith 1993, Andersen et al. 2004), but the present study is the first to show that cross-frontal changes in DVM behavior is a general characteristic of fronts in the SCCS, and covaries with the optical characteristics of the water column.

One of the most interesting results from Chapter 4 involved inferred changes in zooplankton assemblages across fronts. In general, offshore of fronts smaller-bodied zooplankton contributed more to the overall zooplankton biomass compared to inshore of fronts, where larger bodied-zooplankters contributed proportionally more to the overall biomass. Combined with the marked increase in DVM amplitude offshore of fronts, I interpreted these results to mean that fronts separate waters with different zooplankton assemblages. Cross-front changes in zooplankton assemblage have been observed in many ship-based studies of individual fronts (Mackas et al. 1991, Ohman et al. 2012), but this is the first study to determine that this is a general property of fronts in the SCCS.

Inclusion of a multi-frequency or broadband scientific echosounder in the *Spray* instrument package would provide much greater insight into the kinds of changes in zooplankton assemblage seen across fronts. This could be particularly useful for determining the foraging potential of fronts for mobile predators such as tuna, seabirds, and whales.

A new model for discovery in Biological Oceanography

With more gliders, better sensors, satellite data, increased ship-based sampling, it may indeed be possible to better identify ocean conditions that lead to biomass accumulation, increased primary and secondary production, and altered species assemblages at fronts. This is the traditional observational approach to biological oceanography.

However, there is a fundamental problem with this approach. It is inherently backward looking. While we have increased the number of snapshots of the system, we still have not turned these snapshots into a true video which shows the time-evolution of the system. In other words, we may have better described the probability density functions of the different outcomes in response to known conditions, but we have not demonstrated a true mechanistic understanding necessary to describe how fronts impact the wider region. Will increasing the number of snapshots of the SCCS allow us to predict primary and secondary production? Perhaps in a probabilistic way. Will we be able to predict community succession patterns, recruitment, or population dynamics? Can we begin to understand what role fronts might play in regional ecosystem stability and resilience, or ecosystem change? Will we be able to predict ecosystem functioning under future climates? We are not yet at that point.

A true mechanistic understanding of how fronts impact the ecology of the region can only be explored with coupled physical-biological models. However, modeling ocean ecosystems is inherently difficult. Even the simplest analytical models, such as Nutrient-Phytoplankton-Zooplankton-Detritus (NPZD) models, can display complex behavior depending upon initial parameterizations. Moreover, there are fundamental problems with the way we currently use models. As Franks (2009) points out, the assumptions underlying the formulation and parameterization of models are rarely closely examined. Often, the model formulation and parameterization is inappropriate to the

investigation. More importantly, models are rarely treated as real hypotheses (i.e., those which can be falsified by new empirical data). Instead of testing which model amongst many best explains the data, the same model is often used again and again to describe a variety of situations.

Biological Oceanography employs both empirical methods (observation and experimentation) and theoretical methods (modeling). The problem is that the empirical and theoretical approaches are not well integrated. As Franks (2009) succinctly puts it: “we do not model what we measure, and we do not measure what we model.”

There is a better way to do biological oceanography. We need to build a better integrated observing system that combines glider and satellite data with extensive real-time modeling. Automatically assimilating glider and satellite data into high-resolution regional nowcast and forecast models will accomplish two goals: first, we will be able to simultaneously test multiple ecosystem models and discover which model best explains the data. Second, high-resolution regional models will enable adaptive sampling by gliders or small, fast boats to target areas where models are underperforming. “Just in time” boat-based sampling (as opposed to traditional ship-based sampling which is often scheduled years in advance) would collect data and samples not generally collected by the gliders (e.g., DNA sequencing, enzymatic assays, species identification, etc.).

Not only will this integrated approach finally allow us to model what we measure, and vice-versa, it will significantly accelerate the iteration cycle of

hypothesis, measure, test, analysis from a period lasting several years to one lasting only weeks or months. The ability to quickly formulate multiple alternate hypotheses and test them is critical to strong inference (Platt 1964), and is what distinguishes a healthy scientific discipline from an ailing one.

Positive trends in four technology areas will enable this new mode of discovery. First, advances in low-power computing are enabling sophisticated software to run on everything from autonomous vehicles to smartphones. For the past several decades, the energy required per bit of computation has fallen by half every 1.5 years (Kooimey et al. 2011). In other words, in ten years only 1% of the battery capacity will be required for a given computational load as is required today. This translates into increased mission durations and more sophisticated computing available for onboard data analysis and data reduction.

Second, coupled physical-biological ecosystem models will greatly improve due to advances in high performance computing. Supercomputing performance (measured in floating point operations per second) has doubled nearly every year for the last two decades (Service 2012). Additionally, powerful new methods such as probabilistic programming and quantum computing (Watrous 2008) are being developed that can rapidly search a model space of functional forms and parameters to automate the optimization of complex ecosystem models. This will help researchers rapidly update, explore, and test suites of models simultaneously.

Third, advances in materials science and nanotechnology are fostering new battery technologies. For example, within five years Lithium-seawater batteries may provide a 300% increase in mass-specific energy capacity (1500 Wh/kg compared with 500 Wh/kg) and a 50% increase in volumetric energy capacity (1500 Wh/liter compared with 1000 Wh/liter). Better batteries will enable longer missions and provide increased power for sensors and on-board data processing.

Fourth, low-power electronics and sensor technology is advancing rapidly. A wide range of advanced instrumentation has already been deployed (at least in prototype form) on AUVs or gliders, including doppler profilers, side-scan sonars, didson sonars, echosounders, passive acoustic arrays, camera systems, flow-through imagers (e.g., ISIS), ctds, oxygen sensors, pH sensors, nutrient sensors, mass spectrometers, to name a few. A primary goal for glider development should be the creation of multi-instrumented glider designed to study a wide range of biological oceanography questions. Currently, each sensor handles its own signal conditioning, processing, and data management. Significant power, cost and space savings could be achieved by combining more sensors into an integrated package. With adequate funding, a standard “bio-glider” package (Table 5.1) could be developed within 10 years. Such a bioglider would greatly improve our ability to model pelagic ecosystems, particularly with regard to what happens at dynamic features like fronts.

A call to arms: what are the big questions?

A regional, glider-based integrated observation and modeling system capable of resolving oceanic and ecosystem processes at high resolution will allow us to tackle the big outstanding questions in biological oceanography: How are primary and secondary production controlled in a dynamic ocean? How do low frequency environmental forcings such as PDO and NPGO modulate production at the fine-scale? Can fisheries recruitment, standing stocks, and spatial distributions be predicted? Can mortality patterns be predicted? What are the real barriers to speciation and how are populations interconnected? What changes can we expect in production, carbon uptake, species abundance under future climates? How will ocean acidification alter ecosystem function?

Of course, these are not novel questions, but we have never had the tools to adequately answer them before. Our efforts thus far have been too limited in scope due to insufficient sampling, a lack of tight coupling between field data and hypothesis-driven, adaptive modeling, and an inability to rapidly iterate the hypothesis cycle. The old model dominated by ship-based sampling is inadequate and rapidly becoming outdated. Ship time is becoming more expensive, and overall funding for the scientific fleet is declining (Kintisch 2013). Alternatively, some would argue that the Ocean Observing Initiative is the way forward for biological oceanography and pelagic ecology. In my opinion, it is not. The OOI system is too dependent upon a comparatively sparse network of expensive, fixed infrastructure (e.g., moorings and cabled

sea-bed infrastructure). A glider-based network is much less expensive, more flexible in terms of adapting to future sensor technology, and most importantly, covers a broader area with more sensors.

However, perhaps the most important reason to build such a network lies in its potential to answer the as yet unasked questions. The most interesting questions will be the ones which completely redefine our understanding of how the ocean works. In physics, the holy grail for the experimentalist and the theoretician alike is to discover something that completely overturns the existing understanding of how things work – in other words, new physics. I don't see this overarching desire in biological oceanography. More often, it seems we merely try to square observations or model results with our current understanding. This is a consequence of insufficient sampling and moribund modeling efforts. The new approach advocated here can put us on the right track.

So, where might we look for “new physics” in biological oceanography? I would argue that we need to be looking for emergent ecosystem behaviors which can only be explained by coordinated behavior of disparate components. Marine communities are interconnected networks of species and individual organisms. We see emergent behavior in many other biological networks (e.g., social insects, the human brain, genome regulation, and the human-microbial complex), so it is reasonable to assume that emergent behaviors may be important at the ecosystem level as well. What determines ecosystem stability and resilience? To what extent are pelagic ecosystems structured by positive

species interactions (mutualisms and commensalisms) compared to negative species interactions (predation and competition)? What are the feedbacks between the biotic and abiotic components of the system? Are there an infinite or finite number of states in an ecosystem? Can an ecosystem be considered a super-organism which adapts to, or even anticipates changing physical conditions? These were the types of questions that were previously the exclusive domain of the theoretical ecologist. Glider-based networks coupled with continual model testing and just-in-time sampling will allow us to quantitatively examine these questions. The future is bright, and wet.

References

- Andersen, V., C. Devey, A. Gubanov, M. Picheral, V. Melnikov, S. Tsarin, and L. Prieur. 2004. Vertical distributions of zooplankton across the Almeria-Oran frontal zone (Mediterranean Sea). *Journal of Plankton Research* **26**:275-293.
- Belkin, I. M., P. C. Cornillon, and K. Sherman. 2009. Fronts in large marine ecosystems. *Progress in Oceanography* **81**:223-236.
- Castelao, R. M., T. P. Mavor, J. A. Barth, and L. C. Breaker. 2006. Sea surface temperature fronts in the California Current System from geostationary satellite observations. *Journal of Geophysical Research: Oceans* **111**: C09026, doi:10.1029/2006JC003541.
- Deyle, E. R., M. Fogarty, C.-h. Hsieh, L. Kaufman, A. D. MacCall, S. B. Munch, C. T. Perretti, H. Ye, and G. Sugihara. 2013. Predicting climate effects on Pacific sardine. *Proceedings of the National Academy of Sciences*.
- Franks, P. J. S. 2009. Planktonic ecosystem models: perplexing parameterizations and a failure to fail. *Journal of Plankton Research* **31**:1299-1306.

- Hastie, T. and R. Tibshirani. 1987. Generalized Additive-Models - Some Applications. *Journal of the American Statistical Association* **82**:371-386.
- Kahru, M., E. Di Lorenzo, M. Manzano-Sarabia, and B. G. Mitchell. 2012. Spatial and temporal statistics of sea surface temperature and chlorophyll fronts in the California Current. *Journal of Plankton Research* **34**:749-760.
- Kintisch, E. 2013. A Sea Change for U.S. Oceanography. *Science* **339**:1138-1143.
- Koomey, J. G., S. Berard, M. Sanchez, and H. Wong. 2011. Implications of Historical Trends in the Electrical Efficiency of Computing. *Annals of the History of Computing, IEEE* **33**:46-54.
- Lemon, D., P. Johnston, J. Buermans, E. Loos, G. Borstad, and L. Brown. 2012. Multiple-frequency moored sonar for continuous observations of zooplankton and fish. Pages 1-6 *in Oceans, 2012*.
- Mackas, D. L., L. Washburn, and S. L. Smith. 1991. Zooplankton Community Pattern Associated with a California Current Cold Filament. *Journal of Geophysical Research-Oceans* **96**:14781-14797.
- Moser, H. G. and P. E. Smith. 1993. Larval fish assemblages and oceanic boundaries. *Bulletin of Marine Science* **53**:283-289.
- Ohman, M. D., J. R. Powell, M. Picheral, and D. W. Jensen. 2012. Mesozooplankton and particulate matter responses to a deep-water frontal system in the southern California Current System. *Journal of Plankton Research* **34**:815-827.
- Platt, J. R. 1964. Strong Inference: Certain systematic methods of scientific thinking may produce much more rapid progress than others. *Science* **146**:347-353.
- Service, R. F. 2012. What It'll Take to Go Exascale. *Science* **335**:394-396.
- Watrous, J. 2008. Quantum Computational Complexity. arXiv:0804.3401v1.

Table 5.1. Sensors that might be integrated into single multi- instrument package on future gliders.

| Sensor | Scientific Rationale |
|---|--|
| Hydrographic | |
| CTD | Water column structure |
| Dissolved Oxygen | Oxycline, community respiration |
| pH and pCO ₂ | Ocean acidification, community respiration |
| Nitrate sensor | Nutrient profiles, upwelling tracer |
| PAR | Light availability, primary productivity |
| ADCP | Current structure, fine scale patchiness studies |
| Bio-Acoustic | |
| Multi-frequency or Broadband Echosounder | Fish and zooplankton |
| Passive acoustics | Marine mammals |
| Bio-Optical | |
| Zooplankton Imager | Estimates of abundance, biomass, species distributions, and secondary production |
| Advanced Laser Fluorometer | Estimates of phytoplankton taxa distributions, biomass, primary production |

Appendix I

Supplement to chapter 2

1. Sampling Apparatus
2. Sampling Site
3. Mocness Samples, Zooplankton Taxa Analyzed
4. Zooplankton Carbon Biomass Calculations

1. Sampling Apparatus

A self-powered, internally-recording Sontek Acoustic Doppler Profiler (ADP) as used on the *Spray* gliders (e.g., Davis et al., 2008) was used to record acoustic backscatter in situ while the Mocness collected zooplankton samples. The ADP was mounted so as to align two of the three acoustic beams with the same depth strata that the net was sampling (Fig. S1). Due to the geometry of the ADP sensor head, the two beams aligned along the same depth strata as the net pointed horizontally away from the mouth of the net at an angle of 25°. While this can lead to increased variance between Acoustic Backscatter (ABS) and net-measured biomass due to small-scale patchiness, this sampling geometry allows simultaneous acoustic and net sampling that is much more spatially overlapped than previous ADCP-biomass studies.

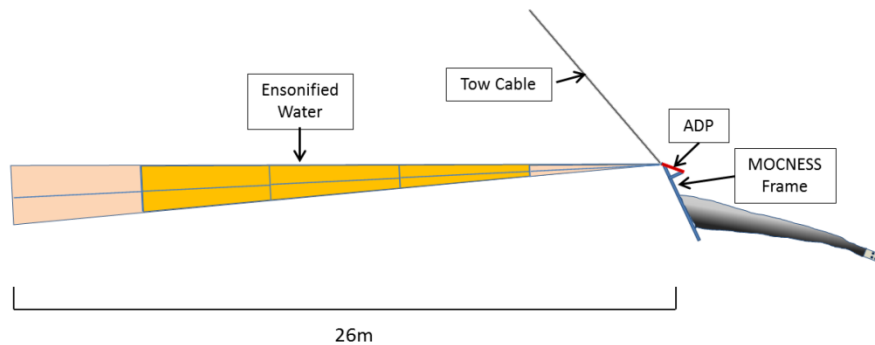


Fig. S1. Sampling geometry of Mocness-mounted ADP. The ADP was mounted to the frame so that two of the three acoustic beams were roughly level with the mouth of the net. The third beam points up to the surface, and was not used in analysis. Only one of the two beams is pictured here. The tow level beams point away from each other with a solid angle between them of 50°. Of the five total range cells recorded for each beam by the ADP, only cells 2 through 4 (depicted in darker yellow) were used in this study.

2. Sampling Site

All Mocness tows were completed within the Santa Barbara Basin within 5 km of each other between the dates of 26 September 2010 and 2 October 2010.

Table S1. Station locations for Mocness tows.

| Tow | Start Date (PST) | Start Time (PST) | Latitude (° N) | Longitude (° W) | Maximum Tow Depth |
|-----|------------------|------------------|----------------|-----------------|-------------------|
| 2 | 26 Sept. | 02:00 | 34.2958 | 120.0379 | 449 |
| 3 | 28 Sept. | 11:20 | 34.3082 | 120.0009 | 522 |
| 4 | 29 Sept. | 21:51 | 34.2523 | 119.9360 | 517 |
| 8 | 1 Oct. | 06:22 | 34.2805 | 119.9953 | 524 |
| 9 | 2 Oct. | 01:57 | 34.2934 | 120.0255 | 526 |

3. Mocness Samples, Zooplankton Taxa Analyzed

Forty-three individual Mocness samples were collected during five tows. Each sample was preserved in 1.8% formaldehyde and then processed ashore using Zooscan, an optical imaging and image processing system (Gorsky *et al.*, 2011). In Zooscan, an aliquot of each sample is scanned with a modified flatbed scanner. The images are then processed using automated image analysis routines which classify each individual plankter within the scanned image as a member of a given category. The categories used in this project are listed in table S2. After all samples have been processed with Zooscan, and the classification results have been manually checked (and corrected, if necessary) by a person, biomass concentration is then estimated in terms of organic carbon or cross-sectional area (as Summed Area Concentration). Biomass estimation procedures are described below in section 4.

Table S2. Taxon Categories Identified by Zooscan in this study.

| | | | |
|--------------------------|----------------------------------|-------------|----------------|
| amphipods | copepods (<i>Oithona</i> -like) | euphausiids | pneumatophores |
| appendicularia | copepods (others) | fish larvae | Polychaetes |
| bryozoan larvae | copepods (poecilostomatoids) | medusae | pteropods |
| chaetognaths | other crustacea | multiples | siphonophores |
| copepods (calanoids) | ctenophores | nauplii | |
| copepods (eucalanids) | doliolids | ostracods | |
| copepods (harpacticoids) | eggs | other misc. | |

The influence of the composition of zooplankton assemblages upon measured acoustic backscatter has been a topic of intense study in bioacoustics. Both General Additive Model (GAM) and multiple linear regression analysis (figure 3 in paper) indicated that increasing relative contribution of the euphausiids and “others” categories to a sample’s biomass was associated with increased backscatter, whereas increasing contribution of copepod biomass was generally associated with decreased backscatter. These trends can be seen when biomass is plotted on a percentage basis by taxa and compared with RMVBS (Fig. S2)

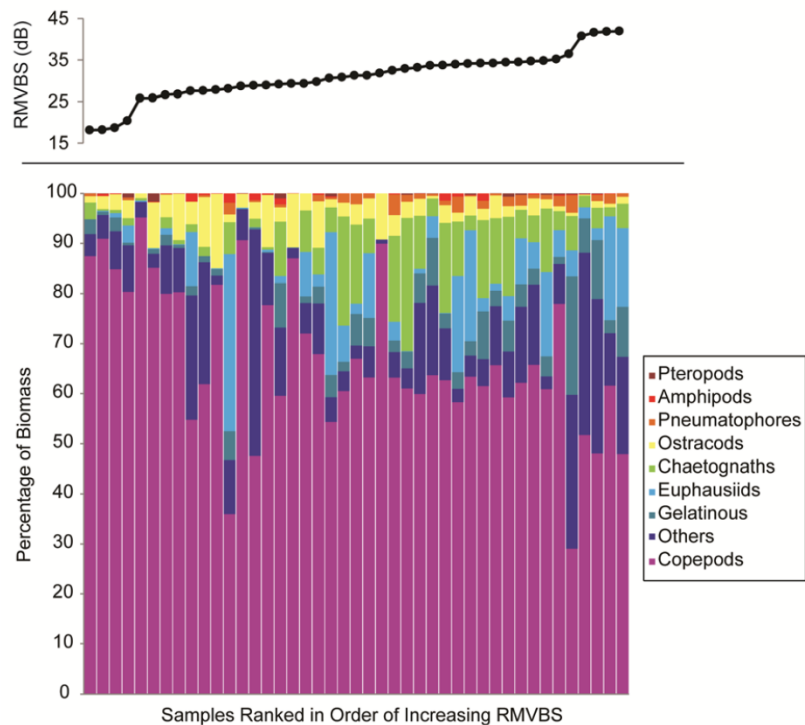


Fig. S2. Relationship between sample taxonomic composition and RMVBS. Each net sample's taxonomic composition is displayed in terms of percentage biomass within the sample (lower panel). Six of the categories represent single taxa from table S2 and three taxa categories are composed of multiple taxa. "Gelatinous" includes ctenophores, doliolids, medusae and siphonophores. "Copepods" includes all six sub-categories of copepods listed in table S2. "Others" includes all other categories from table S2. The samples are ranked in increasing order of RMVBS and each sample's RMVBS is plotted in the upper panel.

4. Zooplankton Carbon Biomass Calculations

The carbon biomass estimation procedure for each taxon relies on an empirically derived equation from previous studies of zooplankton length-carbon relationships (Ohman and Lavaniegos, 2007; Gorsky *et al.*, 2010). In this study, it was found that the Zooscan-generated length measurements of individual plankters could be under-estimated (e.g. if the animal was coiled upon itself) or overestimated (e.g. long antennae of a plankter led to an erroneously large total length estimate). Thus, a more robust length estimate was derived from a plankter's total scanned surface area (excluding open regions of background) that was converted to Equivalent Circular Diameter (ECD). ECD was then converted to total length using taxon-specific total length-ECD relationships determined manually from scanned organisms. In a few cases where conversions were not available, a general cross-sectional area-carbon relationship (Alcaraz *et al.*, 2003) was substituted. A comparison between estimated carbon biomass ($\mu\text{gC m}^{-3}$) and Summed Area Concentration (SAC, $\text{mm}^2 \text{m}^{-3}$) shows that the two quantities are highly correlated (Fig. S3A), though they tend to diverge more at the high end of the biomass range within the samples (Fig. S3B).

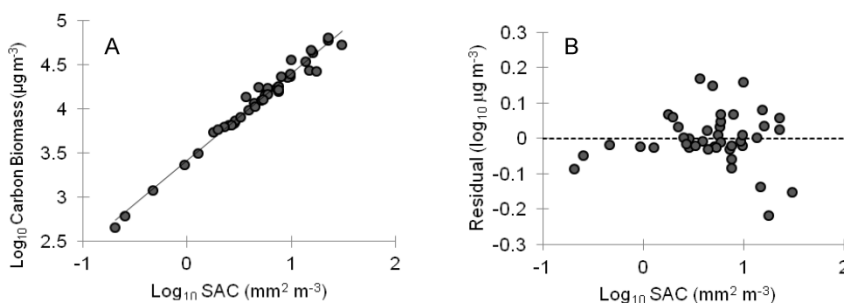


Fig. S3. Relationship between carbon biomass estimates and Summed Area Concentration, SAC. Panel A depicts the correlation between the two variables across all 43 Mocness samples. The line is a simple linear regression. Panel B shows the residual (predicted log_{10} carbon biomass – measured log_{10} carbon biomass) as a function of the logged SAC.

A regression of logged carbon biomass with RMVBS (Fig. S4) yields an r^2 value (0.47) nearly as high as the log_{10} SAC-RMVBS correlation. However, the use of this ADP to measure carbon biomass in the field must be approached with caution. At each point, predicted carbon biomass can deviate from actual carbon biomass by almost an order of magnitude, though when measurements are binned at an appropriate scale it should be possible to compare at least the relative biomass of different locations in the field.

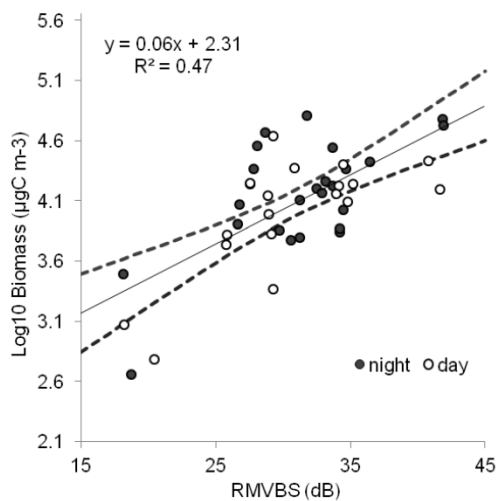


Fig. S3. Relationship between \log_{10} carbon biomass and Relative Mean Volume Backscatter (RMVBS, dB). The regression of RMVBS against \log_{10} carbon biomass is depicted by the solid line, with 5% and 95% confidence intervals for the regression illustrated by dashed lines. Night and day samples are indicated by closed and open circles, respectively.

REFERENCES

- Davis, R. E., Ohman, M. D., Rudnick, D. L., *et al.* (2008) Glider surveillance of physics and biology in the southern California Current System. *Limnol. Oceanogr.*, **53**, 2151-2168.

Appendix II

ADP calibration protocols

The *Spray* acoustic doppler profiler (ADP) was specially designed for the *Spray* by Sontek YSI, Inc. to measure current velocities. In my dissertation, I have also used the *Spray* ADP as an echosounder to map and quantify zooplankton distributions. The Ohman lab has developed protocols to test ADPs in an instrument test pool at Scripps Institution of Oceanography before and after each glider deployment. The purpose of these protocols is to 1) for each transducer, measure the acoustic backscatter (ABS) from a known target located in the center of the acoustic beam at a fixed distance from the ADP, 2) record the beam pattern for each transducer, and 3) to discover any potential problems with an ADP before it is deployed.

Calibration setup

The ADP is tested in an oval-shaped, freshwater pool (Fig. A2.1) whose interior dimensions are 5.5 m width, 12.5 m length and a minimum 4 m in depth. Prior to instrument calibration, the pool pumps are turned off and the pool is allowed to de-gas for at least 12 hr.

At one end of the pool (e.g., approximately 3 m from the one end of the oval), the ADP is suspended from an aluminum beam 2 m below the surface, along the long-axis of the pool. The ADP is mounted in a bracket so that the

beam being tested is aligned along the long axis of the pool, and is parallel to the surface of the water.

At a distance of 5 m from the ADP transducer face, a computer-controlled X-Y stepper motor stage is mounted to a wooden bridge spanning the pool. The target sphere (a 1 cm tungsten-carbide ball) is suspended by monofilament into the pool from the X-Y stepper motor stage so that the ball can be moved in a 1 m² grid perpendicular to the beam axis.

The maximum backscatter is achieved when the sphere is located at the exact center of the beam. It was discovered in late 2008 that air-bubbles can be trapped on the thread that holds the target sphere, leading to erroneously high backscatter. This problem was overcome by soaping the thread with dish soap.

A Matlab script controls the position of the target sphere in the X-Y grid via serial commands to the motor controller. The Matlab script also controls when the ADP pings the target, and records the post-ping ABS from the target. The script systematically moves the target through a 5 cm grid spaced series of positions (i.e. 400 positions total), and records ABS from 3 pings at each of these positions. The script then determines the likely center of the acoustic beam and records pings from an additional 100 positions (2 cm grid spacing) centered on this location. After finishing this second grid pattern, the script determines the maximum backscatter measured by the ADP at the center of the

beam and posts this result to a private website along with an image of the beam pattern to archive the data.

Beam Pattern

Since the *Spray* ADP uses a simple circular monostatic transducer, the resulting beam pattern recorded during the calibration should be circular (Fig. A2.2). The beam map also allows calculation of the half-beamwidth, or the angle off-axis that the recorded beam strength drops by 6dB. For example, using the approximately 18 cm off-axis distance observed in the beam pattern in figure 1, and the 5 m distance to the target, the half-beamwidth angle is equal to $\text{atan}(0.18/5)$, or 2° .

Maximum ABS from a known target

In order to track instrument drift over time in any particular ADP, and to ensure comparability between different ADP instruments, I recorded the maximum return from the target for each beam for each ADP before and after it was deployed. Figure A2.2 shows the acoustic backscatter (80 dB) measured by the ADP when the acoustic return was maximal (i.e. when the target was in the center of the beam). Compiled results from these calibrations are presented in Tables A2.1 and A2.2.

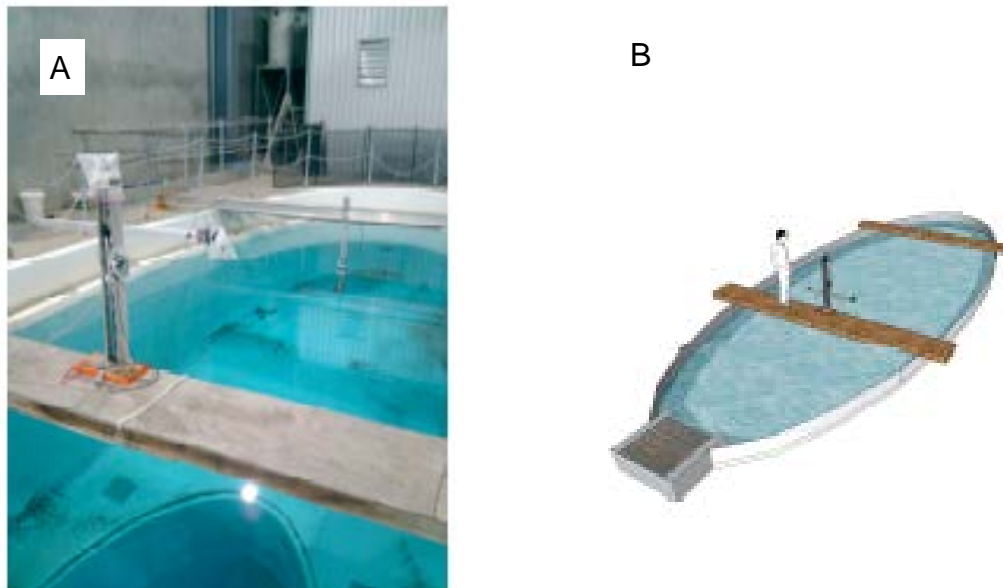


Fig. A2.1. (A) ADP testing set-up in the SIO OAR pool. The ADP is shown 2 m underwater in the photo at a distance of 5 m from the stepper motor system (in the foreground) that controls the position of the target sphere relative to the acoustic beam. (B) A drawing of the pool is shown for scale.

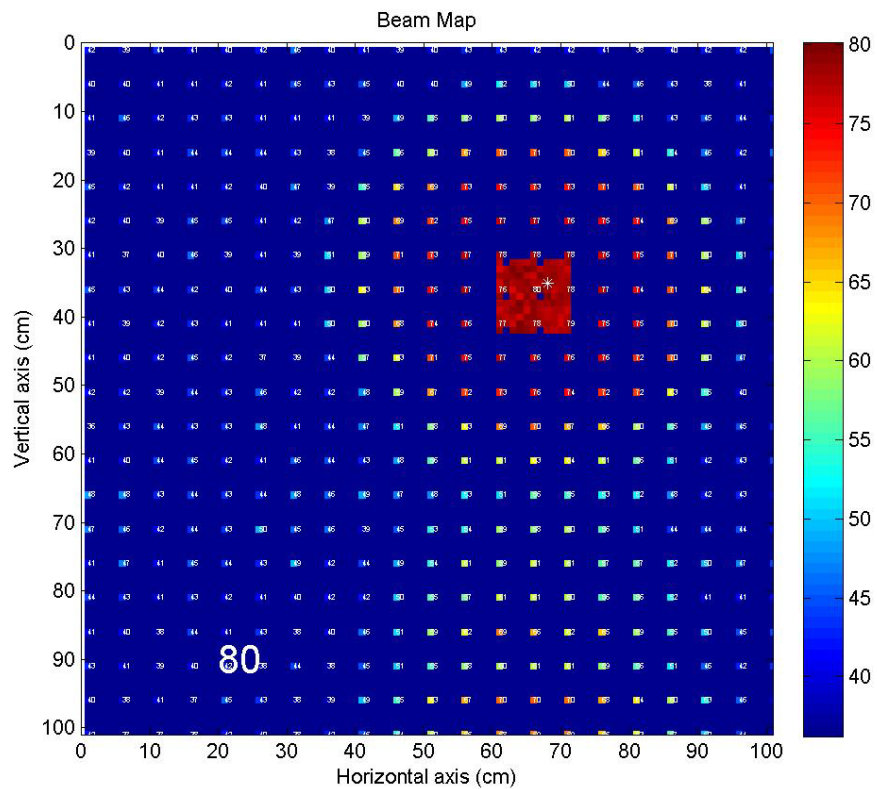


Figure A2.2. Example beam map generated during the calibration of ADP M685 on March 23, 2011. The color scale depicts recorded acoustic backscatter in decibels. The number 80 refers to the maximum ABS recorded during the calibration from a point near the center of the beam.

Table A2.1. ADP calibration results. All data reported in decibels.

| ADP SN | Calibration Date | Beam 1 | Beam 2 | Beam 3 | Analyst | Average interbeam difference | Mean Change since last deployment | Mean all deployments |
|--------|------------------|--------|--------|--------|-------------|------------------------------|-----------------------------------|----------------------|
| M1125 | 30-May-11 | 76 | 76 | 77 | S. Gordon | 0.67 | | 76 |
| M1126 | 11-Jul-12 | 76 | 74 | 75 | | 1.33 | | 75 |
| M1128 | 31-May-11 | 79 | 79 | 79 | S. Gordon | 0.00 | | |
| M1128 | 10-Apr-12 | 77 | 78 | 78 | Jesse | 0.67 | 1.33 | |
| M1128 | 27-Jan-13 | 80 | 78 | 79 | C Nickels | 0.99 | 1.30 | 79 |
| M1234 | 14-Dec-09 | 83 | 82 | 86 | J. Powell | 2.67 | | 84 |
| M479 | 6-Oct-06 | 81 | 81 | 81 | B. Maurer | 0.00 | | |
| M479 | 30-Mar-07 | 81 | 81 | 82 | J. Powell | 0.67 | 0.33 | 81 |
| M489 | 8-Jan-07 | 83 | 84 | 83 | J. Powell | 0.67 | | |
| M489 | 2-Jul-07 | 83 | 82 | 81 | J. Powell | 1.33 | 1.33 | |
| M489 | 10-Dec-07 | 83 | 83 | 82 | J. Powell | 0.67 | 0.67 | |
| M489 | 20-Sep-11 | 79 | 79 | 79 | S. Gordon | 0.00 | 3.67 | 82 |
| M513 | 6-Oct-06 | 85 | 84 | 85 | B. Maurer | 0.67 | | 85 |
| M578 | 8-Sep-07 | 84 | 84 | 84 | J. Powell | 0.00 | | |
| M578 | 30-Mar-08 | 87 | 87 | 88 | J. Powell | 0.67 | 3.33 | |
| M578 | 26-Jan-13 | 83 | 84 | 84 | Cat | 0.94 | 3.65 | 85 |
| M583 | 28-Dec-07 | 93* | 92* | 93* | J. Powell | 0.67 | | |
| M583 | 31-Jul-08 | 84 | 85 | 85 | J. Powell | 0.67 | 8.00 | |
| M583 | 16-Jan-09 | 85 | 85 | 86 | J. Powell | 0.67 | 0.67 | |
| M583 | 27-Nov-09 | 81 | 81 | 82 | J. Powell | 0.67 | 4.00 | |
| M583 | 10-Aug-10 | 83 | 83 | 84 | S. Gordon | 0.67 | 2.00 | |
| M583 | 23-Sep-11 | 82 | 83 | 83 | S. Gordon | 0.67 | 0.67 | 85 |
| M588 | 15-Jul-08 | nan | 87 | 88 | J. Powell | | | |
| M588 | 28-Oct-12 | 79 | 82 | 80 | Cat_Nickels | 1.88 | 6.63 | 83 |
| M672 | 22-Sep-11 | 83 | 80 | 83 | S. Gordon | 2.00 | | |
| M672 | 28-Oct-12 | 82 | 84 | 79 | Cat_Nickels | 3.22 | 2.93 | 82 |
| M673 | 14-Jul-08 | 82 | 82 | 82 | J. Powell | 0.00 | | |
| M673 | 19-Jan-09 | 80 | 81 | nan | J. Powell | | 1.50 | 81 |
| M678 | 10-May-08 | 86 | 85 | 84 | J. Powell | 1.33 | | |
| M678 | 5-Apr-09 | 84 | 84 | 83 | J. Powell | 0.67 | 1.33 | |
| M678 | 10-Apr-10 | 83 | 83 | 83 | S. Gordon | 0.00 | 0.67 | |
| M678 | 25-Oct-10 | 87 | 87 | 85 | S. Gordon | 1.33 | 3.33 | |
| M678 | 11-Jul-12 | 81 | 81 | 81 | Jesse | 0.00 | 5.33 | |
| M678 | 27-Jan-13 | 85 | 83 | 84 | C Nickels | 1.74 | 3.17 | 84 |
| M680 | 23-Nov-08 | 84 | 87 | 84 | J. Powell | 2.00 | | |
| M680 | 27-Jul-09 | 82 | 82 | 82 | J. Powell | 0.00 | 3.00 | |
| M680 | 13-Dec-09 | 83 | 82 | 82 | J. Powell | 0.67 | 0.33 | 83 |
| M681 | 28-Sep-09 | 80 | 81 | 80 | J. Powell | 0.67 | | |

Table A2.1 cont.

| ADP SN | Calibration Date | Beam 1 | Beam 2 | Beam 3 | Analyst | Average interbeam difference | Mean Change since last deployment | Mean all deployments |
|--------|------------------|--------|--------|--------|-----------|------------------------------|-----------------------------------|----------------------|
| M681 | 10-Aug-10 | 83 | 83 | 84 | S. Gordon | 0.67 | 3.00 | 82 |
| M685 | 23-Mar-11 | 81 | 80 | 81 | S. Gordon | 0.67 | | 81 |
| M686 | 29-Jul-08 | 82 | 81 | 82 | J. Powell | 0.67 | | |
| M686 | 25-Jul-09 | 80 | 80 | 80 | J. Powell | 0.00 | 1.67 | |
| M686 | 12-Dec-09 | 82 | 81 | 81 | J. Powell | 0.67 | 1.33 | 81 |

Note: Asterisks denote calibrations that were anomalously high for undetermined reasons.

| | M1125 | M1126 | M1128 | M1234 | M479 | M489 | M513 | M578 | M583 | M588 | M672 | M673 | M678 | M680 | M681 | M685 | M686 |
|-------|-------|-------|-------|-------|------|------|------|------|------|------|------|------|------|------|------|------|------|
| M1125 | 76.3 | 75.0 | 78.5 | 83.7 | 81.2 | 81.8 | 84.7 | 85.0 | 85.0 | 83.1 | 81.8 | 81.4 | 83.9 | 83.1 | 81.8 | 80.7 | 81.0 |
| M1126 | | 75.0 | | | | | | | | | | | | | | | |
| M1128 | | 3.5 | | | | | | | | | | | | | | | |
| M1234 | | 8.7 | 5.1 | | | | | | | | | | | | | | |
| M479 | | 6.2 | 2.6 | 2.5 | | | | | | | | | | | | | |
| M489 | | 6.8 | 3.2 | 1.9 | 0.6 | | | | | | | | | | | | |
| M513 | | 9.7 | 6.1 | 1.0 | 3.5 | 2.9 | | | | | | | | | | | |
| M578 | | 10.0 | 6.5 | 1.3 | 3.8 | 3.3 | 0.3 | | | | | | | | | | |
| M583 | | 10.0 | 6.5 | 1.3 | 3.8 | 3.3 | 0.3 | 0.0 | | | | | | | | | |
| M588 | | 8.1 | 4.5 | 0.6 | 1.9 | 1.3 | 1.6 | 1.9 | 1.9 | | | | | | | | |
| M672 | | 6.8 | 3.3 | 1.9 | 0.6 | 0.1 | 2.9 | 3.2 | 3.2 | 1.3 | | | | | | | |
| M673 | | 6.4 | 2.9 | 2.3 | 0.2 | 0.3 | 3.3 | 3.6 | 3.6 | 1.7 | 0.4 | | | | | | |
| M678 | | 8.9 | 5.3 | 0.2 | 2.7 | 2.1 | 0.8 | 1.1 | 1.1 | 0.8 | 2.0 | 2.5 | | | | | |
| M680 | | 8.1 | 4.6 | 0.6 | 1.9 | 1.4 | 1.6 | 1.9 | 1.9 | 0.0 | 1.3 | 1.7 | 0.8 | | | | |
| M681 | | 6.8 | 3.3 | 1.8 | 0.7 | 0.1 | 2.8 | 3.2 | 3.2 | 1.3 | 0.0 | 0.4 | 2.0 | 1.3 | | | |
| M685 | | 5.7 | 2.1 | 3.0 | 0.5 | 1.1 | 4.0 | 4.3 | 4.3 | 2.4 | 1.1 | 0.7 | 3.2 | 2.4 | 1.2 | | |
| M686 | | 6.0 | 2.5 | 2.7 | 0.2 | 0.8 | 3.7 | 4.0 | 4.0 | 2.1 | 0.8 | 0.4 | 2.9 | 2.1 | 0.8 | 0.3 | |

mean difference = 3.1
 Standard deviation = 2.5

Table A2.2. Pairwise differences between each ADP instrument's mean calibration test result. The mean and standard deviation of these differences is shown at the bottom of the table. All data reported in decibels.